T. J. Wipf, F. W. Klaiber, J. D. Rhodes, B. J. Kempers

Effective Structural Concrete Repair
Volume 1 of 3

Repair of Impact Damaged Prestressed Concrete Beams with CFRP

March 2004

Sponsored by the
Iowa Department of Transportation
Highway Division and the
Iowa Highway Research Board

Iowa DOT Project TR - 428

Iowa Department of Transportation

Final

REPORT

IOWA STATE UNIVERSITY
OF SCIENCE AND TECHNOLOGY

Department of Civil, Construction and Environmental Engineering

T. J. Wipf, F. W. Klaiber, J. D. Rhodes, B. J. Kempers

Effective Structural Concrete Repair
Volume 1 of 3

Repair of Impact Damaged Prestressed Concrete Beams with CFRP

March 2004

Sponsored by the
Iowa Department of Transportation
Highway Division and the
Iowa Highway Research Board

Iowa DOT Project TR - 428

Final

REPORT

IOWA STATE UNIVERSITY
OF SCIENCE AND TECHNOLOGY

Iowa Department of Transportation

Department of Civil, Construction and Environmental Engineering

General Abstract

Structural concrete is one of the most commonly used construction materials in the United States. However, due to changes in design specifications, aging, vehicle impact, etc. – there is a need for new procedures for repairing concrete (reinforced or pretressed) superstructures and substructures. Thus, the overall objective of this investigation was to develop innovative cost effective repair methods for various concrete elements. In consultation with the project advisory committee, it was decided to evaluate the following three repair methods:

- Carbon fiber reinforced polymers (CFRPs) for use in repairing damaged prestressed concrete bridges
- Fiber reinforced polymers (FRPs) for preventing chloride penetration of bridge columns
- Various patch materials

The initial results of these evaluations are presented in this three volume final report. Each evaluation is briefly described in the following paragraphs. A more detailed abstract of each evaluation accompanies the volume on that particular investigation.

Repair of Impact Damaged Prestressed Concrete Beams with CFRP (Volume 1-*this volume*) Four full-sized prestressed concrete (PC) beams were damaged and repaired in the laboratory using CFRP. It was determined that the CFRP repair increased the cracking load and restored a portion of the lost flexural strength. As a result of its successful application in the laboratory, CFRP was used to repair three existing PC bridges. Although these bridges are still being monitored, results to date indicate the effectiveness of the CFRP.

Use of FRP to Prevent Chloride Penetration in Bridge Columns (Volume 2) Although chemical deicing of roadways improves driving conditions in the winter, the chlorides (which are present in the majority of deicing materials) act as a catalyst in the corrosion of reinforcement in reinforced concrete. One way of preventing this corrosion is to install a barrier system on new construction to prevent chloride penetration. Five different fiber reinforced polymer wrap systems are being evaluated in the laboratory and field. In the laboratory one, two, and three layers of the FRP system are being subjected to AASHTO ponding tests. These same FRP wrap systems have been installed at five different sites in the field (i.e. one system at each site). Although in the initial stages of evaluation, to date all five FRP wrap systems have been effective in keeping the chloride level in the concrete below the corrosion threshold.

Evaluation of Repair Materials for Use in Patching Damaged Concrete (Volume 3) There are numerous reasons that voids occur in structural concrete elements; to prevent additional problems these voids need repaired. This part of the investigation evaluated several repair materials and identified repair material properties that are important for obtaining durable concrete repairs. By testing damaged reinforced concrete beams that had been repaired and wedge cylinder samples, it was determined that the most important properties for durable concrete repair are modulus of elasticity and bond strength. Using properties isolated in this investigation, a procedure was developed to assist in selecting the appropriate repair material for a given situation.

Effective Structural Concrete Repair

General Introduction

Structural concrete is one of the most commonly used construction materials in the United States. Due to changes in the design specification for bridges, increases in legal loads, potential for over-height vehicle impacts, and general bridge deterioration, there is need for new procedures for strengthening and/or rehabilitating existing reinforced and prestressed concrete bridges. In this investigation, strengthening and rehabilitating are considered to be specific means of repairing. The problems previously noted occur in the superstructure as well as in the substructure and are commonplace for state bridge engineers, county engineers and consultants.

In the past, several different materials and procedures have been used for strengthening/rehabilitating structural concrete with varying degrees of success. Some of the procedures used may be effective initially, however, they may not be effective long term especially if the deterioration is due to chloride contamination. Thus, research was needed to develop successful repair methods/materials for strengthening/rehabilitating various structural concrete bridge elements.

Overall Research Objectives

The overall objective of this project was to develop innovative repair methods that employ materials which result in the cost effective repair of structural concrete elements. Carbon Fiber Reinforced Polymers (CFRPs) were found to be the most effective material for long term repair. They have shown promise for use in strengthening and/or rehabilitating various bridge elements. These materials have the advantage of large strength/weight ratios, excellent corrosion and fatigue properties, and are relatively simple to install.

To insure the success of this project, a project advising committee (PAC) consisting of members from the Iowa DOT Office of Bridges and Structures and the Iowa County Engineers Association was formed. The research team met with the PAC on six different occasions. During the initial meetings, the numerous problems engineers have with structural concrete bridge elements were discussed. In later meetings, the research team proposed some potential solutions to the problems previously noted. The outcome of the last PAC meeting was that the following three repair methods should be investigated:

1.) Evaluation of CFRP for use in repairing/strengthening damaged prestressed concrete bridges,

2.) Evaluation of FRP for preventing chloride penetration into bridge columns,

3.) Evaluation of various patch materials.

This project involved a combination of laboratory and field tests. In two cases (1 and 2 noted above), there were laboratory investigations prior to investigating the procedure/material in the field in demonstration projects. The procedures/materials used in the demonstration projects will be periodically inspected until the end of the contract which is Dec., 2008. A log noting the date of the inspection, condition of strengthening system, etc. will be kept for each demonstration project. If a significant change in the strengthening system is observed at one of the demonstrate sites, the structure could be tested if such a test would provide additional information on the repair material/system.

Reports

Since there were three unique repair systems/materials investigated in this project, the results are presented in three separate volumes. Laboratory as well as field test results are presented in this three volume final report. Following this initial report, brief interim reports on the demonstration projects will be submitted approximately every two years. At the conclusion of the project (Dec. 2008), a final summary report will be submitted.

As previously noted, each volume of this final report is written independently. Thus, the reader may read the volume of interest without knowledge of the other two volumes. To further assist the readers in their review of this final report:

- Each volume has a unique abstract, summary, and conclusions, which are pertinent to that part of the investigation. Application guides for installing CFRP on damaged prestressed concrete beams and FRP on columns are presented in Volumes 1 and 2, respectively. A general abstract briefly summarizing the entire project is presented at the beginning of each volume. Thus, the three volume report has four abstracts.
- Each volume has a reference list that is unique to that part of the project. A limited number of references have been cited in more than one volume of the final report.
- The three volumes have different authors – the senior members of the research team plus the graduate research assistant(s) who worked on that part of the investigation.

Volume 1 Abstract

As a result of frequent over-height vehicular collisions with prestressed concrete (P/C) bridge girders around the state of Iowa, this project was initiated to investigate the use of carbon fiber reinforced polymers (CFRPs) to repair and/or strengthen damaged P/C girders. A literature review was completed to identify research on the use of CFRP in the repair/strengthening of structural concrete. Although there was a significant amount of literature on the use of CFRP on reinforced concrete, there was very little on the use of CFRP to repair/strengthen P/C bridges.

To obtain unpublished information, a questionnaire was distributed nationally to state agencies to determine how they are currently or are planning to use CFRP material to repair/strengthen P/C bridges. The return rate for the survey was excellent – 49/60 (82%). Of those returning the questionnaire, 98% indicated they would consider using FRPs in future bridge repairs if research verifies their effectiveness.

Four full-size, repaired, P/C beams were tested in the laboratory. Impact damage to the beams was simulated by removing a portion of bottom flange concrete and by severing several prestressing strands. To restore the flexural capacity of the specimens, the original shape of the bottom flange was restored using a concrete patch after which CFRP sheets were bonded to the bottom flange. Three of the beams were subjected to service loading prior to being loaded to failure. The fourth beam was subjected to simulated traffic (i.e., cyclic loading) before being loaded to failure. From the laboratory load tests, it was determined that the addition of CFRP increased the cracking load and restored a portion of the lost flexural strength.

Based upon the results from the laboratory tests, CFRP was used in the repair/strengthening of three existing bridges that had been damaged by over-height vehicle collisions. The southbound I-65 bridge near Altoona, IA, the westbound IA-34 bridge near Osceola, IA, and the westbound I-80 bridge near DeSoto, IA all had significant loss of concrete on one or more girders as well as severed prestressing strands. Prior to being repaired with CFRP, all bridges were load tested in their damaged condition. The Altoona bridge was retested after installation of the CFRP to determine changes in its structural behavior after being repaired. Although the bridge was only subjected to service loads during testing, experimental results indicated some improvement in its structural behavior.

Based on the work on the Osceola Bridge, a design/application guide was developed for designing and installing a CFRP repair/strengthening system for a damaged P/C beam.

TABLE OF CONTENTS

LIST OF FIGURES

LIST OF TABLES

1. INTRODUCTION

1.1. Background

Every year several prestressed concrete (P/C) bridges are damaged by overheight vehicles. Shanafelt and Horn (1980) have shown that approximately 160 P/C bridge impacts are reported each year by transportation departments in the United States. This number is also likely to increase as the amount of traffic on the nation's highways continues to grow.

In Iowa, approximately 5 to 6 significant bridge impacts due to overheight vehicles are reported each year (Phillips, 1995). The average estimated cost to repair each damaged bridge is $38,900. Minor impact damage (i.e. chips and scrapes) is repaired by patching but is generally not reported. The majority of the bridge impacts are caused by construction equipment being hauled on flatbed trailers. It is interesting to note that approximately 50% of the vehicles involved in recorded impacts had the necessary permit or were hauling loads that did not require a permit. This indicates that human error is a major factor in bridge impacts.

Traditional P/C girder repair strategies includes internal strand splices, external post-tensioning, and welded steel jackets. These types of repairs are both labor intensive and vulnerable to future corrosion. Girder replacement is another option often considered for moderately to severely damaged bridges. Unfortunately, replacing damaged girders is very expensive and disruptive to traffic. One possible alternative to these traditional techniques is to repair/strengthen impact damaged P/C girders with carbon fiber reinforced polymers (CFRP). CFRP is a relatively new material that has been used extensively in bridge applications in Europe and Japan (Hooks and Siebels, 1997). These types of materials have the advantage of large strength/weight ratios, excellent corrosion/fatigue properties, and are relatively simple to install. For these reasons, composite materials are beginning to gain acceptance in bridge applications in the United States.

1.2. Objective and Scope

The primary objective of this research was to evaluate the effectiveness of repairing/strenghthening impact damaged P/C girders with CFRP sheets and plates. The

main components of the investigation included a literature review, a survey sent to transportation officials, laboratory testing of full-size beam specimens, field testing of damaged bridges, and analyses of the experimental data.

A second primary objective was to evaluate the effectiveness of FRP sheets in repairing/strengthening substructures of bridges. FRP wrap systems were installed on a slab specimen in the laboratory and cylindrical columns at different test sites in the field. These wraps were installed to prevent chloride intrusion of the concrete specimens. Analysis of the testing is forthcoming and will be reported at a later date in a second report.

A literature review was completed to provide background information related to the project. Relevant material was summarized to help provide a more complete understanding of the topic. A questionnaire was also distributed nationally to transportation officials to help determine how other states are using or are planning to use CFRP materials to repair P/C bridge structures. Also included is a case study of traditional versus conventional repair costs from the IA DOT. The results of the literature review and the questionnaire responses are presented in Chapter 2.

Four full-size test specimens were constructed, subsequently damaged, and then repaired. Impact damage was simulated by removing a portion of concrete from the bottom flange and by severing multiple prestressing strands. The damage inflicted was intended to represent the level of damage typically found on moderately damaged girders in the field. Repairs were made by restoring the original shape of the bottom flange with a concrete patch material. Externally applied CFRP sheets were then bonded to the bottom flange to restore the flexural capacity of the specimens. CFRP sheets (jackets) were also used to help confine the patch material and to prevent premature debonding at the CFRP/concrete interface.

Along with the four beams, three damaged bridges were also investigated. Bridges near Altoona, Osceola, and De Soto, Iowa were struck by overheight vehicles. They were subsequently strengthened and repaired using CFRP sheets and plates. The full-size beam specimens, bridge schematics, and test setups are discussed in Chapter 3. The installation of the patch and CFRP is presented in Chapter 4.

Analyses and interpretation of the test results are discussed in Chapter 5. Beam deflection and strain data are presented for various levels of damage before and after the

repairs. Changes in beam stiffness and the distribution of forces due to the severed prestressing strands are also discussed. Strains were also monitored along the length of the CFRP and on the transverse CFRP jackets. The experimental results from the CFRP strengthened beams are compared with the ultimate strength analytical values and discussed.

A summary of the research is presented in Chapter 6. Suggested guidelines were also developed to help engineers and transportation officials decide when to use CFRP products to strengthen damaged girders. The appendix includes the national questionnaire, bridge damage reports, and a design/installation guide for CFRP repair on bridges.

2. LITERATURE REVIEW

A literature review relating to this phase of the project was completed. The literature search was performed using a number of sources: the Transportation Research Information Services (TRIS) at the Iowa Department of Transportation (Iowa DOT), the university library, the Internet, and a questionnaire distributed to state bridge engineers. The information in the following sections is a summary of the literature relating to this project.

2.1. Damage Classifications

Impact damage to P/C girders can range from simple scrapes to large section loss and severed prestressing strands. In 1980, Shanafelt and Horn (1980) published National Cooperative Highway Research Program (NCHRP) Report 226. This report contained detailed information concerning damage evaluation and repair methods for P/C bridges. One of the results of their work was a set of guidelines for inspectors and engineers to classify various levels of damage. They classified damage to P/C girders in four different levels:

1) Minor Damage
   - damage only to concrete portions of girders
   - no exposed reinforcing bars or prestressing strands
   - cracks in spalled areas must be less than 3 mils in width

2) Moderate Damage
   - damage only to concrete portions of girders
   - extensive spalled areas may expose reinforcing bars and/or prestressing strands
   - cracks in spalled areas are wider than 3 mils, but are closed below the surface damage
   - no severed prestressing strands

3) Severe Damage
   - damage to concrete and reinforcing include one or more of the following:
   - cracks extending across the width of the bottom flange but closed below the surface
   - major or total loss of concrete section in the bottom flange
   - major loss of concrete section in the web, but not at the same location as the loss of concrete in the bottom flange

   - severed prestressing strands or strands that are visibly deformed
   - minor horizontal and vertical misalignment of bottom flange (within allowable limits)

4) Critical Damage

- open cracks extending across the bottom flange and/or in the web directly above the bottom flange (indicating that the prestressing strands have exceeded yield strength)
- an abrupt lateral offset or lateral distortion of exposed prestressing strands (another indication that the prestressing strands have exceeded yield strength)
- loss of prestress force to the extent that calculations show that repairs are not feasible
- vertical misalignment in excess of allowable limits
- longitudinal cracks at the interface of the web and the top flange that are not substantially closed below the surface damage (indication of permanent deformation of stirrups)

In a more recent report, Feldman, et al. (1996) developed another set of guidelines for classifying impact damage. They classified damage to P/C girders in three different levels:

1) Minor Damage
   - shallow concrete cracks and nicks, shallow spalls, and/or scrapes

2) Moderate Damage
   - large concrete cracks and spalls
   - exposed undamaged prestressing strands

3) Severe Damage
   - loss of significant portions of concrete cross section
   - exposed damage prestressing strands
   - girder distortion resulting in lateral misalignment

There are a number of similarities in the two definitions of damage levels. Both classification systems have essentially the same descriptions of minor and moderate damage. The method proposed by Shanafelt and Horn (1980) is much more explicit when describing severe impact damage. However, no two impact damaged P/C beams appear the same in the field and it is difficult describe all possible types of damage in a brief set of guidelines. The damage classification system commonly used by state bridge engineers responding to the questionnaire is presented in Section 2.3. It is interesting to compare the slight differences in classifications. Damage descriptions made by practicing engineers tend to be much more general and do not include the extreme or critical damage levels. P/C girders that experience critical damage are almost always replaced.

2.2. Traditional Prestressed Concrete Repair Methods

Traditional P/C Repair Methods are outlined in NCHRP Reports 226 and 280 (1985). The two basic methods for restoring prestressing force are internal splices and external post-

tensioning. Internal strand splices use mechanical devices that consist of standard prestressing chucks and high strength turnbuckles to restore the original prestressing force to the severed strands. After the splices are installed and fully tensioned, a preload is applied to the beam and the concrete is repaired. Preloads can consist of loaded trucks, stacked barrier rails and/or steel plates, or hydraulic jacks. After the patch has attained sufficient strength the preload is removed. This method can be used to repair multiple severed strands in the same girder.

The second method involves post-tensioning with external tendons. This technique requires jacking corbels located outside the damage area. The corbels should be located so that holes can be drilled through the beam without interfering with the prestressing strands or web reinforcement. After the corbels are in place, high-strength tendons are installed and post tensioned. The primary disadvantage with external post-tensioning is that the hardware is exposed to the elements and therefore more susceptible to corrosion.

A third possible method for repairing damaged girders is a metal sleeve splice. This is a welded steel jacket that wraps around the bottom flange. Bolts extend through the concrete web to secure the splice in place. Preloading the girder before placing the patch can be used to restore partial or full prestressing. Note that the jacket does not provide any prestressing force. In this case, the stress ranges in the remaining strands would be increased. After the jacket is in position, epoxy is injected between the steel/concrete interface to bond the two materials together. Metal sleeves are also susceptible to corrosion.

Olsen, et al. (1992) evaluated the performance of internal splices and external post-tensioning repairs on P/C girders removed from a bridge in the field. The objective of the research was to rate the different repair methods under static, fatigue, and ultimate loads. The girders used for the research were standard AASHTO III type beams with a total length of 64 ft – 8 in. Damage was simulated on the girders by removing concrete from the corner of the bottom flange and flame cutting strands. In one girder, two strands were severed and then repaired with internal splices. Static and fatigue load tests indicate that the repaired strands carry a higher load than the undamaged strands. This behavior was attributed to the relatively high stiffness of the turnbuckles and indicates a potential fatigue problem. Also, during the ultimate strength test, the concrete patch fell out at a load of only 67% of the

girder strength. The turnbuckle dimensions did not allow for adequate concrete cover. Another beam was damaged in an identical manner and repaired with external post-tensioning. One of the corbels broke away as a result of flexural cracking after 12 in. of vertical displacement (78% of the undamaged capacity). A significant amount of girder concrete was also removed when the corbel failed. The concrete patch also fell out during the ultimate load test. Fatigue tests also indicated a small amount of strand damage (10%) resulted in an 80% reduction in the expected fatigue life of the remaining prestressing strands.

In a more recent report, Zobel, et al. (1996) repaired impact damaged P/C girders with internal strand splices as well a number of different patching materials. Preloads were applied to the damaged girders to restore their original profile and to assist in removing loose/fractured concrete. Damaged concrete was removed using a chipping hammer. After the concrete surfaces had been prepared, a plywood formwork was built to hold the repair materials in place. Prepackaged materials applied with forms included Set 45 (Masterbuilders Inc.) and Patchroc 10-61 (Fosroc Industries). Repairs were also completed without formwork using nonsag or vertical and overhead (V/O) repair materials. Products selected included Burke V/O (Burke), Renderoc HB2 (Fosroc Industries), and EMACO S88CA (Masterbuilders Inc.). A number of conclusions were reached after the experiences with the different repair products. Special care should be taken to match the properties of repair material with the existing concrete (e.g. similar color/texture, compressive and tensile strengths, modulus of elasticity, and thermal expansion characteristics). Working time of the patch material should also be considered when selecting a prepackaged material. For example, Set 45 only has a working time of 10 minutes. This would probably not be sufficient to property repair a girder in the field.

Four different strand splice designs were tested and evaluated to determine which types were the most effective. The names of the four different splices were the Alberta Splice Sleeve, Muti-Bolt Splice, Grab-It^{TM}, and Dual Strand Splice. There were installation problems associated with all four of the internal splices. It was difficult to keep the threaded components of the splices clean and properly lubricated. When the threads became damaged or dirty, it was extremely difficult to reach the desired tension. As before, the splices (wedge

details) tended to be prone to fatigue problems because of the high axial stiffness and stress concentrations at the wedge anchorages. Internal splices can be used to restore the ultimate flexural design strength of girders when the remaining service life of the structure is not a major concern. The authors recommended not repairing girders with splices when more than 10 to 15% of the strands in a single girder are severed.

2.3. Innovative Prestressed Concrete Repair Methods (CFRP)

Traditional P/C repair methods have a number of disadvantages. Installation of internal splices, external post-tensioning, and steel jackets systems can be time consuming and susceptible to corrosion. Another problem with internal splices and external post-tensioning is that it is possible for pieces of the patch to fall out and damage passing vehicles. An alternative is to repair impact damaged P/C girders with externally bonded carbon fiber reinforced polymers (CFRP). These types of materials appear to be very promising in the field of bridge repair. Their high strength to weight ratios and the excellent corrosion resistance make them attractive materials for structural applications. In addition, CFRP is flexible and can quickly be applied to flat or curved surfaces. CFRP laminates are generally bonded directly to concrete surfaces with a high strength epoxy. Applied to impact damaged P/C girders, CFRP have to potential to restore flexural strength and confine the patch material (Klaiber et al., 1999).

2.4. Questionnaire Results

A questionnaire was distributed to all of the state bridge engineers to help determine what techniques and materials are being used to repair impact damaged P/C girders. Another goal of the questionnaire was to determine how innovative materials such as CFRP are currently being applied to bridge structures. In addition to the fifty states, the survey was also sent to several U.S. national transportation officials and Canadian Departments of Transportation. The return rate for the survey was 82% (49/60). A copy of the questionnaire is presented in Appendix A.

Of the agencies responding, 44% indicated that they have some form of a strengthening/rehabilitation/repair program for impact damaged concrete bridges. A number

of states indicated that impact damage is handled on a case-by-case basis. The following damage levels summarize the types of damage reported by the different agencies:

1. Minor Damage
- some spalling and cracking
- small areas of concrete loss

2. Moderate Damage
- large amounts of loose or missing concrete
- minor cracks in the flange and web
- minor damage to prestressing strands, i.e. one strand severed

3. Severe Damage
- major cracking of the web and flange
- significant damage to the prestressing strands

Other comments suggest that impacts generally either cause minor damage or completely destroy the bridge. Typical repairs consist of removing fractured concrete and cleaning of the damaged section, mechanical splicing of severed prestressing strands, epoxy injection of cracks, and encasement of the damaged area with a patch material. Twenty-one different patch materials were listed by those responding to the questionnaire. None of the patch materials were repeated more than three times. Concrete is generally used for large volume repairs. Welded wire fabric and steel drive pins are also commonly used to help secure the patch material. These are essentially the same procedures described in NCHRP Report 226. The majority of agencies reporting indicate that damaged P/C girders with moderate to severe section loss are preloaded prior to the replacement of the concrete section. The vertical pre-load helps put the repair material in compression and therefore improves the durability characteristics of the patch. Preloading also helps maintain the original profile of the P/C girder.

Criteria for replacing damaged prestressed girders varies from state to state. For example, in California the entire girder is removed if the prestressing system is affected by the impact. North Carolina generally removes girders if one of more prestressing strand is severed. Wisconsin replaces girders if more than two prestressing strands have been severed.

Finally, Oregon reports that if more than 25% of the prestressing strands are severed the member is replaced.

The following is a list of R/C and P/C bridge related work that was reported in the questionnaire:

- Massachusetts has applied for Federal funding under the Innovative Bridge Construction program to use CFRP products to repair and strengthen two bridges. One of these proposed projects is the repair of a deteriorated P/C deck beam. The beam in question has lost seven prestressing strands. It is estimated that the entire project will cost $65,000. The "innovative materials" for this construction project account for $15,000 or 23% of the total program. The other project mentioned was the strengthening of a R/C bridge deck.
- Michigan has strengthened R/C bridge beams with CFRP sheets.
- Minnesota is considering a pier cap strengthening project.
- North Carolina plans to make a number of repairs to deteriorating columns and pier caps with GFRP.
- Kentucky is considering strengthening a prestressed box beam bridge with CFRP fabric that has shear cracks at the beam ends.
- Georgia has used or is planning to use FRP materials on pier cap repairs, deck strengthening, and P/C beam repairs.
- Missouri has funded research on strengthening of concrete slab bridges with FRP.

An overwhelming majority of those returning the questionnaire (98%) indicated that if FRP products appear to be effective, they would consider using them on future bridge repair projects. Virginia was the only state or agency not willing to consider using FRP.

2.5. Case Study

Some repair data was collected from the Iowa DOT involving different bridge repairs that had been performed. From this data, some comparisons were drawn between the steel jacket and CFRP repair costs. The data came from five bridges repaired in Iowa in recent years, four using the steel jacket and one using CFRP. Most of the bridges were from the Central Iowa area, but one was from the western side of the state. These bridges had all incurred damage due to vehicular impact and were in need of various repairs. Some of the bridge data used to draw comparisons are shown in Table 2.1, which includes bridge locations, dimensions, beams, damage amount, and the extent of the repair work.

Table 2.1. Bridge description, locations, and damage levels.

Bridge	No. of beams repaired	Length of repair	Location	Extent of Repair Needed	Degree of Traffic Control
Polk 3498 (Steel)	1	30 ft	Euclid over I-235	1*	Moderate
Polk 2095 (Steel)	2	29 ft	Beaver Road over I 80/35	2*	Extreme
Woodbury 597 (Steel)	1	15.7 ft	Local K25 over I-29	3*	Total Shutdown of K25
Warren 599 (Steel)	1	13.5 ft	Iowa 92 over I-35	4*	Little
Polk 3400 (CFRP)	6 total, 1 extensive	6 ft, and 80 ft	US-65 over US-6	5*	Little

*See repair description below.

1. This bridge required repair of two relatively large areas of concrete on the damaged beam. Steel plate assemblies were attached to the upper and bottom portion of the beam. It was then sealed using an epoxy gel and injected with an epoxy resin. The welded area was painted with zinc paint. The steel jacket continues higher up the web for bridge #1 and #4 than it does for bridge #2.
2. This bridge needed repair of two relatively large areas of concrete on the beam. Steel plate assemblies were attached to the upper and lower portion of the beams. It was sealed using an epoxy gel and injected with an epoxy resin. The welded area was painted with zinc paint.
3. This bridge had incurred more damage than the others and required the repair of one beam and total replacement of another. This makes it hard to compare with the other repair jobs.
4. This repair was approximately the same as repair #1.
5. The concrete on this bridge was repaired using shallow repair and/or regular repair techniques. FRP plates were installed under the heavily damaged areas on one beam. CFRP was wrapped around damaged areas (8-15 ft.), and then down the entire length of the heavily damaged beam.

Bids were taken separately for the five jobs. The costs and bids varied widely from company to company and bridge to bridge. Table 2.2 shows a summary of the bids with the winning bids in bold type.

Table 2.2. Bids for different bridge repairs.

Bridge	Bidding Company	Cost of Traffic Control	Mobilization	Beam Repair
Polk 3498 (Steel)	Shaw	***$5,200***	***$2,000***	***$24,952***
	Cramer	$5,700	$5,500	$23,252
	Jensen	$7,700	$5,000	$28,717
	Herberger	$7,700	$5,000	$36,101
Polk 2095 (Steel)	Cramer	***$17,061***	***$2,400***	***$5,500***
	Jensen	$17,477	$2,000	$15,000
Woodbury 597 (Steel)	Elk Horn	***$30,535***	***$12,000***	***$23,440***
	Christensen	$54,701	$15,000	$39,312
Warren 599 (Steel)	Shaw	***$2,920***	***$3,500***	***$12,050***
	Jensen	$4,720	$2,500	$16,900
	Cramer	$2,920	$5,000	$14,375
	Herberger	$4,220	$4,000	$23,400
Polk 3400 (CFRP)	Cramer	***$3,150***	***$5,500***	***$34,000***
	Shaw	$5,550	$3,500	$35,000
	BRB	$4,000	$5,000	$61,000

Drawing direct comparisons from the steel jacket vs. the CFRP wrap is difficult because in the field most beams are not exactly alike, and if they are, the damage on one beam is going to be different from the damage on an identical beam. The length of the beams, the amount of damage, the damage location on the beam, the damage location over the roadway, the need for extensive traffic control, and the amount of time to do the repair, are all factors in figuring which method is the cheaper.

The first impression of the tables indicates that the CFRP method looks to be more expensive than the steel jacket. This is a result of possibly three things: the length of the beam wrapped with CFRP was 75 feet, the wrapped beam also had its flexural strength enhanced by carbon fiber plates, and the CFRP process is very new.

The cost to repair a 30 ft beam for the Polk 3498 bridge was $24,952, which included $15,312 for structural steel. This is approximately $826 per lineal foot. The Polk 3400 bridge repair cost $34,000. With 80 feet being wrapped and ignoring the cost of the other

five beams, the cost of this repair was $425 per lineal foot. This does not include the fact that the bridge repaired with CFRP was also flexurally strengthened.

Unlike the bridges repaired with the steel jacket, the Polk 3400 bridge was flexurally enhanced with carbon fiber plates. The plates used for this job were 4 in. Sika S1012 plates, which cost $44 per lineal foot. Four plates were placed side by side along the bottom with a length of 75 feet for a total of 300 lineal feet. This means that the plates alone cost $13,000. Subtract that from the $34,000 total, and the price is $262.50 per lineal foot for the CFRP wrap, which is less than 1/3 of the cost of the steel jacket repair.

As more companies continue to use the CFRP the cost should decrease as the competition increases. Hopefully more repairs can be documented to increase the data bank of bridge repair costs. This will make it easier to see the advantages of CFRP.

2.6. Reinforced Concrete and CFRP

In the past ten years, a significant amount of research has been completed on the concept of strengthening of R/C beams with FRP. The majority of these projects are based on small-scale tests. These types of tests are helpful in understanding the general characteristics of beams with bonded FRP materials.

2.6.1. Debonding

One common problem encountered by a number of researchers is the phenomena of debonding. Debonding is best described as the peeling of the CFRP sheets from the concrete surface. This behavior is the result of crack propagation along the CFRP/concrete interface. Generally, debonding takes place before the ultimate strength of the CFRP material is reached.

Arduini and Nanni (1997) investigated the effects of repairing precracked R/C beams with CFRP sheets. The beams used in this study (12 in. x 6 in. x 6 ft) were tested in four-point loading. The beam specimens were initially subjected to a load equal to 30% of the nominal flexural capacity. This service load was sufficient to cause cracking in the constant moment region. The beams were than repaired with a variety of different CFRP configurations. Debonding at the adhesive-concrete interface was the controlling mode of failure. The debonding generally started at one of the vertical flexural cracks in the constant

moment region and propagated along the CFRP sheet. It was found that sandblasting the concrete surface was only slightly more effective than grinding in controlling debonding. The impact of CFRP strengthening is a function of beam cross-section and the amount of reinforcing steel. The response of heavily reinforced beams repaired with CFRP will not be as pronounced.

A set of small scale beam (4 in. x 4 in. x 40 in.) tests were conducted by Quantrill, el al. (1996) to determine how concrete strength, adhesive thickness, and plate cross-sectional area influenced the predicted stress levels at the ends of FRP plates. Higher strength concrete was found to carry increased levels of shear and normal stress before debonding occurs. The stress concentration factors at the plate ends were determined to be independent of concrete strengths, and were found to vary with adhesive thickness. Increasing the adhesive thickness tended to decrease the bond strength. FRP plates were also bonded to both sides of the concrete beams in the vicinity of the plate ends. This technique was found to have little affect on the beam strength.

A number of studies have investigated different anchorage techniques in an attempt to prevent the FRP sheets or plates from debonding. Varastehpour and Hamelin (1996) tried to confine the plate ends by both mechanical anchors (bolts) and FRP angle wraps in the areas of high shear. The bolts only slightly increased the ultimate strength of the beams and did not prevent the FRP plates from debonding. The full flexural capacity was reached when the angle wraps were used to anchor the longitudinal FRP.

Sharif, et al. (1994) investigated various schemes designed to prevent FRP debonding on precracked R/C beams. Steel anchor bolts were found to prevent debonding only for thick FRP plates. However, the beams repaired with anchor bolts failed due to diagonal tension (shear) cracks that formed at the ends of the FRP plates. A variety of other jackets or wraps were also considered. These included additional plates bonded to the sides of the beams in the areas that experienced debonding. One variation included an I-shaped FRP plate. This continuous “I-jacket” anchorage system was the most effective in preventing debonding and developing the full flexural strength of the repaired beams.

Arduini, et al. (1997) completed a study in the area of brittle failure of CFRP sheets and plates bonded to scaled R/C beams. Debonding was the predominate mode of failure for

beams strengthened with multiply layers of CFRP sheets. Wrapping the entire length of the beam with a transverse CFRP wrap was found to increase the strength of the section by 20% as opposed to those beams without confinement. The wrap also increased the ductility of the beam by 15%. Also, tests indicated that the shear strength of the FRP-adhesive interface was three times the shear strength of the concrete-adhesive interface.

2.6.1.1. Predicting Normal and Shear Stress

Premature debonding failures at plate ends are the result of shear and normal stress concentrations in the adhesive. This undesirable behavior became an issue in early tests with R/C beams strengthened with bonded steel plates. Roberts (1989) developed the following approximate procedure to predict the magnitude of the shear and normal stresses at the ends of bonded steel plates:

$$\tau_o = \left(F_o + \left(\frac{K_s}{E_p b_p d_p} \right)^{\frac{1}{2}} M_o \right) \frac{b_p d_p}{I b_a} \left(h_p - h \right) \tag{2.1}$$

$$\sigma_o = \tau_o d_p \left(\frac{K_n}{4 E_p I_p} \right)^{\frac{1}{4}} \tag{2.2}$$

Where:

$$K_s = G_a \frac{b_a}{d_a}$$

$$K_n = E_a \frac{b_a}{d_a}$$

τ_o = maximum shear stress in the adhesive.
σ_o = maximum normal stress in the adhesive.
K_n = normal stiffness/unit length of adhesive layer.
K_s = shear stiffness/unit length of adhesive layer.
E_p = modulus of elasticity of the steel plate.
E_a = modulus of elasticity of the adhesive.
G_a = shear modulus of the adhesive.

b_p = width of steel plate.

b_a = width of adhesive.

d_p = depth of steel plate.

F_o = shear force in the beam.

M_o = bending moment.

I = total moment of inertia of the composite transformed steel section.

I_c = moment of inertia of the concrete.

I_p = moment of inertia of the steel plate.

h = depth of neutral axis.

h_p = effective depth of steel plate.

h_s = effective depth of conventional steel reinforcement.

This type of analysis laid the groundwork for later work dealing specifically with FRP plates. Malek, et al. (1996) developed a set of expressions to represent the high interfacial shear and normal stress at the ends of FRP plates. These equations were developed from equilibrium and compatibility requirements of an infinitesimal piece of FRP bonded to the tension face of a R/C beam. Assumptions used in the development of these expressions included linear elastic behavior for all materials and an uncracked concrete cross-section. Microcracks and slip effects of the FRP were ignored. The following equations represents the shear stress between the FRP and the adhesive material (x = 0 represents the termination point of the FRP plate):

$$\tau(x) = t_p\left(b_3\sqrt{A}\cosh\left(\sqrt{A}x\right) - b_3\sqrt{A}\sinh\left(\sqrt{A}x\right) + 2b_1x + b_2\right) \qquad (2.3)$$

The maximum shear stress occurs when x = 0:

$$\tau_{max} = t_p\left(b_3\sqrt{A} + b_2\right) \qquad (2.4)$$

Where:

$$b_1 = \frac{\bar{y}a_1E_p}{I_{tr}E_c}$$

$$b_2 = E_p\left(\frac{\bar{y}}{I_{tr}E_c}\left(a_1L_o^{\,2} + a_2L_o + a_3\right) + 2b_1\frac{t_at_p}{G_a}\right)$$

$$b_3 = \frac{\bar{y}E_p}{I_{tr}E_c}\left(2a_1L_o + a_2\right)$$

$$A = \frac{G_a}{t_a t_p E_p}$$

t_p = thickness of the FRP plate.
t_a = thickness of the adhesive.
E_p = elastic modulus of the FRP plate.
E_c = elastic modulus of concrete in tension.
E_a = elastic modulus of the adhesive.
G_a = shear modulus of the adhesive.
$\bar{y}$ = distance from the neutral axis to the FRP.
I_{tr} = moment of inertia or the transformed section.
L_o = distance between the origin of x_o and the cut-off point.
a_1,a_2,a_3 = constants related to the type of loading.

Using a similar approach, the following expression was developed for the maximum normal or peeling stress:

$$f_{n_{max}} = \frac{K_n}{2\beta^3}\left(\frac{V_p}{E_p I_p} - \frac{V_c + \beta M_o}{E_c I_c}\right) \qquad (2.5)$$

Where:

$$K_n = \frac{E_a}{t_a}$$

$$\beta = \left(\frac{K_n b_p}{4E_p I_p}\right)^{\frac{1}{4}}$$

$$V_p = -b_p \frac{t_p^2}{2}\left(b_3\sqrt{A} + b_2\right)$$

$$V_c = V_o - b_p t_p \bar{y}\left(b_3\sqrt{A} + b_2\right)$$

K_n = represents the normal stiffness of the adhesive.
M_o = bending moment at the cut-off point.
V_o = shear at the cut-off point.
b_p = width of FRP plate .

Results from these two expressions for shear and normal stress were compared with a finite element (FE) model and experimental results. The results from the FE solution closely resembled the analytical solution. Stress concentrations tended to only be present in the area near the ends of the FRP plate.

2.6.1.2. CFRP Design Guidelines

A number of researchers have presented flexural design guidelines for R/C beams that consider the stress concentrations at the end of FRP plates. In a procedure by Chaallal, et al. (1998), both classical and premature failure modes are checked. The two classical failure modes are tensile failure (rupture) of the CFRP material or concrete crushing before or after steel yielding. Note that tensile failure of the FRP is only possible for lightly reinforced sections. There were also two modes of failure defined as premature. These failure types include debonding of the FRP material at the concrete interface and the other is debonding of the FRP/concrete cover at the level of reinforcing. Similar design guidelines were also suggested by Saadatmanesh and Malek (1998). In this procedure, Equations 2.4 and 2.5 were incorporated to check for premature localized failures.

2.6.2. Durability Issues

Durability and long-term performance of CFRP systems is a major concern when repairing or strengthening concrete bridge structures. The epoxy bond must be able to withstand a combination of freeze/thaw cycles, elevated moisture levels, chorides from deicing chemicals, and ultraviolet radiation. Fatigue is another long-term factor that needs to be considered when using CFRP systems. Unfortunately, very little long-term behavior data are currently available for bonded fibers.

The majority of the information that has been published on durability focuses on the results of accelerated environmental tests on small-scale specimens. Toutanji and Gomez (1997) published a paper focusing on the bond strength of FRP sheets when exposed to harsh environmental conditions. Concrete beam specimens were placed in an environmental chamber and subjected to 300 cycles; one cycle consisted of four hours of exposure to simulated salt water and than 2 hours of drying. The dimensions of the beams used in these tests were 2 in. x 2 in. x 14 in. The specimens were than tested in four point bending and compared with identical control beams that had been kept at room temperature. All of the beams failed as a result of debonding at the fiber/concrete interface. Reduction in strength was found to range from 7 to 33 % for beams with CFRP sheets. This strength reduction was attributed to the deterioration of the epoxy. A slight reduction in ductility also occurred after exposure to the wet/dry environment.

A similar paper was published by Chajes, et al. (1995). This research focused on the effects of wet/dry and freeze/thaw cycles on small-scale concrete beams (1.5 in. x 1.5 in. x 13 in.) strengthened with CFRP. The wet cycle of the wet/dry exposure also included chlorides. Specimens were subjected to 100 cycles for each environmental condition. The mode of failure for all of the CFRP strengthened beams was described as rupture of the fabric with partial debonding. The wet/dry and freeze/thaw exposure conditions were both found to decrease the ultimate capacity of the beam specimens by approximate 20% at 100 cycles.

Hoa, et al. (1996) also conducted a series of environmental tests on concrete beam specimens (3 in. x 2 in. x 11 in.) strengthened with CFRP. The beams were subjected to water immersion, freeze/thaw cycles, and outdoor exposure. Outdoor exposure specimens were subjected to Canadian (Montreal) weather conditions for 28 months. All of the beam specimens were tested to failure in 3-point bending. The water immersion tests did not significantly influence the capacity of the beams. The freeze/thaw and long-term specimens exhibited a 7% reduction in load carrying capacity. It was concluded from the results of these tests that temperature is more influential than moisture in reducing the bond strength at the concrete/fiber interface.

A similar conclusion was reached about the effect of temperature changes and bond strength by Green and Soudki (1997). Freeze/thaw tests were conducted on CFRP

strengthened concrete cylinders (6 in. x 12 in.) and beams (4 in. x 6 in. x 47 in). The cylinders and beams were subjected to 200 and 50 complete cycles, respectively. It was noted that the cracking load for the beams strengthened with CFRP was slightly lower than the control beams. No significant differences in ultimate strength or ductility were observed between the beam specimens exposed to freeze/thaw cycles and those kept at room temperature. The typical mode of failure was debonding of the CFRP sheet. The debonding generally started at a flexural or shear crack and then propagated to the end of the beam.

Sen, et al. (1999) also investigated the affects of different environmental conditions on bonded CFRP samples. Throughout this two-year study, slab specimens were subjected to wet/dry cycles with salt water, wet/dry cycles with salt water combined with thermal cycles, and continuous outdoor exposure. The CFRP samples were rated using visual inspection, tension, and torsion tests. It was determined that visual inspection was not a reliable method for evaluating bond degradation. Also, the torsional shear test was found to be a more reliable than the tension tests for quantifying the bond strength of the CFRP. The wet/dry cycles were the most harmful to the CFRP samples. Those samples exposed the wet/dry cycles had an average bond strength approximately 30% lower than the control group.

2.6.3. Creep and Shrinkage

Plevris and Triantafillou (1994) developed an analytical model to investigate the creep and shrinkage characteristics R/C beams strengthened with CFRP laminates. In this model, time-dependent deformations of the adhesive layer between the CFRP and concrete interface were neglected. In the development of the analytical model, it was assumed that the CFRP was applied to the R/C beam 200 days after construction. The results of the parametric study indicated that CFRP laminates have a positive effect on the long-term behavior of strengthened R/C concrete beams. Increasing the amount of CFRP on the tension face of a beam decreases the creep strains in the compressive zone. This results in reduced deflections over time due to creep. The results of this analytical model were also confirmed with experimental tests.

Ligday, et al. (1996) also investigated the effects of creep on R/C concrete beams strengthened with CFRP sheets. Two beams were tested under sustained loads for a period

of 50 days. Both beams were strengthened in the longitudinal direction with CFRP sheets bonded to the tension face. Also, one beam was wrapped with a full-length transverse CFRP wrap and the other beam was left unwrapped. The results indicated that the transverse wrap decreased concrete strains by approximately 70% over time when compared to the unwrapped beam. A modified form of the ACI creep model (Eqn. 2-8, (ACI, 1994)) was also suggested to represent the creep characteristics of the wrapped beam.

2.6.4. Static Performance

Shahawy and Beitelman (1999) looked at static performance of T-beams strengthened with CFRP. They statically tested ten T-beams, nineteen feet long, with differing wrap patterns varying from fully wrapped to partially wrapped stems. The partially wrapped stems only had CFRP on the bottom of the stem and not on the sides. The beams had from 0 to 4 layers of CFRP attached to them. Two-point loading was used for the tests. From their static tests, ultimate flexural strength was shown to increase from 19% to 70% with a rate of increase beginning to diminish past two layers. They determined that concrete crushing was occurring before the full strength of more CFRP layers could be realized.

It was also concluded that perhaps partial wrapping was not the best way to wrap the beams. When a CFRP layer was only placed on the bottom of the stem, horizontal cracks developed along the level of the reinforcing steel causing delamination of the concrete. The fully wrapped beams were found to be more ductile than the partially wrapped beams, which seems odd and does not seem to follow what most other researchers are saying.

Copozucca and Cerri (2002) looked at the behavior of RC beam models strengthened after cracking with CFRP. After running single point bending tests on different beams with one and two layers of CFRP, they concluded that models with more layers of CFRP will have more strength but less ductility then those with fewer or no layers of CFRP. This could lead to undesirable brittle failures. With only one layer of CFRP, a good level of ductility was shown from their Moment-Curvature plots.

2.6.4.1. Shear

Chaallal et al. (2002) performed tests looking into shear strengthening with CFRP fabric. They tested fourteen 20 ft long RC T-girders with various stirrup spacings a total of

twenty-eight times to determine the effect of CFRP shear reinforcement. They drew several conclusions from their tests. The failure mode for the unwrapped beams was concrete crushing. For the wrapped beams the failure mode was usually fabric delamination near the support because of sliding along the line of the shear crack. The concrete in the wrapped beams appeared to have undergone significant deformations pas its ultimate capacity due to the wrap confinement.

The researchers stated that for wrapped beams the maximum shear force generally increased with the number of layers of CFRP, but the shear forces were not a function of the number of layers. The optimum number of layers depended on the steel reinforcement. The shear reinforcement also increased the ductility of the members. They also claim that a certain combination of CFRP layers and steel stirrups exists that would create a maximum increase in ductility. Norris et al. (1997) concluded that certain combination of fibers and orientations could provide a ductile yielding response similar to steel plate retrofits that is more satisfactory for concrete design. Chaallal et al. (1998) gives a design procedure for shear strengthening using CFRP fabrics including an example problem.

Tann et al. (2001) presented a design approach for externally bonded shear using FRP composites as well as a major literature review of previous research. This literature review documented growths in shear design technology and included names such as Al-Sulaimani et al.(1994), Chajes et al.(1995), Sato et al.(1997), Triantaffilou (1998), and Swamy et al. (1999). The review spanned the years from 1993-2000.

2.6.5. Fatigue Performance

Shahawy and Beitelman (1999) also looked at fatigue performance of strengthened T-beams. Six beams, nineteen feet long, were cyclically loaded for up to 3,215,000 cycles. There was one control beam, two beams had 2 layers of CFRP with the stem fully wrapped and two beams had 3 layers of CFRP with the stem fully wrapped. A sixth beam was damaged in fatigue for 150,000 cycles before 2 layers of CFRP were added to its stem.

The damaged beam that had been rehabilitated showed improved fatigue life similar to the undamaged beams that were wrapped before they were loaded. This led to the conclusion that severely cracked beams in the field could be successfully repaired with CFRP. From the tests it was also concluded that the stiffness of all of the wrapped beams

was greater than the unwrapped control beam. Finally the testers concluded that full wrapping of beams with CFRP is an effective method of rehabilitating and strengthening fatigue critical structures.

Barnes and Mays (1999) conducted some fatigue tests on reinforced concrete beams with CFRP plates attached. Five identical beams were tested in fatigue, two original and 3 strengthened beams. Three different aspects of loading were addressed. These aspects included the following: apply the same loads to plated and unplated beams, apply loads that would give the same stress range in the rebar to each, or apply the same percentage of ultimate load capacity to both beams. All three of these aspects were addressed in this single test.

The final results of this experiment showed that a plated beam had significantly longer fatigue life than an unplated beam with the same loading. A plated beam also has a longer fatigue life than an unplated beam when the rebar is loaded to identical stress ranges. Finally it was noted that an unplated beam had a longer fatigue life than a plated beam when each was loaded to the same percentage of the predicted ultimate strength.

2.6.6. Field Testing

Stallings et al. (2000) tested a bridge in Alabama that had been damaged and repaired with CFRP. The bridge was a 4 girder, 7 span bridge with 34 ft spans. The bridge had not been impacted but needed to be strengthened due to additional load requirements. It had developed flexural cracks near the midpoint of several spans. The plans called for FRP strengthening of one span with CFRP plates along the bottom of the flanges for flexural strengthening and GFRP along the sides of the flanges to prevent flexural cracks from opening further. The intent of the design was to increase the bending moment 20% so the needed CFRP was calculated based on this requirement.

The girders were repaired according to the recommendations provided by the manufacturer. These recommendations included grinding and sandblasting the concrete, creating a smooth surface on the plates and correctly mixing and applying the epoxy as well as using rollers to create a better bond.

Static and dynamic load tests were done before and after the repair using ALDOT trucks. Decreases in reinforcement stresses for the static tests ranged from 4% to 12%.

Decreases in mid-span deflection for the static tests ranged from 2% to 12%. For the dynamic tests, reinforcement stresses decreased from 4% to 9%, and mid-span deflection decreased from 7% to 12%.

The testers concluded that application of the CFRP was a simple, straightforward process with little or no need for special equipment or tools. They also found that deflections and reinforcement stresses in the girders strengthened with GFRP on the sides were noticeably less than for the girder without the GFRP. This led them to conclude that cheaper GFRP plates may be added to the sides of girders to increase stiffness while the more expensive CFRP plates could be added to the bottom flanges to increase load capacity.

Masoud and Soudki (2000) investigated the serviceability of corroded RC beams that had been strengthened with CFRP sheets. They tested 8 strengthened beams that had been corroded with a chloride solution. They concluded that the CFRP was capable of restoring strength lost due to corrosion. Their results also showed that longitudinal crack widths were reduced about 20% from unstrengthened to strengthened beams, and mid-span deflection was also reduced an average of 33% for strengthened beams.

Watson (2001) reported on several aspects of CFRP uses including column wraps, corrosion inhibition, and beam strengthening, including laboratory and field beams. One investigation included a bridge in South Carolina that had been significantly damaged by vehicular impact. The state had to choose the best possible repair option. It was determined that the replacement of the beam would have cost upwards of $250,000. Finally a CFRP strengthening option was designed and approved that only took 3 weeks, saved the state over $150,000, as well as minimized traffic disruption.

Many other people have conducted tests on RC bridges strengthened with either CFRP and/or GFRP. Some of the more recent include Nanni et al. (2001), Brena et al. (2001), Kachlakev (2001), and Keble et al. (2001). There are also up to hundreds more not mentioned.

2.7. Prestressed Concrete and CFRP

To date, very little work has been published in the area of P/C and FRP. Aboutaha, et al. (1997) reported on the effectiveness of using CFRP to repair and strengthen a damaged AASHTO type II P/C girder. The girder had been tested in flexure at two different points to

its ultimate capacity in a previous FHA project. These initial tests resulted in major flexural cracks at the loading points that extended into the top flange (indicating the strands had yielded). The loads also caused concrete crushing in the compression flange and the prestressing strands to slip. In short, this girder was heavily damaged.

The repair strategy consisted of injecting the cracks with epoxy and applying multiple layers of CFRP sheets to both the tension flange and the web. To develop the full strength of the CFRP sheets, they were extended 54 in. past the existing flexural cracks at the loading points. Load tests were conducted before and after the application of the repair materials to determine the effectiveness of the repairs. The failure mode of the repaired girder was bond-shear or peeling between the ends of the CFRP sheets and the concrete interface. The load-deflection curve for the repaired girder indicated a tri-linear behavior. In the first slope region, the CFRP sheets increased the beam stiffness to 50% of the original, undamaged value. The second slope region represents the opening of shear cracks in the web near the supports. It was noted that the CFRP sheets were more effective in controlling flexural cracks. The last slope region corresponded to the peeling at the ends of the CFRP sheets. Lack of ductility was not an issue with the repaired girder. It would not have been practical to fully restore the elastic stiffness of the damaged girder. Fully restoring the elastic stiffness would have tripled the calculated flexural strength of the original girder. Shear type failures need to be carefully considered when the original flexural design strength is exceeded. Increasing the beam stiffness is difficult due to the small cross-sectional area of the CFRP sheets.

Shahawy and Beitelman (1995) completed an experimental investigation on the strengthening of damaged P/C slabs with externally bonded CFRP. Prestressed solid and voided slabs specimens (0.66 ft x 3.9 ft x 21.5 ft) were loaded to failure under 2-point loading and then strengthened with unidirectional carbon fiber tape. Approximately 90% of the original flexural strength was restored by adding the CFRP to the damaged solid slabs. Strain levels in the prestressing strands also decreased by 38% in the retrofitted specimens. The effect of the CFRP on the voided slab specimens was much more pronounced. The flexural strength of the voided slabs increased by 78% compared to the initial strength test. However, the voided slab specimen experienced a sudden bearing failure at one of the

supports. These prestressed slabs were not designed to carry these increased concentrated forces at the ends. Installing large amounts of tensile reinforcement (CFRP) can result in undesirable changes in the failure modes.

There have been relatively few papers published concerning CFRP and prestressed concrete. Klaiber et al. (1999) tested a P/C beam with 3 of the 12 strands cut to simulate impact damage. The beam was repaired using a corrosion inhibitor followed by a mortar patch. The beam was fitted with CFRP plates for flexural strengthening. A GFRP wrap was also put on at the end of the plates to prevent debonding and near the middle to prevent patch fallout and restrain peeling as a result of flexural cracks in the maximum moment region. Following an ultimate load test, it was concluded that the CFRP and GFRP contributed to a gain of 17% from the unstrengthened to the strengthened beam. They concluded that the repair was effective in restoring stiffness and providing strength increases in the damaged beams.

2.7.1. Shear Strengthening of Prestressed Concrete Girders

CFRP materials have been used in a number of cases to increase the shear strength of P/C girders. The majority of these projects have been completed in Canada. Drimoussis and Cheng (1994) strengthened full-scale “E” girders that had been removed from a bridge with CFRP sheets in the areas of high shear. An “E” girder is similar to a double tee in cross-section. A variety of different sheet orientations were investigated. One layer of CFRP oriented vertically increased the shear strength from 18-64%. All of the applied sheets experienced debonding type failures.

Hutchinson, et al. (1997) increased the shear capacity of scaled down I-shaped P/C girders with CFRP sheets. The test specimens were 1:3.5 scale models of Maryland bridge girders. CFRP sheets were applied to the webs in both the vertical and diagonal directions. Diagonal sheets were the most efficient in reducing the stress levels in the traditional stirrups.

Alexander and Cheng (1996) strengthened a number of P/C bridge girders for shear near Edmonton, Alberta. Two CFRP sheet layouts were used in this project. One layout had continuous sheets bonded in the transverse direction. In the other configuration, sheets were placed at regular intervals. Spaces between the CFRP sheets should allow moisture to escape from the concrete. The bridge will be monitored in the field for a period of four years. The

girders will then be removed from the bridge and tested in the laboratory to failure. When completed, these tests will help determine which sheet configuration is the most effective in strengthening P/C girders in shear when exposed to long-term environmental conditions.

2.8. CFRP Bridge Repairs

Taljsten and Carolin (1998) described the strengthening of a 3-span CIP concrete box girder railroad bridge in Sweden with CFRP sheets. The owners of the bridge wanted to increase the allowable axle load by 20% to accommodate larger trainloads. Minor concrete damage was also present due to a number of vehicle impacts.

The concrete surface was prepared by sandblasting and grinding. Almost 10,000 ft of unidirectional carbon fiber sheets were applied using a hand lay-up method in both the longitudinal and transverse directions. The fibers used had a modulus of elasticity of 34,000 ksi and a final thickness of 0.0315 in. It was not necessary to stop train traffic during the application of the CFRP sheets.

Bridge deflections and strains were recorded before and after the strengthening process. These tests indicate that transverse stiffness was increased by almost 16%. The strain levels of transverse steel reinforcing also decreased by 15%. No increase in stiffness was found in the longitudinal direction. The bridge cross-section was uncracked. It was suggested the contribution of the CFRP would have been substantially higher if the section was cracked. This bridge will be monitored over time to evaluate the long-term behavior of the CFRP sheets. Humidity levels in the concrete will also be recorded to determine the effect on the bond strength.

Shawhawy and Beitelman (1996) used CFRP to restore strength to impact damaged P/C girders (I-shaped) in Florida. The exterior and first interior girders both experienced significant section loss in the bottom flange and severe cracking in the web. Load tests conducted after the impact indicated that the strength of the two damaged girders had been reduced by approximately 20%. A repair strategy using CFRP was developed primarily because of the high replacement cost. The estimated cost to replace the two damaged girders was $300,000. Each damaged girder was strengthened with 2-layers of CFRP sheets in longitudinal direction to increase the flexural strength. Full depth transverse CFRP sheets were also used to increase the shear strength and seal the cracks. The cracks on the sides of

the beams were not injected with epoxy before the installation of the CFRP sheets. The CFRP material was protected with a layer of UV resistant primer and a layer of fire resistant material. Also, the exterior lane of the strengthened bridge was closed to traffic for 24 hours to allow the CFRP to cure. Load tests conducted after the bridge had been strengthened indicated that the original service condition of the girders was restored.

3. TESTING PROGRAM

3.1. Laboratory Testing Program

The testing program consisted of two parts, a laboratory part and a field part. The laboratory part entailed four prestressed concrete beams that were damaged in the lab and then repaired using CFRP. The beams were then statically load tested to failure, with one beam subjected to fatigue loading prior to the static failure tests. The description of the laboratory testing program is in part one of this chapter.

3.1.1. Beam description

The four prestressed beams used in the laboratory testing portion of this project were Iowa DOT LXA-38 beams. Humboldt Concrete Products of Humboldt, Iowa supplied the four beams. A cross section of the beam along with the orientation of prestressing strands is shown in Figure 3.1. Twelve of the fourteen prestressing strands were located in the bottom flange of the beam. Each beam was 39 ft – 6 in. long from end to end. The average midspan camber of the beams on arrival was measured to be 3/4 in. This is close to the theoretical value of 0.67 in. published by the Iowa DOT (Standard, 1990) for this beam type.

3.1.1.1. Cast-In-Place Composite Slab

It was necessary to cast a composite slab on the beams to develop the full tensile strength of the CFRP repair material and to simulate typical field conditions. The slab selected for this project was 4 ft wide and 8 in. deep (See Figure 3.2). These dimensions were chosen after reviewing plans from a variety of P/C bridges in Iowa. The maximum permissible spacing for LXA-38 beams is 7 ft – 6 in. for HS 20 loading. This spacing limit is applicable to girders with both steel and concrete diaphragms. However, the majority of P/C bridges in the state typically do not use this maximum allowed girder spacing. The effective slab width is a function of the effective beam span, the slab depth (slab stiffness), and the beam spacing. Using the AASHTO specifications (1998), the effective slab width of the test specimen was calculated to be 48 in. Therefore, the full slab width (48 in.) was considered effective and was used in computing section properties of the composite beam. This slab

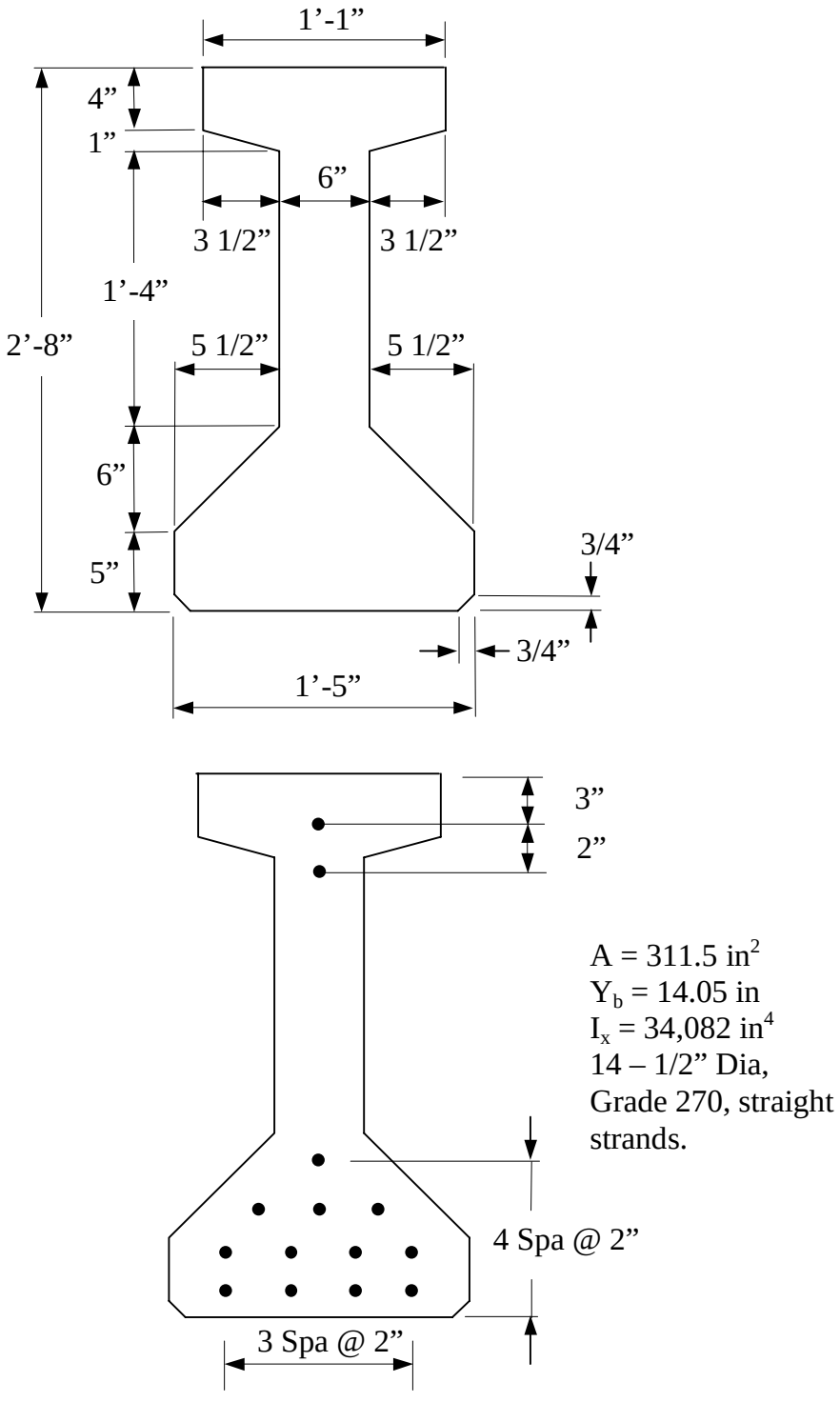

Figure 3.1. LXA-38 dimensions and properties.

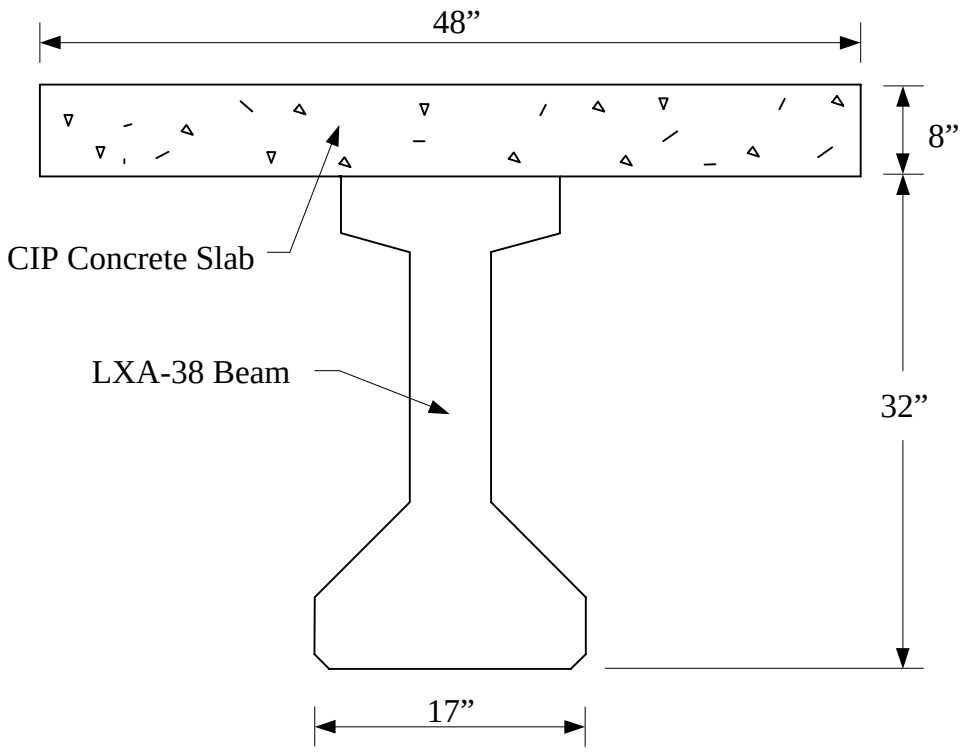

Figure 3.2. Dimension of CIP concrete slab.

width is slightly conservative when compared to the effective slab widths associated with girder spacings commonly used in the field. The measured deflections and strains values will also be slightly larger because of the smaller effective slab width (i.e. smaller moment of inertia). For example, the moment of inertia for a composite beam with a 7 ft – 6 in. wide slab is 22% larger than the same beam with a 4 ft wide slab. Limiting the width of the slab also significantly increased the stability of the test specimen in the laboratory. After adding the slab, the total depth of the composite section was increased from 32 in. to 40 in. Composite beam action was provided by a combination of steel stirrups that extended from the P/C beam and the intentionally roughened concrete on the top surface of the P/C beam. Formwork for the slab was completed with 2x4’s and 3/4 in. plywood. In traditional construction situations, steel beam hangers would be used to support the formwork. In this particular case, it was found to be more economical to use sets of 2x4 legs spaced on 32 in. centers. Transverse supports were spaced on 16 in. centers to ensure that the 3/4 in. plywood was not overstressed and to control deflections. A typical cross-section of the formwork is

shown in Figure 3.3; as shown in this figure, concrete screws were used to anchor the formwork against the beam. They were positioned so they would not interfere with instrumentation (i.e. strain gages). A photograph of the completed formwork for the CIP slab is shown in Figure 3.4.

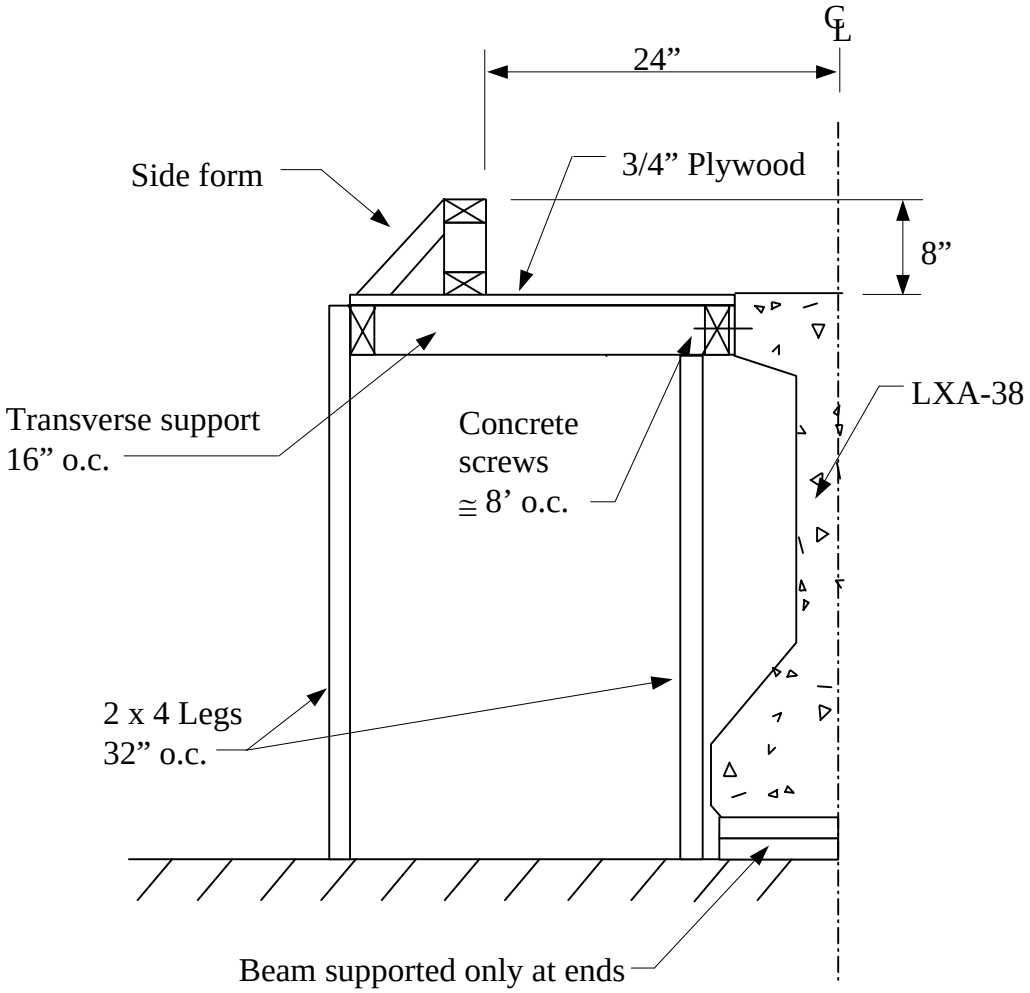

Figure 3.3. Slab formwork.

The same formwork was used to cast all four concrete slabs. To simplify analysis, the formwork was designed and constructed to follow the 3/4 in. camber in the beams. This was necessary to create a slab with a uniform thickness and therefore a beam with constant cross section. The composite slab was cast without a haunch. Also, all of the exposed wooden surfaces were coated with form oil before the reinforcing steel was placed.

All of the concrete slabs were reinforced with #4's spaced 12 in. O.C. in both the transverse and longitudinal directions. The reinforcement was Grade 40 deformed bars and was designed according to AASHTO LRFD Specifications (54). Temperature and shrinkage requirements were the controlling factor in the design of the slab reinforcement. The secondary purpose of the deformed bars was for the negative moment in the cantilever slab. All of the steel reinforcement was placed on 6 in. high steel chairs.

The concrete used in the slabs was a standard Iowa DOT mix (C4) with a design strength of 4,000 psi. The concrete compressive strength test results from the first three individual pours are shown in Table 3.1. Each value shown represents a three-cylinder average. Standard construction methods were used to place the concrete. An electric vibrator was used to ensure that the concrete was properly consolidated; the top surface of the slab was finished with steel trowels. The concrete was covered with plastic sheets to enhance the curing process; the formwork and plastic sheets were not removed until the slab had cured for at least three days.

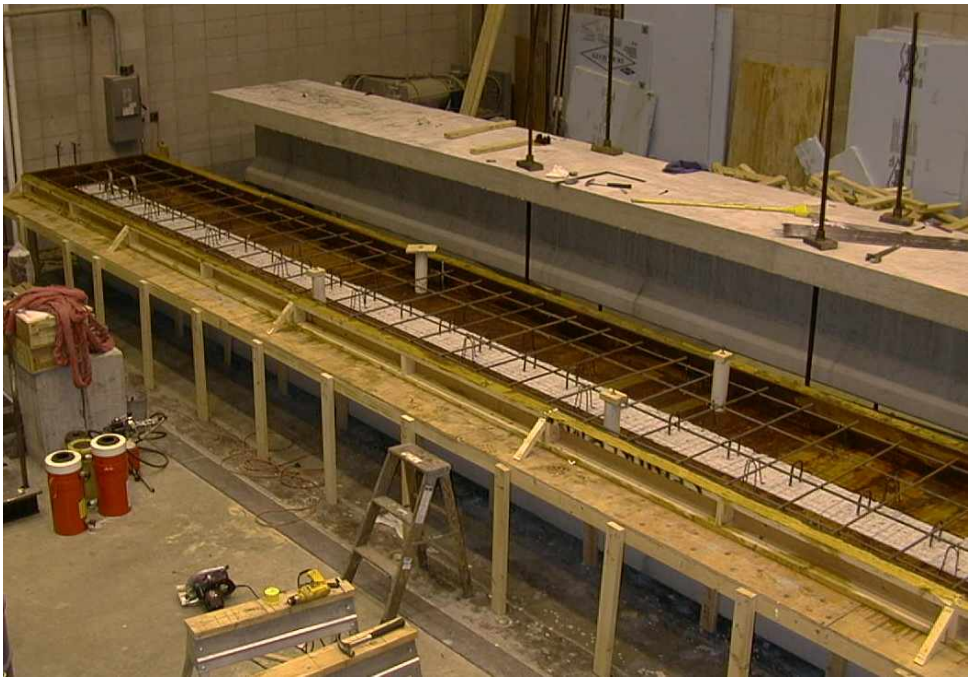

Figure 3.4. Completed formwork.

Table 3.1. Summary of concrete compressive strengths.

Concrete Pour Number	3 Day Strength (psi)	28 Day Strength (psi)
1	3,500	5,850
2	3,110	6,030
3	2,100	4,250

3.1.1.1.1 Slab Details

To simplify loading the specimens, it was necessary to create four holes in the concrete slab corresponding to the holes in the tie down floor. Another alternative was to cast the entire slab and then to core the holes in the slab in the appropriate locations. A problem with this method was containing the large amounts of cooling water in the laboratory. A simpler solution was to include the holes in the slab as it was being poured. This was done by using 4 in. diameter x 12 in. long PVC pipe sections; these were held in place, by 1/2 in. diameter threaded rods as shown in Figure 3.5. A "wooden cap" was used to apply pressure to the PVC to keep it in place and to keep the inside of the PVC pipe clear of concrete. The exteriors of the PVC pipe sections were also coated with form oil to simplify their removal. Finally, the threaded rod was tensioned to hold the PVC pipe sections securely in place. The pipe sections were removed after the concrete had been allowed to cure by twisting them out with a pipe wrench.

Figure 3.5. Completed PVC assembly.

3.1.2. Load Test Setup

All of the P/C beams were tested in four-point bending as shown in Figure 3.6. Each support consisted of 2-W21 x 83 sections welded together. The webs of the steel support sections also had bearing stiffeners to accommodate for the large concentrated reactions. Neoprene pads (12 in x 12 in. x 1 in.) were used between the steel supports and the P/C beams. This reaction was idealized in the analysis as a concentrated force acting through the center of the neoprene pads. Therefore, the effective span length was taken to be 38 ft - 4 in.

The live load was applied to the beams using a system consisting of two hydraulic loading cylinders and an electric pump. A cross-section of the loading setup is shown in Figure 3.7. Load cells positioned below the hydraulic cylinders were used to monitor the two applied loads. The hydraulic hoses were run in parallel so that the pressure in each cylinder would always be equal. Neoprene bearing pads (12 in. x 12 in. 1 in.) and steel plates (12 in. x 12 in. x 3 in.) were also used to evenly transfer the force from the hydraulic jacks to the composite beam.

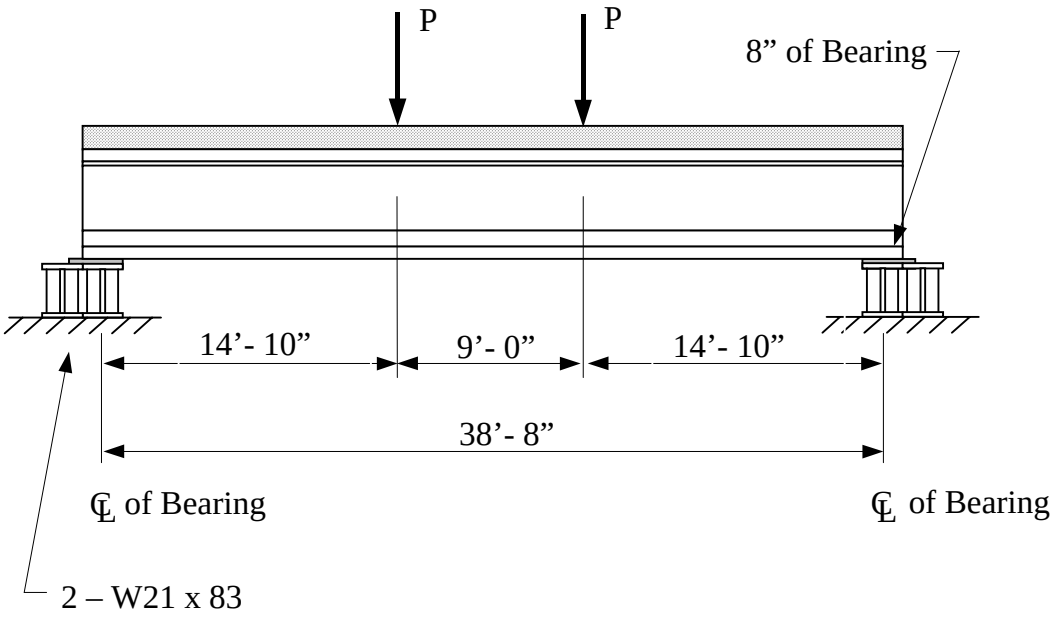

Figure 3.6. Prestressed beam test setup.

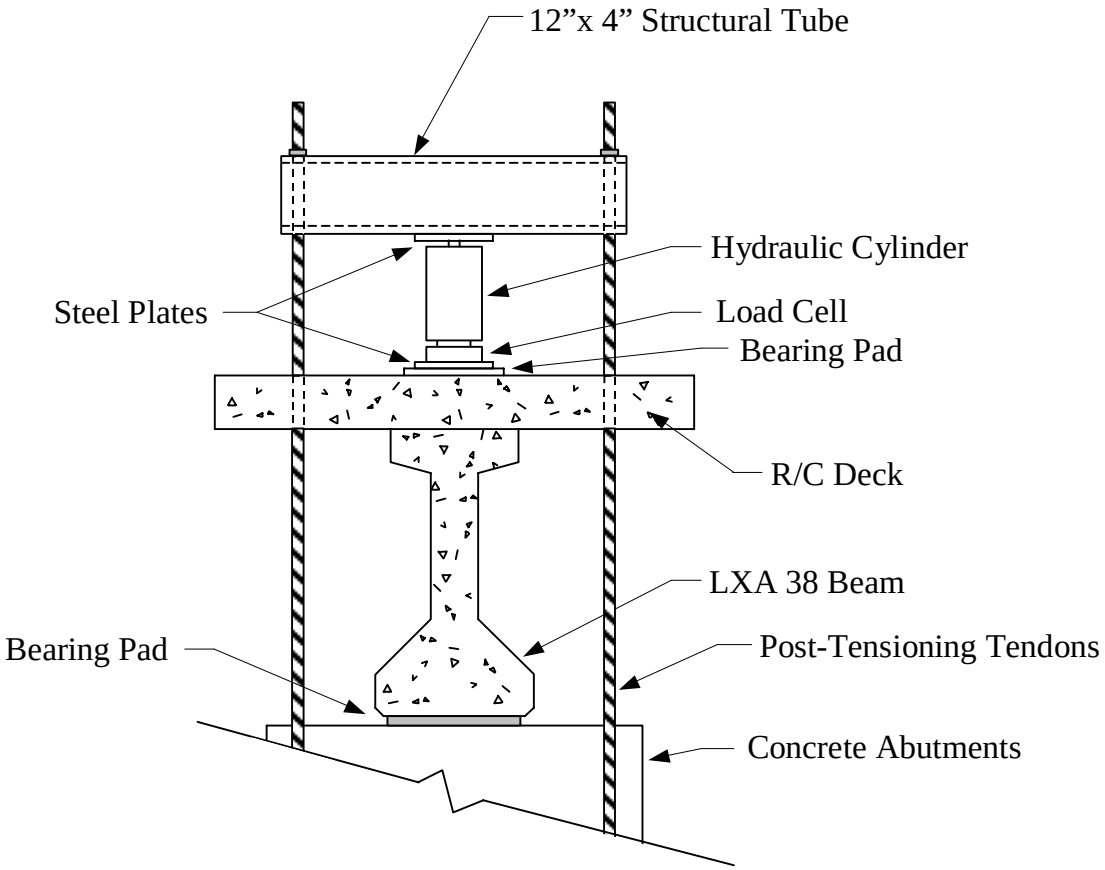

Figure 3.7. Cross-section of loading setup.

3.1.3. Instrumentation

Each beam was instrumented with electrical resistance strain gages (henceforth referred to as strain gages) and string potentiometer displacement transducers. Concrete strain gages were manufactured by Precision Measurement Co., Ann Arbor, Michigan. Steel strain gages used on the prestressing strands and on CFRP sheets were produced by Measurements Group, Inc., Micro-Measurements Division, Raleigh, North Carolina. All strain gages were temperature compensating and were applied using recommended preparation and adhesive materials. Celesco type string potentiometer displacement transducers were manufactured by Transducer Products, Inc., Canoga Park, California. A computer controlled data acquisition system (DAS) was used to measure and record all of the test data.

3.1.3.1. Concrete Gages

A total of eight concrete strain gages were used on each of the first three beam specimens. Only six were deemed needed on the fourth beam. Figure 3.8 indicates the location of concrete strain gages used for monitoring strains in the CIP slab. Three gages (D2, D3, D4) were located at midspan to measure the compressive strain in the constant moment region. Corresponding gages (GB1 and GB2) shown in Figure 3.9 were placed on both sides of the top flange of the P/C beam. A single concrete strain gage was located on the bottom of the beam at midspan. Only one gage was used on the bottom because concrete in that area was later removed. These gages were used to determine strain profiles in the undamaged midspan cross-section. Concrete strain gages were also placed on the slab to measure the compressive strains at the sections were the CFRP sheets were terminated (D1 and D5).

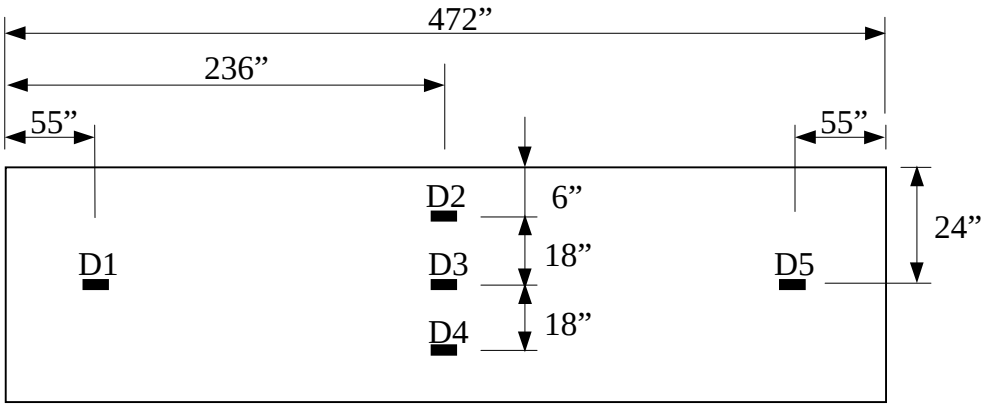

Figure 3.8. Plan view of concrete strain gage locations on top of slab.

3.1.3.2. CFRP Gages

Nine strain gages (labeled B1-B9 in Figures 3.9 and 3.10) were applied to the CFRP sheets on the bottom of each beam. These strain gages were located at the ends of the CFRP sheets, both quarter points, and at midspan. All of these gages were orientated to measure strains in the longitudinal direction. A number of additional strain gages were added to this basic configuration in later tests. For example, additional strain gages were included to

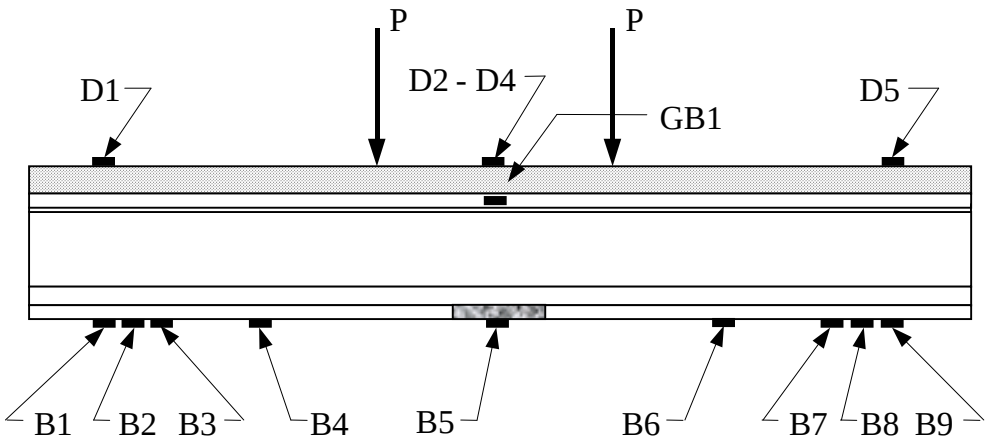

Figure 3.9. Basic strain gage orientation on repaired P/C beam.

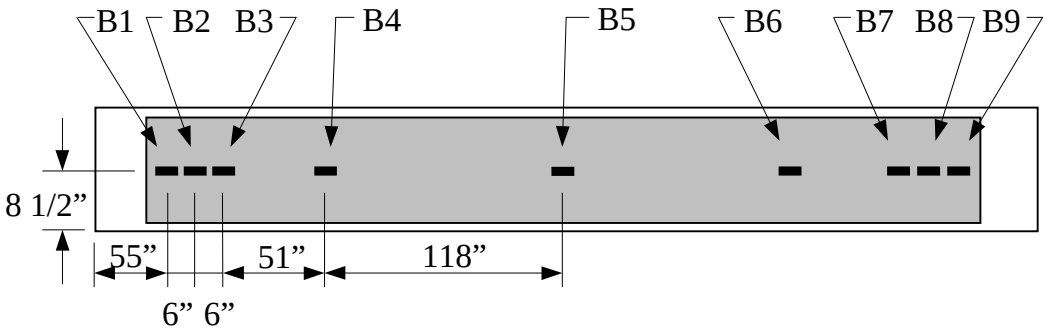

Figure 3.10. Plan view of strain gages on CFRP sheets on the bottom of P/C beam flange.

monitor transverse CFRP wraps. These differences will be discussed in detail in Chapter 4. The basic strain gage configuration is shown in Figures 3.8 through 3.10.

3.1.3.3. Steel Strain Gages

In addition to the concrete and CFRP strain gages, strain gages were also installed on the exposed prestressing strands after all of the concrete was removed. A total of eight gages (two per strand) shown in Figure 3.11 were used to monitor the strain levels in the bottom level of prestressing strands. The gages were positioned as closely as possible to one end of the exposed prestressing strands. This was necessary to minimize vibrations at the location of the strain gages when the strands were severed which could damage the soldered

connections on the strain gage. Also, the strain gages were oriented along the axis of the individual wires in the seven wire prestressing strand. Therefore, the strain gages were slightly skewed because of the twist in the wires. The two gages on each strand were located on different wires in the strand.

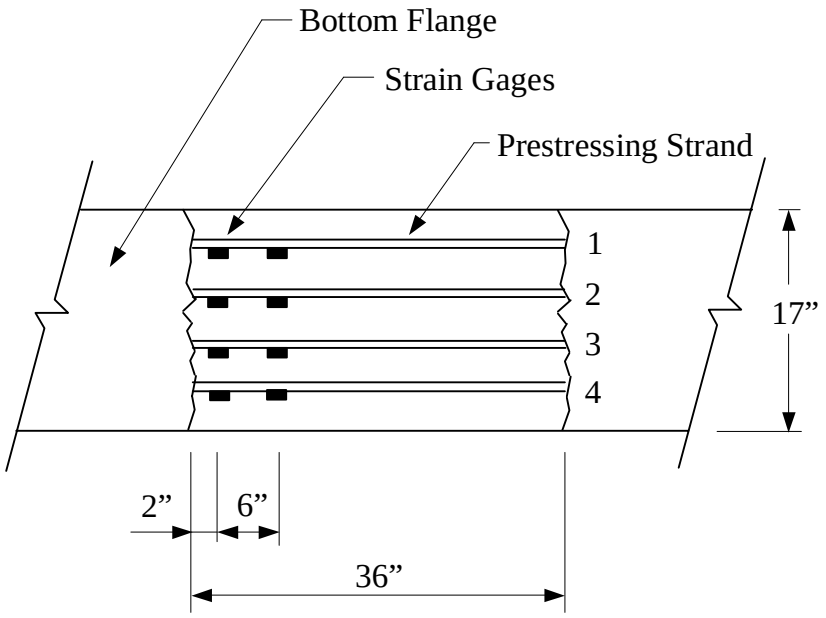

Figure 3.11. Plan view showing the location of the strand strain gages.

3.1.4. Vehicle Damage

It is difficult to simulate impact damage to a P/C beam in a laboratory environment. Vehicle impacts are highly variable; each impact produces different types of section loss and cracking patterns. For this project, vehicle impact damage was simulated by removing a portion of the concrete in the bottom flange and severing multiple prestressing strands. Load tests were completed as concrete and prestressing steel was removed to determine the relative changes in beam stiffness and stress ranges on the concrete, CFRP, and prestressing strands. Beam 3 was also laterally loaded through the bottom flange in an attempt to produce the diagonal cracks typically found in the webs of impact damaged girders in the field.

3.1.4.1. Concrete Removal

Concrete was removed from the bottom flange of the P/C beams using a handheld demolition hammer. The section of the bottom flange removed was 3 ft long and 4 in. deep across the entire width of the bottom flange. This was enough to expose two layers of prestressing strands (i.e. eight prestressing strands). Special care was taken to avoid damaging the exposed prestressing strands with the demolition hammer. To produce the maximum effect from the given loading, the damage was located at the beam centerline as shown in Figure 3.12. After the concrete was removed, a service load test with a maximum load P of 25 kips (i.e. 50 kips applied to the beam) was conducted to determine changes in the stiffness characteristics of the beam. The results of these tests are presented and discussed in Chapter 5. A photograph of the beam with 4 in. of concrete removed is shown in Figure 3.13. Two exposed stirrups are also clearly visible in this photograph.

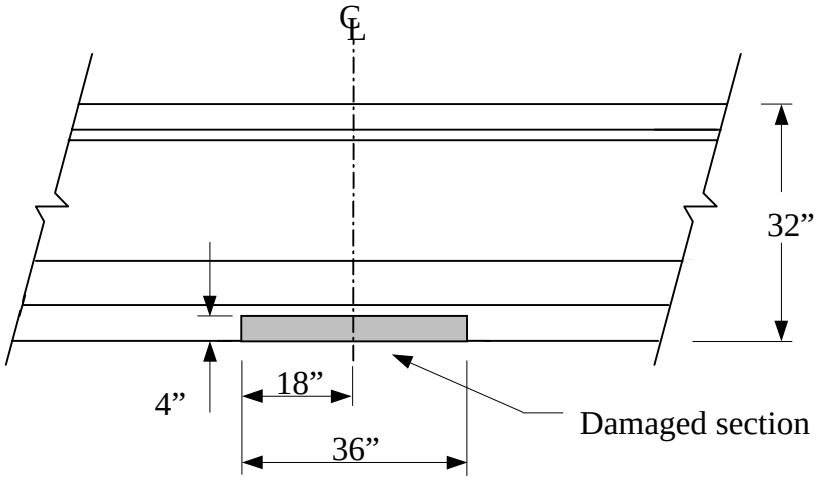

Figure 3.12. Location of beam damage.

Figure 3.13. Damaged beam with concrete removed.

3.1.4.2. Severing of Prestressing Strand

Once the concrete was removed, the first two prestressing strands (Strands 1 and 2 shown in Figure 3.11) on the bottom row were severed with a cutting torch. Strands were heated slowly to allow the wires to neck down under the prestressing force. Strand strain readings were taken during the cutting process to determine the effective prestressing force and to determine how the released forces were distributed to the remaining strands. Metal heat shields were used to insulate adjacent strands from the extreme heat. After each strand was severed, a service load test was completed to determine the change in beam stiffness and the changes in stress levels in the remaining strands and in the concrete. The strands were cut at the ends opposite the strain gages; they were also clamped to other strands to minimize vibrations.

3.1.5. Fatigue Conditions

The fourth beam tested was subjected to cyclic loading to simulate actual highway loading. The setup for the fatigue portion of the test is shown in Figure 3.14. The lab setup required to accommodate the beam consisted of a large preexisting steel frame anchored to the lab floor. The frame consisted of two W-shaped steel beams about 25 feet long that ran

parallel to each other seven feet apart. Other W-shaped beams provided bracing. The lab was not big enough to allow the P/C beam to be placed parallel or perpendicular to the frame. The only way the beam would fit was to skew it diagonally to the frame. This allowed for just enough room to walk around one end of the beam in order to maintain the functional capacity of the lab, although one end of the beam was supported on the tie down floor and the other on the on grade slab.

Since the P/C beam had to be skewed, the actuators had to be skewed as well. Two hydraulic actuators were used to load the P/C beam. The actuators each had a 55 kip capacity and were attached to the frame using several large C-clamps. They were also braced in several directions, and welded to the frame to prevent them from moving from side to side. Small movements of the actuators did not appear to have a significant effect on the fatigue loading.

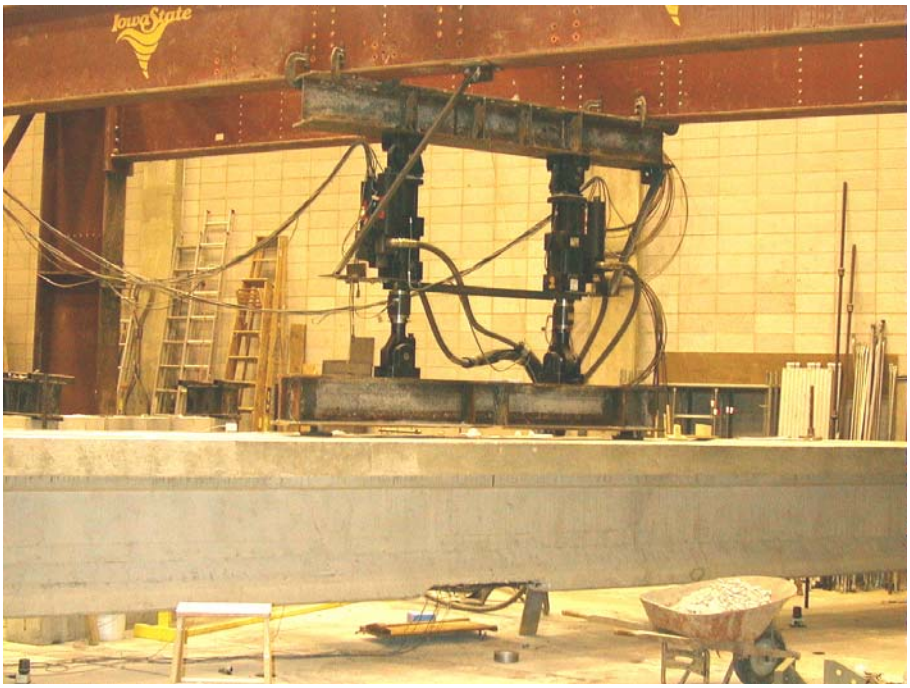

Figure 3.14. Fatigue loading setup.

A cross-sectional view of the fatigue test is provided in Figure 3.15. A 10 ft steel spreader beam was used because the actuators were only 4 feet apart. It was not attached to

the actuators to prevent any potential binding. The spreader beam was supported by the pin and roller on top of the beam. The weight of the actuators kept the spreader from moving. During the fatigue testing, a minimum load of 2 kips was applied at all times to prevent any bouncing or movement of the spreader beam.

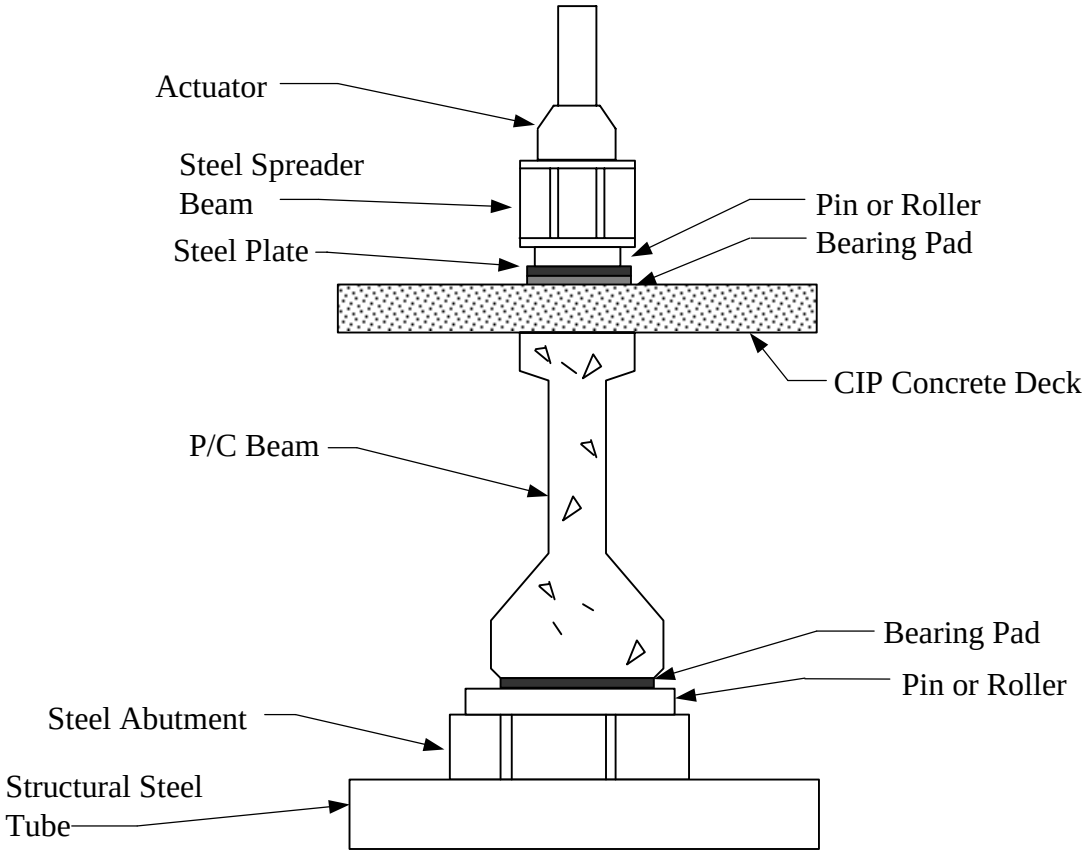

Figure 3.15. Cross-section of fatigue loading setup.

3.1.5.1. Loading and Degradation

The P/C beam was loaded with a load range from 2 to 29 kips per actuator. The maximum moment induced was approximately 35% of the total moment capacity of the beam. The rate of loading was 0.70 cycles per second. The loading was applied for 2.5 million cycles. Service load tests were run frequently, about 20 times throughout the cycling to identify any change in stiffness or strength. The CFRP was also visually inspected throughout the cycling to observe potential debonding. Table 3.2. lists the number of cycles carried out prior to each service test. Each degradation test involved setting the actuators so

there were 2 kips total on the beam, then increasing the load to 58 kips while taking readings at 2 kip intervals.

Table 3.2. Number of cycles at each degradation test.

Number of Test	Number of Cycles	Number of Test	Number of Cycles
1	0	11	899,430
2	64,960	12	958,140
3	115,500	13	1,092,200
4	176,180	14	1,189,610
5	288,060	15	1,361,150
6	330,170	16	1,526,420
7	384,740	17	1,641,800
8	441,240	18	1,769,340
9	694,600	19	2,049,910
10	786,780	Ultimate	2,528,930

Other service load tests were also performed throughout the damage and repair process. A service test was performed after each of the following events: before any damage was done, after the concrete was removed, after the strands were cut, and after the longitudinal and transverse CFRP was applied. These tests were run from 0 to 25 total kips.

3.2. Bridge Testing Program

The field portion of the program involved three bridges around the state of Iowa that had been damaged by overheight vehicles. The bridges were near Altoona, Osceola, and De Soto, Iowa. Each bridge was repaired using CFRP. Table 3.3 lists the bridge numbers and their location.

Table 3.3. Bridge locations and maintenance numbers.

	Approximate bridge location	Bridge number
Bridge 1	Altoona, Iowa	7783.IL065
Bridge 2	Osceola, Iowa	2015.2L034
Bridge 3	De Soto, Iowa	2510.I.080

3.2.1. Altoona Bridge

Bridge 1 had six girders that all carried 4 spans. The 4 spans included a 36’ approach span on the north side, a 46’ exit span on the south side, and two 96.5’ main spans that carry traffic south along IA Highway 65 over IA Highway 6, which runs almost perpendicular. The bridge consists of two travel lanes, a large shoulder lane on the outside, and a smaller shoulder on the inside of the roadway. An overall view of the bridge is shown in Figure 3.16, a schematic view is shown in Figure 3.17, and a cross section is shown in Figure 3.18.

Figure 3.16. Overall view of Altoona Bridge looking east.

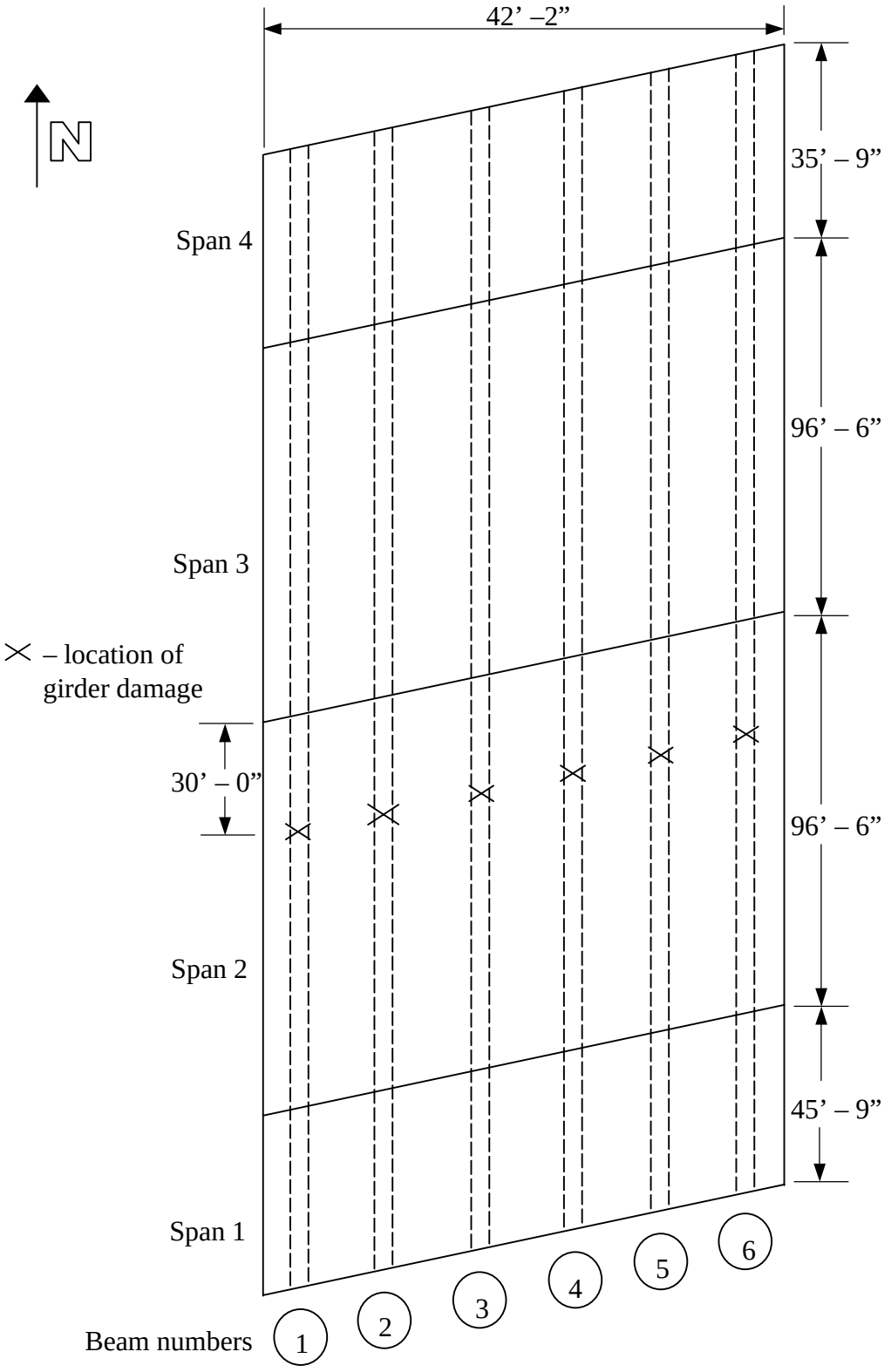

Figure 3.17. Dimensions of Altoona Bridge.

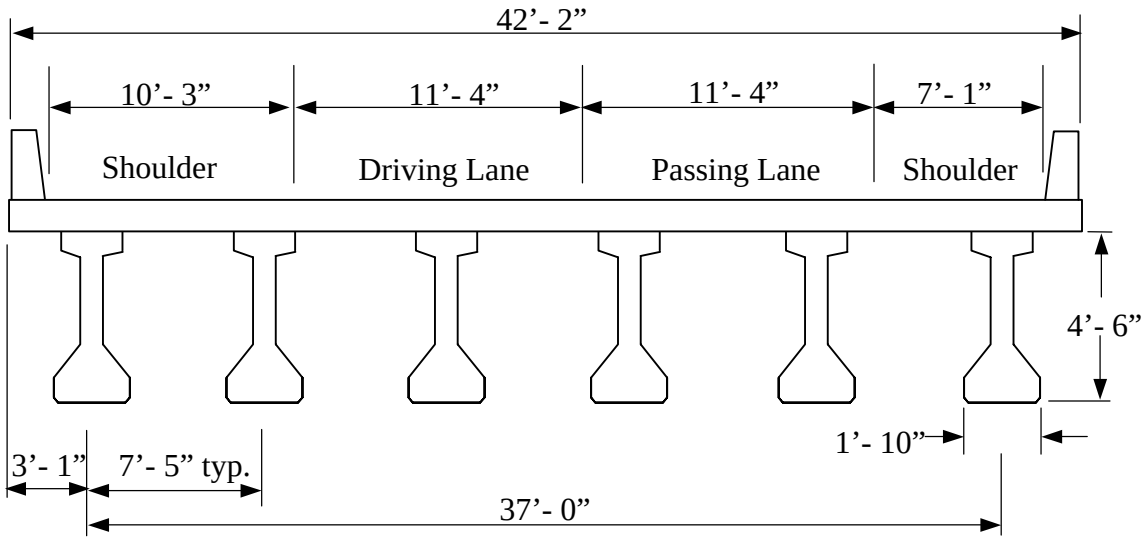

Figure 3.18. Cross section of Altoona Bridge.

3.2.1.1. Description of Damage

An overheight semi-tractor trailer being driven on Highway 6 from west to east impacted the west most girder of the bridge, damaging it slightly. This initial impact caused the truck’s load to retract and then rebound back into the second girder. This impact caused greater damage, to the extent of two strands being severed and some concrete loss. The truck continued traveling under the bridge while the load scraped and superficially damaged the concrete of the remaining 4 girders. A more extensive damage report is located in Appendix B. Beam damage can be seen in the photographs of Figures 3.19 through 3.21.

3.2.1.2. Load Test Set up

The load test took two days to complete. The first day consisted of instrumenting the bridge with strain gages. Displacement transducers were installed at midspan of span 2 on the second day, prior to the load testing. The strain gages were then left in place while the bridge was repaired, but the displacement transducers were removed. Following the repair of the bridge, new strain gages were installed where they had been torn down and the test was repeated.

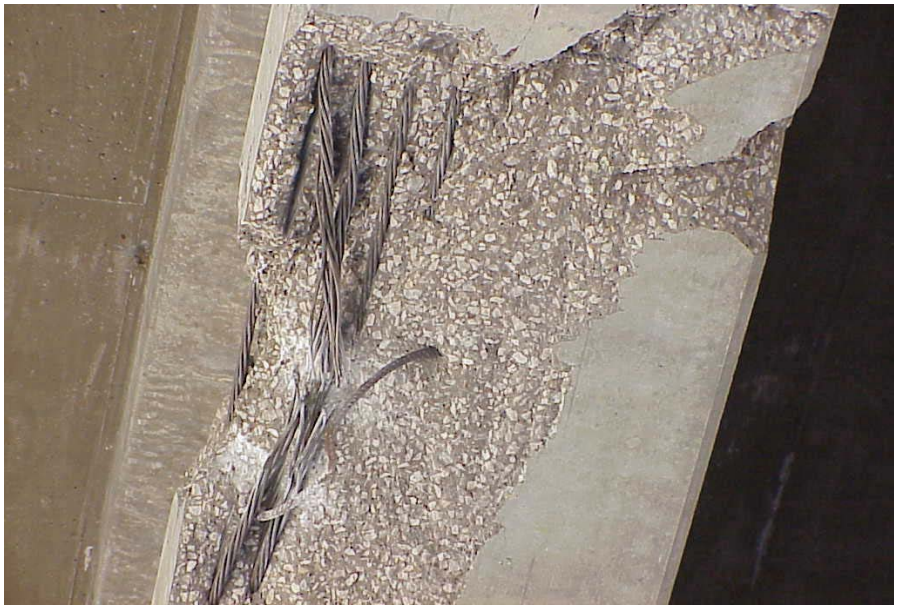

Figure 3.19. Photograph of the damage to Beam 2 in the Altoona Bridge.

Figure 3.20. Photograph of the damage to Beam 1 in the Altoona Bridge.

Figure 3.21. Photograph of the damage to Beam 5 in the Altoona Bridge.

3.2.1.2.1 Instrumentation

Concrete strain gages were placed in several different positions on each of the 6 girders. The gages were glued according to the methods described in the gage manual. The gages were covered with enamel, thin rubber strips, and aluminum tape (see Figure 3.22) to protect them from the elements, as they would remain on the bridge for several months.

Figure 3.22. Photograph of weather protecting tape over a strain gage on the Altoona Bridge.

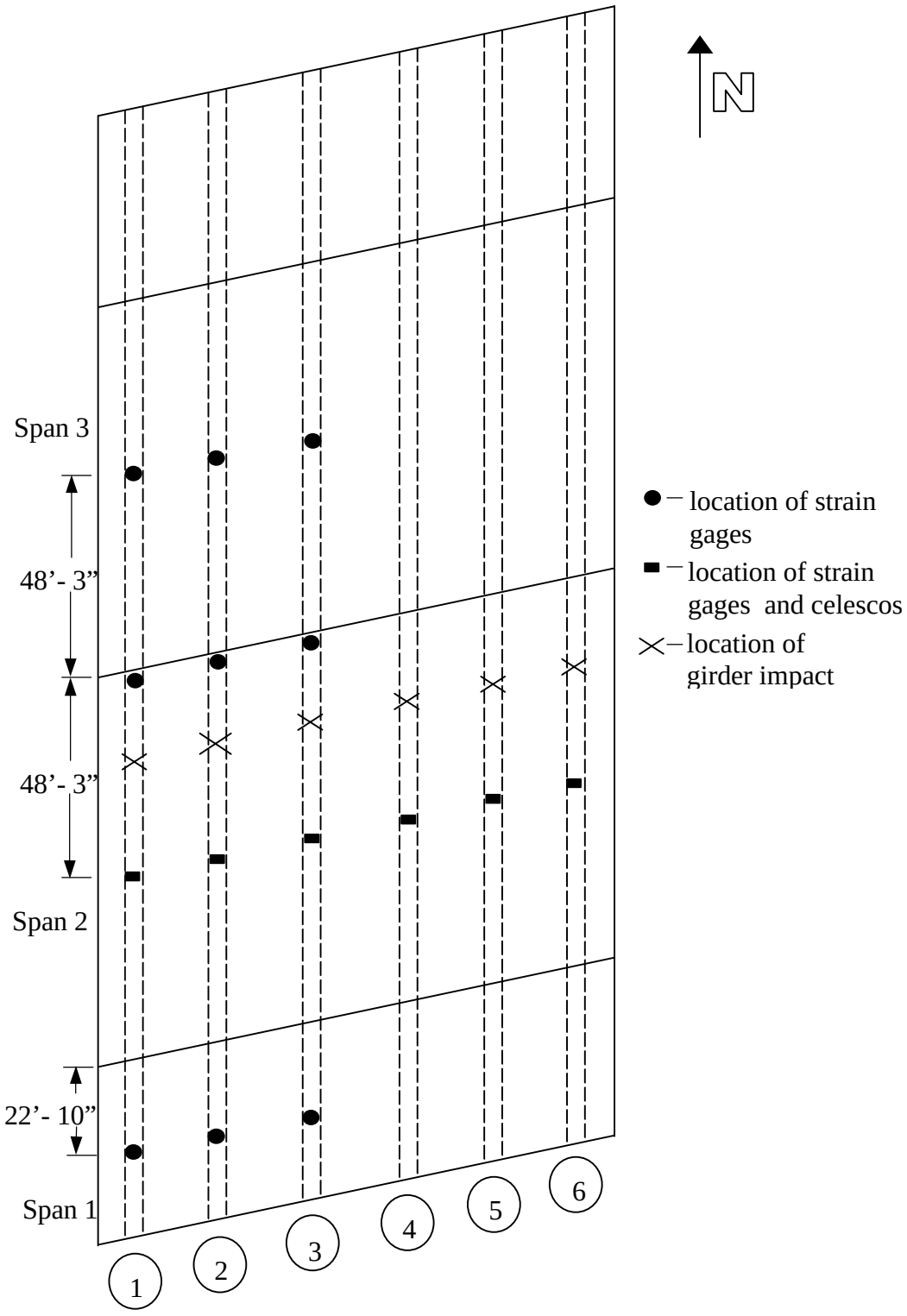

Figure 3.23. Location of strain gages and deflection transducers on the Altoona Bridge.

The strain gage and deflection schematic is shown in Figure 3.23. Six strain gages where placed on girders 1, 2, and 3. These were the girders that surrounded the most heavily damaged area, Girder 2. The eastern three girders, girders, 4, 5, and 6, each had two gages.

For girders 1, 2, and 3, one gage was placed on the side of the bottom flange at mid-span of span 1, the south span. Two gages were placed at mid-span of span 2, with one gage placed on the side of the top flange, and one on the side of the bottom flange. Two more gages were placed near the north pier of span 2 in the same configuration that was just mentioned. This was done so the damaged area would have gages on either side of it. Finally, 1 more gage was placed on the side of the bottom flange at mid-span of span 3.

Girders 4, 5, and 6, had two gages each. The gages were on the side of the top flange and the side of the bottom flange. They were set at mid-span of span 2. These gages made it possible to find the centroids of girders 4, 5, and 6. Deflections were measured on all of the beams at the mid-span of span 2 with celesco type string potentiometer transducers.

3.2.1.2.2. Load Trucks

The trucks used for the static and dynamic load tests were Standard DOT 3-axle dump trucks filled with sand. The weights and dimensions for each of the four trucks can be found in Table 3.4, with the accompanying figure (Figure 3.24). Dimensions are listed to the nearest one tenth of a foot. Trucks 1 and 2 were used for loading during the original test while trucks 3 and 4 refer to the trucks from the second test. The center of gravity of the trucks was taken to be at the center of the rear tandem axle.

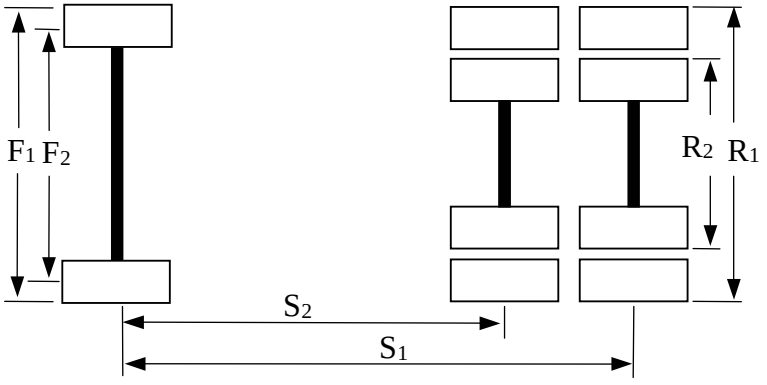

Figure 3.24. Dimensions of the trucks used in the Altoona Bridge Test. (see Table 3.4)

Table 3.4. Weights and dimensions of trucks.

Truck	Truck Number	Weight (lbs.)	F_1 (ft)	F_2 (ft)	R_1 (ft)	R_2 (ft)	S_1 (ft)	S_2 (ft)
1	A29244	53,800	8.0	7.0	8.0	6.0	18.5	14.5
2	A29532	48,400	8.0	7.0	8.0	6.0	18.5	14.5
3	A29244	46,180	8.0	7.0	8.0	6.0	18.5	14.5
4	A25857	47,220	8.0	7.0	8.0	6.0	19.0	15.0

3.2.1.3. Static and Dynamic Test Procedures

Two tests were conducted on this bridge; before and after repair. Both a static test and a dynamic test were conducted. The dynamic test was performed to provide a better indication of the bridge continuity.

3.2.1.3.1 Static Test Procedure

A static load test was conducted using various load cases. The purpose was to get reliable transverse strain and deflection data. The static load tests were performed in the midst of moving traffic. One or two lanes (including the shoulder as a lane) were blocked off at a time, while an open lane allowed traffic to continue to flow over the bridge. Although traffic continued to flow, all test readings were taken when the bridge was free of traffic.

The strain gages were zeroed when there was no traffic or trucks on the bridge or the approach spans. The trucks were positioned in the marked positions corresponding to the 32 different load cases. Strain and deflection data was taken for a series of approximately five of the load cases in series, and then the gages were zeroed again. All of the measurements were taken when there was no traffic on or near the bridge. The procedure was repeated until data had been collected for all load cases. The procedure for the static tests remained consistent from the damaged bridge test to the repaired bridge test.

3.2.1.3.2 Load Cases

There were 32 different load cases used for the static portion of the test (see Table 3.4 and Figure 3.24) involving one or two trucks. The positions were chosen to produce positive and negative moment data. The land column refers to the shoulder as Lane 1, the driving lane as Lane 2, and the passing lane as Lane 3. The location column refers to the location on

the specified span, ½, ¼, or ¾ of the way across from north to south. For the cases that involved two trucks, trucks were either placed side-by-side in adjacent lanes, front to back in the same lane, or in the same lane at different points of the spans (i.e. positions 1 & 3, 2 & 3, etc.). Photos of the trucks in side-by-side and front to back positions are shown in Figure 3.26 and 3.27. The load cases are listed in Table 3.5. The lanes and dimensions of the cross-section are shown in Figure 3.25.

Table 3.5. Listing of load cases for Altoona Bridge tests.

Load Case	Lane(s)	Truck(s)	Span(s)	Location
1	1	1	1	1/2
2	1	1	2	1/4
3	1	1	2	1/2
4	1	1	2	3/4
5	1	1	3	1/2
6	2	1	1	1/2
7	2	1	2	1/4
8	2	1	2	1/2
9	2	1	2	3/4
10	2	1	3	1/2
11	1 & 2	1 & 2	1	1/2
12	1 & 2	1 & 2	2	1/4
13	1 & 2	1 & 2	2	1/2
14	1 & 2	1 & 2	2	3/4
15	1 & 2	1 & 2	3	1/2
16	1	1 & 2	1 & 2	1/2
17	1	1 & 2	1 & 3	1/2
18	1	1 & 2	2 & 3	1/2
19	1	1 & 2	2 & 2	1/2
20	2	1 & 2	1 & 2	1/2
21	2	1 & 2	1 & 3	1/2
22	2	1 & 2	2 & 3	1/2
23	2	1 & 2	2 & 2	1/2
24	3	1	1	1/2
25	3	1	2	1/4
26	3	1	2	1/2
27	3	1	2	3/4
28	3	1	3	1/2
29	3	1 & 2	1 & 2	1/2
30	3	1 & 2	1 & 3	1/2
31	3	1 & 2	2 & 3	1/2
32	3	1 & 2	2 & 2	1/2

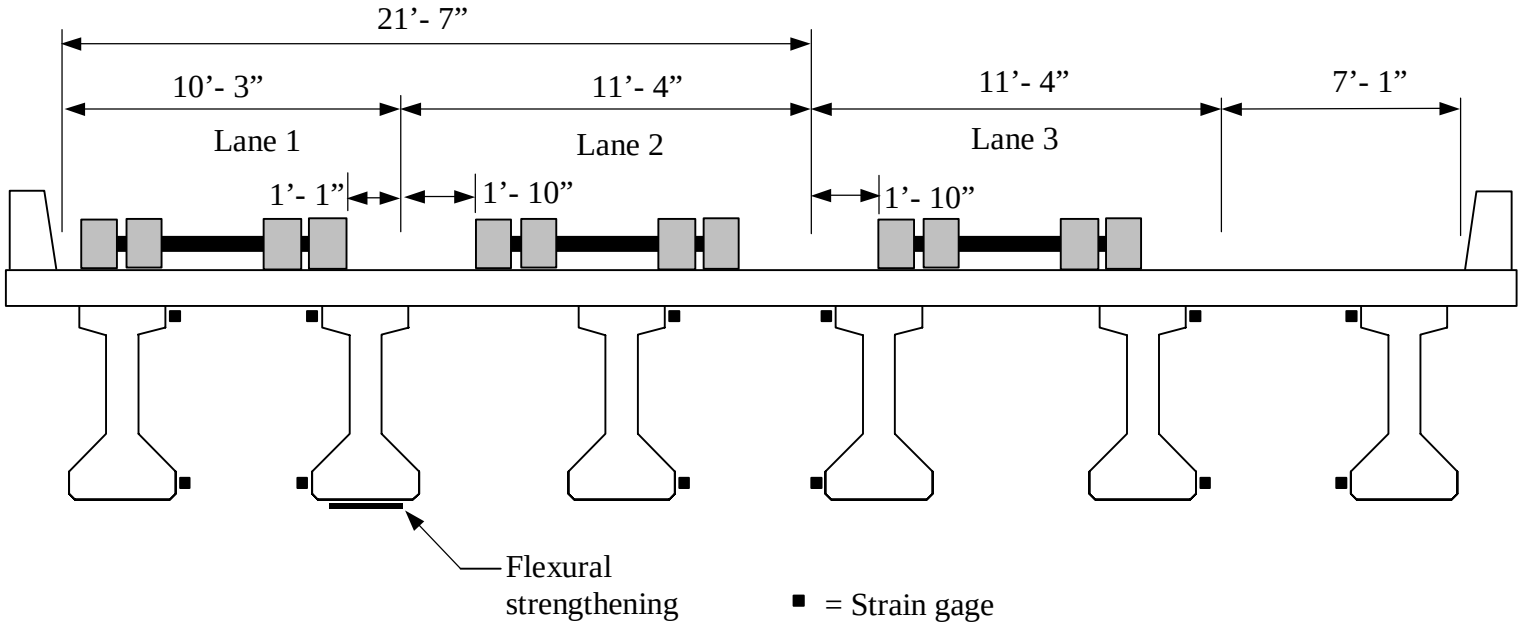

Figure 3.25. Truck lanes used in the Altoona Bridge Test.

Figure 3.26. Photograph of trucks in Lane 1 and 2 in the Altoona Bridge test.

Figure 3.27. Photograph of trucks in Lane 3 in the Altoona Bridge test.

3.2.1.3.3 Dynamic Procedure

The same strain gage and deflection schematic from the static procedure was used for the dynamic procedure. Several trials were measured at different speeds, with one truck traversing the bridge at a time. The different speeds included several crawl runs

(approximately 3-8 mph) and some faster runs (approximately 30-35 mph). Several ambient vehicles traveling highway speeds (65-70 mph) were also measured. The dynamic tests helped to check the continuity of the gages as loads crossed the bridge, as well as confirming the data from the static tests.

3.2.2. Osceola Bridge

The second bridge tested, Bridge 2, has eight prestressed concrete beams and carries traffic west on Highway 34 over Interstate 35 north and southbound near Osceola, Iowa. The bridge is a two-lane bridge, both westbound, and includes two main spans and two approach spans (see photo in Figure 3.28). The approach span from the east is 48'- 7" long. The next span, which carries traffic over northbound I-35, is 64'- 7" long and is the span that sustained the impact damage. The span that carries traffic over southbound I-35 is 56'- 3" long, and the exit span is 48'- 7" long. A schematic of the bridge can be seen in Figure 3.29, and a cross section of the bridge is shown in Figure 3.30.

Figure 3.28. Overall view of the Osceola Bridge.

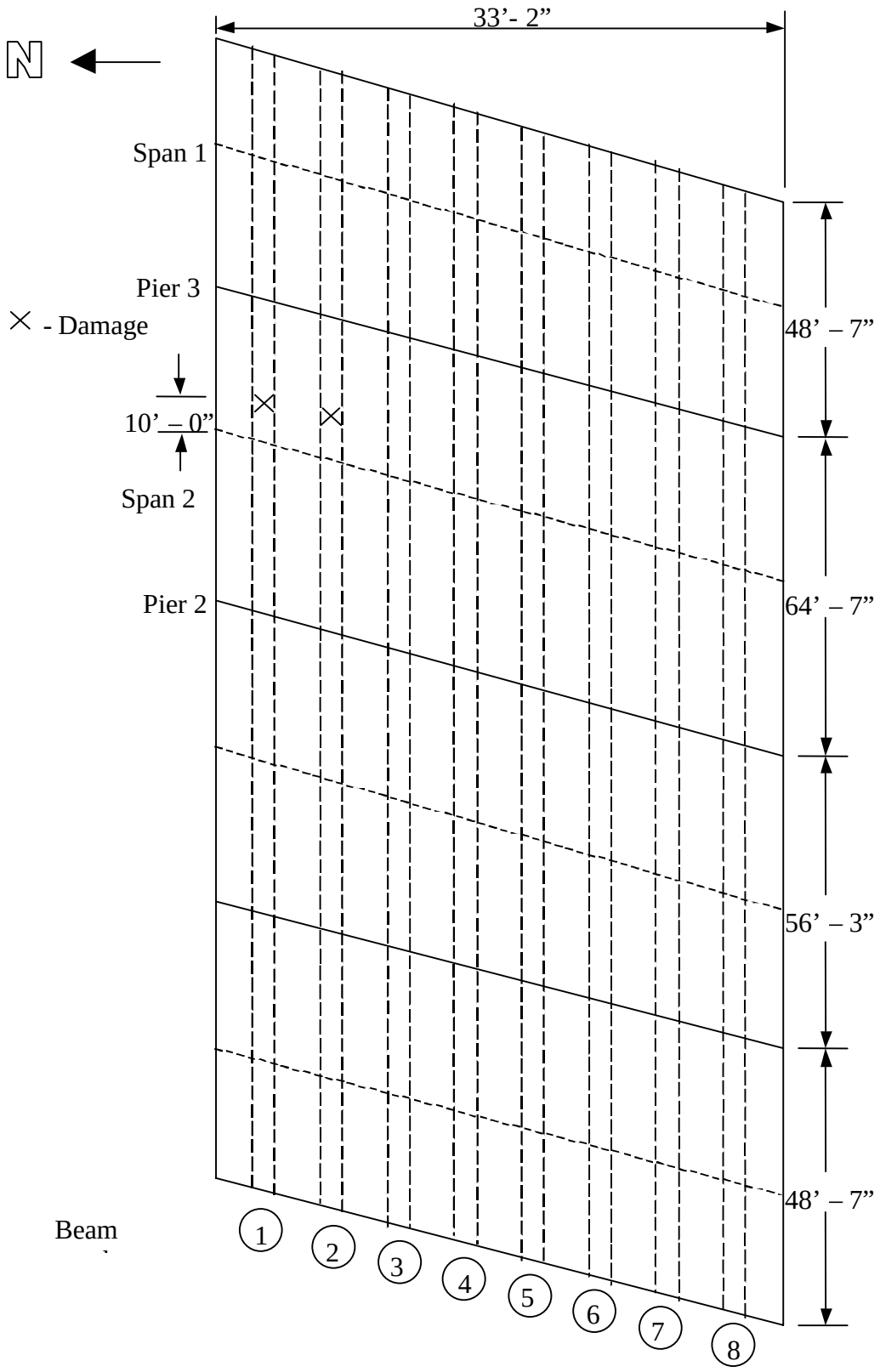

Figure 3.29. Dimensions of the Osceola Bridge.

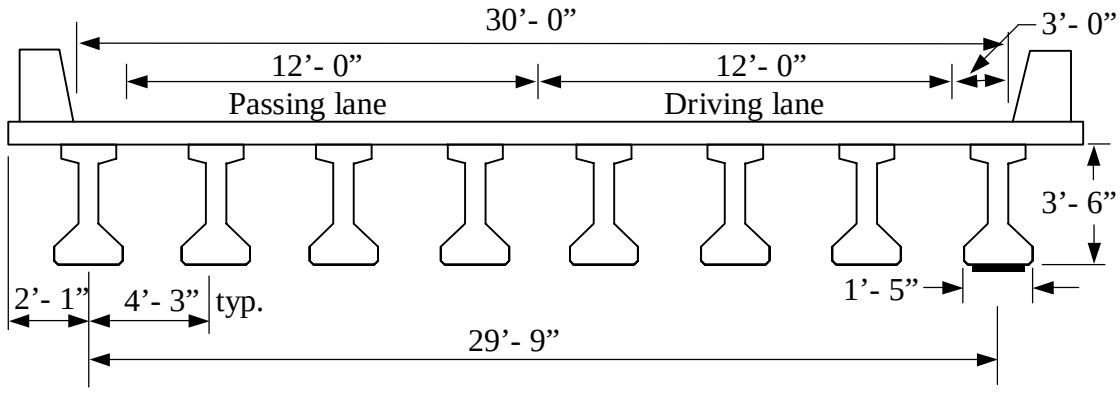

Figure 3.30. Cross section of the Osceola Bridge.

3.2.2.1. Description of Damage

The bridge incurred some damage due to an overheight piece of machinery being transported on a semi-tractor trailer. The vehicle was traveling northbound on I-35. The equipment cleared the southernmost six beams, but due to the grade of the highway, the two beams on the north side were struck. Beam 2 sustained some concrete spalling but no steel damage. Beam 1 incurred the most damage with significant concrete spalling as well as one prestressed steel tendon being severed. The diaphragm between the Beam 1 and Beam 2 near the impacted area also lost some concrete. A bridge schematic and two of the damaged areas are shown in Figures 3.30, 3.31, and 3.32. Appendix B offers a more complete damage report.

3.2.2.2 Instrumentation

Instead of using regular resistance type strain gages, a newer testing system was used. The new system called BDI-STS, Structural Testing System by Bridge Diagnostics, Inc., was used for this test. This system consists of up to 64 strain transducers that are applied to a bridge or other structure in a fraction of the time needed to apply standard foil strain gages. The strain transducers are place in position, and then they are fastened using a quick drying adhesive. All of the gages are then connected to the main data collection system. This system then produces the strain results by measuring the tiny displacements as a general resistance gauge would. A typical BDI gage on the bottom flange of a girder is shown in Figure 3.33.

Figure 3.31. Photograph of the damage to Beam 1 in the Osceola bridge.

Figure 3.32. Photograph of the damage to the diaphragm in the Osceola bridge.

Figure 3.33. Close-up of BDI gage on the Osceola bridge.

Sixteen BDI gages were used in the instrumentation. One gage was placed on the side of the top flange, and one on the bottom of the bottom flange for each of the eight beams. The gages were all placed 3 feet west of the existing bridge diaphragm. This allowed for the easiest gage placement while traffic was flowing under the bridge. The damaged area was located about 3 feet east of the diaphragm, in the center of the driving lane for I-35. Figure 3.29 shows the instrumentation cross-section for the testing.

3.2.2.3. Trucks

One standard DOT 3-axle dump truck filled with sand was used for this test. The center of gravity was assumed to be in the center of the two rear axles. The front axle weighted 13,120 lbs., the rear axles weighed a combined 34,340 lbs., for a total weight of 47,460 lbs. Figure 3.34 shows the layout and dimensions of the truck.

3.2.2.4. Procedure

A total of ten rolling tests were done for the testing of this bridge. The rolling tests consisted of a single truck driving about 5 to 8 mph. along a predetermined straight line. There were five different positions across the transverse direction, with two trials run for each position. These positions will be called 1-5 during the discussion, starting from the

north. A cross section of the bridge including the truck lanes is shown in Figure 3.35, and a gage schematic is shown in Figure 3.36.

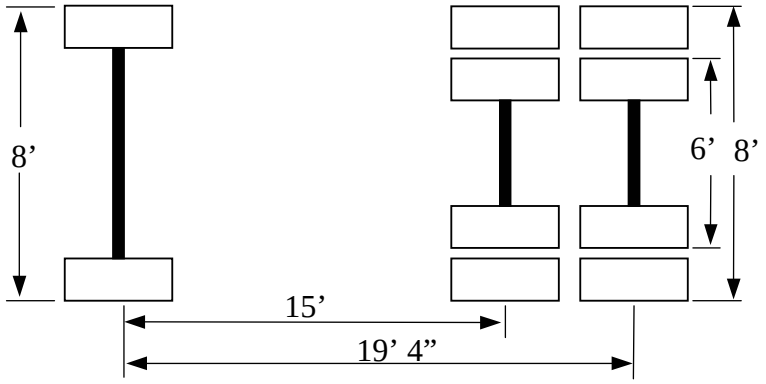

Figure 3.34. Dimensions of truck used in test.

Before the test, the truck was fixed with the BDI auto-clicker that attached near the front left wheel. This device detects a reflective surface that marks every wheel revolution. Before every test, vice-grip pliers with a reflective surface connected would be attached to the front left wheel. The auto-clicker would then click every time the reflective surface would pass it. This allowed for easy determination of spacings and distances when looking at the final data plots.

For each test, the truck was rolled into place right up to the edge of the first approach span. The reflective pliers were attached to the top of the wheel and the truck was backed up one complete wheel revolution, which was 10.8 ft. When the truck started moving, the data acquisition device was activated.

Traffic was stopped before the bridge while the rolling tests were done. One person walked in front of the truck to ensure that it kept rolling in a straight line along the pre-measured lanes, while another person walked alongside the truck to watch the auto-clicker and prevent any malfunctions. The rolling speed of the truck was approximately 8-10 mph. When the truck had exited the bridge, the gages were reset and traffic was allowed to go over the bridge again. Two identical trials were run back to back in each position before the truck was moved to a new lane. After all ten trials were completed, the gages were removed and the bridge was ready to be repaired.

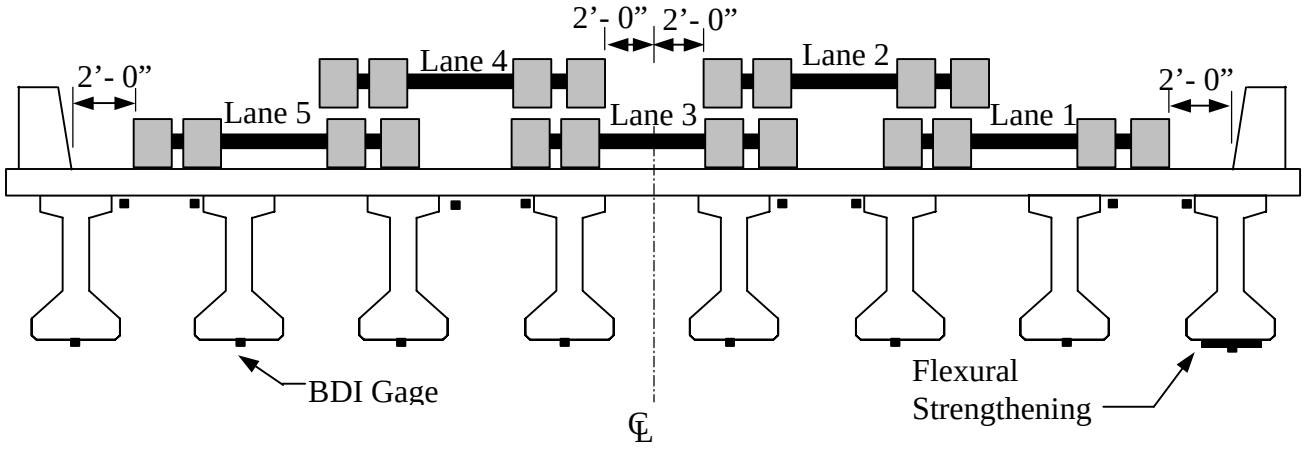

Figure 3.35. Truck lanes and gage positions used in Osceola Bridge test.

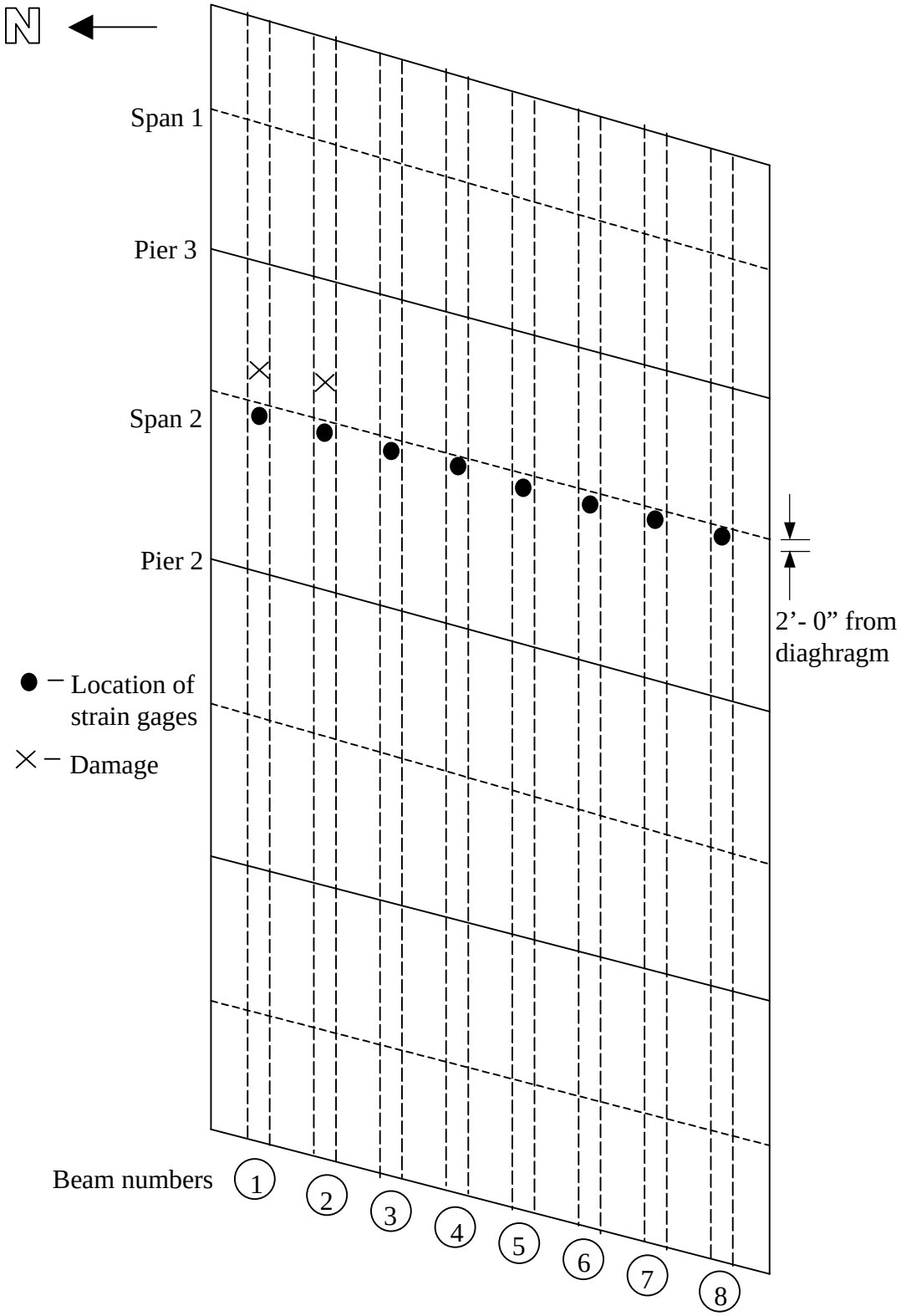

Figure 3.36. Gage schematic of Osceola Bridge.

3.2.3. De Soto Bridge

Bridge 3 has nine prestressed concrete beams and carries traffic west on Interstate 80 over Highway 169 north and southbound near De Soto, Iowa. The bridge is a two-lane bridge, and includes two main spans and two approach spans. The first approach span is 34'- 9". Both main spans are 68'- 9", and the exit span is 39'- 0". The bridge accommodates two 12'- 0" travel lanes as well as a wide shoulder on the driving lane side. An overall view of the bridge is shown in Figure 3.37, a schematic view is shown in Figure 3.38, and a cross section is shown in Figure 3.39.

Figure 3.37. Overall view of De Soto Bridge looking southeast.

3.2.3.1. Description of Damage

The bridge incurred some damage due to an overheight vehicle traveling south on Highway 169. The vehicle missed the seven northernmost beams and struck the final two, Beams 8 and 9. Beam 1 sustained significant concrete loss and also lost a prestressing tendon. Two of the damaged areas are shown in Figure 3.40 and 3.41. Appendix B contains a more thorough report of the damage.

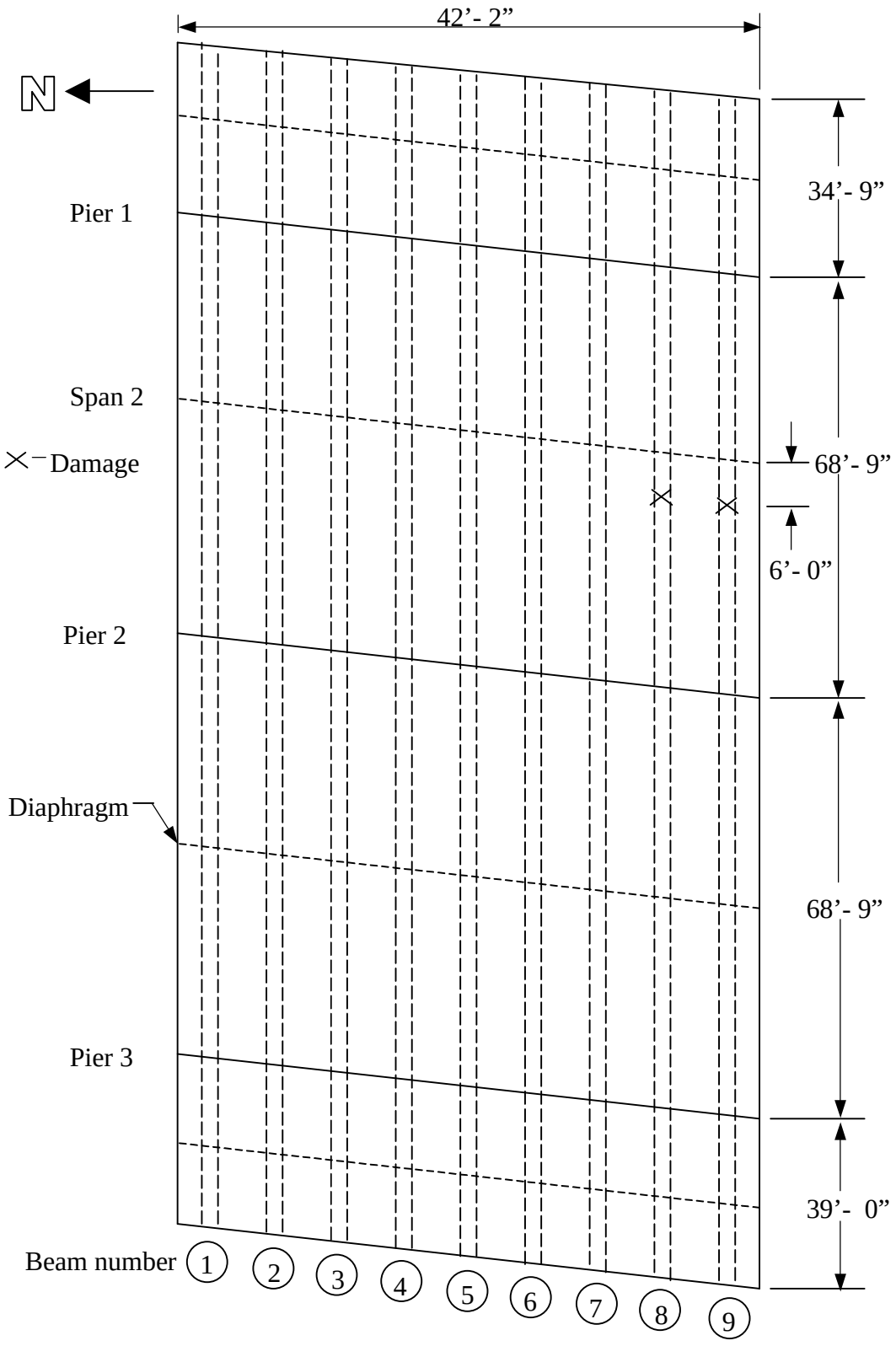

Figure 3.38. Dimensions of De Soto Bridge.

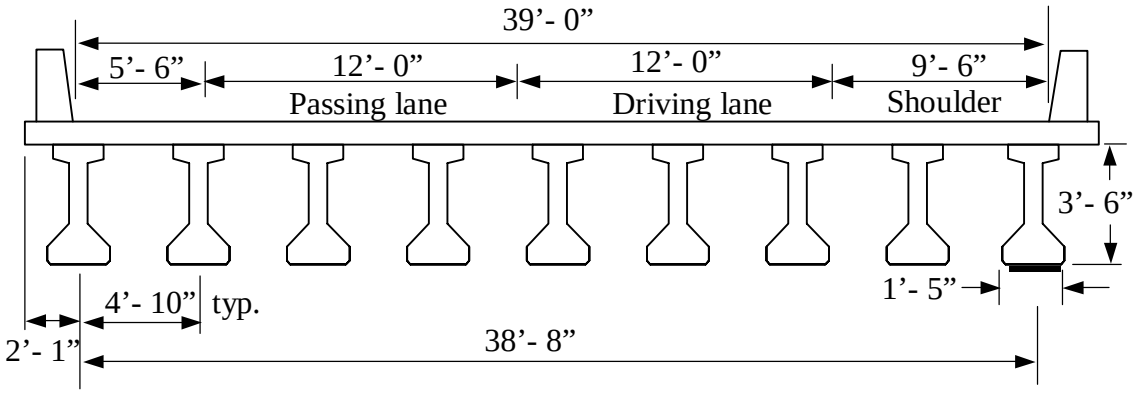

Figure 3.39. Cross section dimensions of the De Soto Bridge.

Figure 3.40. Photograph of severed prestressing strand on Beam 9 in the De Soto bridge.

3.2.3.2. Instrumentation

The BDI-STS, Structural Testing System by Bridge Diagnostics, Inc., was used for running this test. This system was also used for the Osceola bridge test and is described in section 3.2.2.2. Eighteen BDI gages were used in the instrumentation. One gage was placed on the side of the top flange, and one on the bottom of the bottom flange for each of the nine beams (see Figure 3.43). The gages were all placed 1 foot west of the existing bridge diaphragm. The damaged area was located about 3 feet west of the diaphragm, in the center of the driving lane for Highway 169. Figure 3.44 shows the gage schematic.

Figure 3.41. Photograph of severed prestressing strand in the De Soto bridge.

3.2.3.2.1. Trucks

One standard DOT 3-axle dump truck filled with sand was used for this test. The center of gravity was assumed to be in the center of the two rear axles. The front axle weighed 15,060 lbs. and the rear axles weighed a combined 34,140 lbs., for a total weight of 49,200 lbs. Figure 3.42 shows the layout and dimensions of the truck.

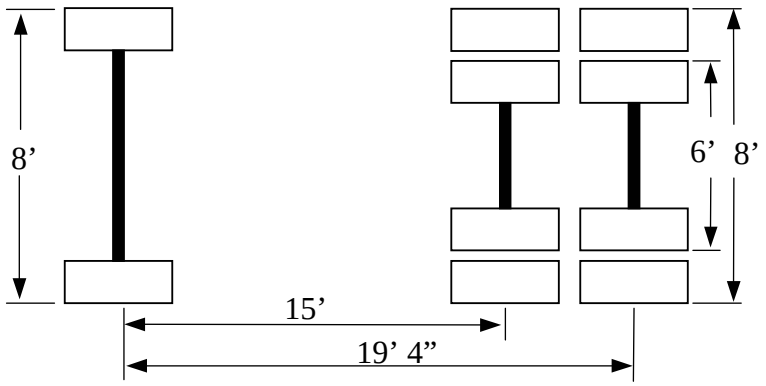

Figure 3.42. Load truck dimensions from De Soto Bridge test.

3.2.3.3. Procedure

Six rolling tests were done for the testing of this bridge. The rolling tests consisted of a single truck driving about 8 mph. in each lane and along the left barrier of the bridge.

There were three different positions across the transverse direction, with two trials run for each position. The truck positions were shown in Figure 3.43.

For each trial, the truck started back about one quarter mile. The driver would then maintain speed trying to avoid any bouncing of the truck. Traffic was only blocked along the lane in which the truck was driving. Traffic could not be stopped along the busy interstate highway. The gages started reading on a command based on visual position. When the truck was nearing the first approach, a radio call started the readings. When the truck had exited the last span, another called was used to stop the gages. When the truck had exited the bridge, the gages were reset. Two identical trials were run back to back in each position before the truck was moved to a new lane. After all six trials were completed, the gages were removed and the bridge was ready to be repaired.

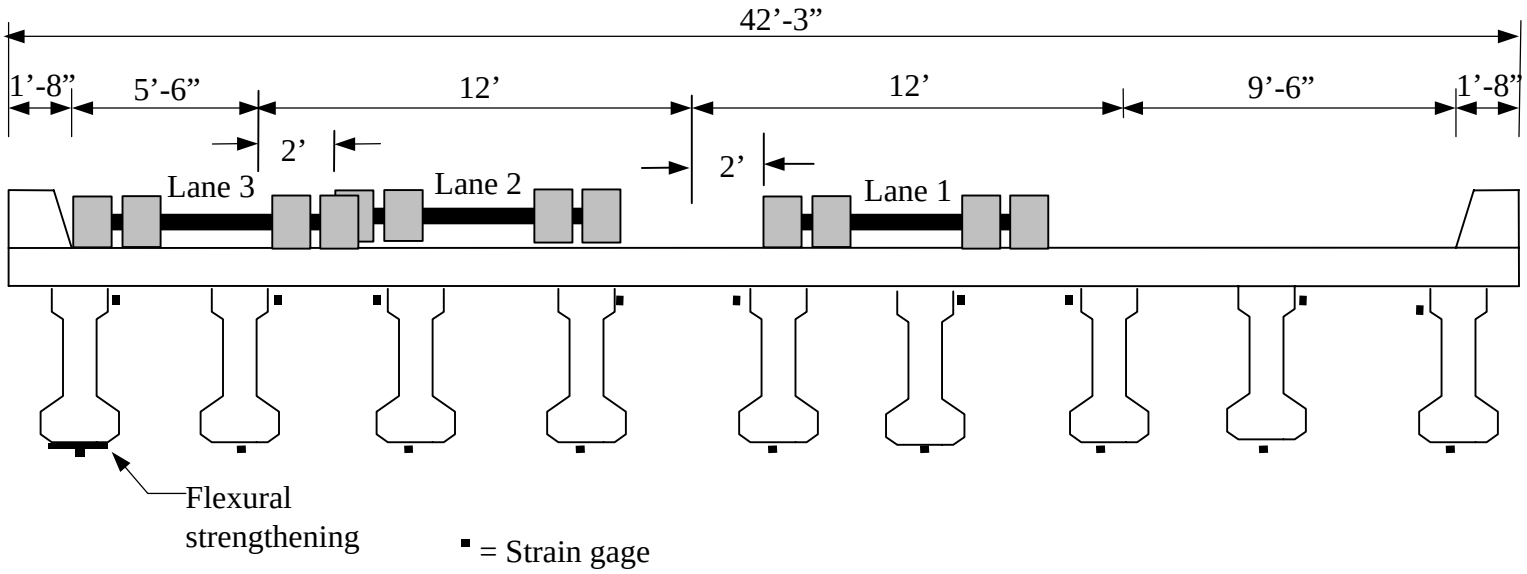

Figure 3.43. Instrumentation cross-section at mid-span of Span 2.

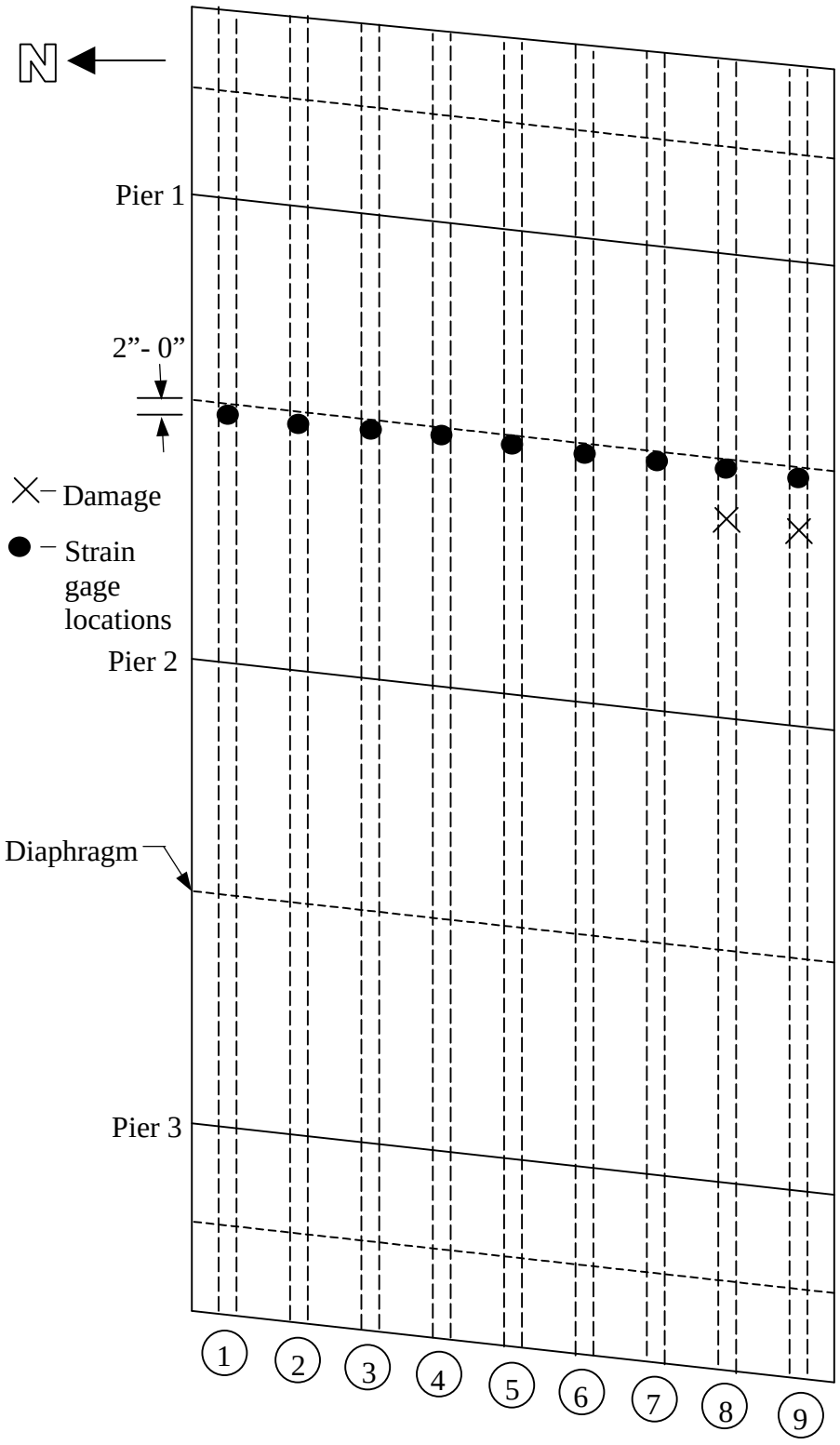

Figure 3.44. Strain gage schematic for De Soto Bridge.

4. REPAIR OF IMPACT DAMAGED LABORATORY AND FIELD P/C BEAMS

4.1. Laboratory Patch Material Properties

The first step in the repair process after a vehicle impact is to patch the damaged concrete beam with a suitable repair material (Raker, 2000). The patch material selected for laboratory portion of this project was EMACO S88 Cl. This is a commercially available structural repair mortar produced by Master Builders Technologies. EMACO S88 Cl is designed especially for overhead concrete repairs and is compatible with the MBrace Composite Strengthening System described in Chapter 5. Material properties (Master, 1998) of the repair mortar at different stages of the curing process are shown in Table 4.1. As can be seen in this table, this product has high early and final compressive strength when compared to normal structural concrete. The primary reason for this increase in strength is that EMACO S88 Cl contains silica fume. Also, notice that the modulus of elasticity (MOE) of EMACO S88 Cl is 28% higher than the MOE of concrete with f'_c = 4,000 psi which is 3,600 ksi.

Table 4.1. Material properties of EMACO S88 Cl.

Test Description	1 Day (psi)	7 Days (psi)	28 Days (psi)
Direct Tensile Bond Strength (ACI 503R, Appendix A)	100	175	300
Modulus of Elasticity (ASTM C 469)	-	-	5,000,000
Splitting Tensile Strength (ASTM C 496)	350	500	900
Flexural Strength (ASTM C 348)	650	1,000	1,300
Compressive Strength (ASTM C 109)	3,500	8,000	11,000

4.1.1. Patch Installation – Laboratory and Field

Using the correct installation procedures is very important to ensure patch performance and durability. All of the recommended installation procedures suggested by the manufacturer were followed in the laboratory. The first step was to saturate the existing

concrete with water to prevent the substrate from drawing moisture from the patch material during curing. One gallon of water was required to mix each 55-lb bag of EMACO S88 Cl. For smaller batch sizes, only half the material in each bag was mixed at one time. A scale was used to ensure that each batch contained the correct amount of material. As suggested by the manufacturer, only 90% of the mixing water was initially added to the mixing container (a 5 gallon bucket). Next, the dry material was slowly added to the water and mixed for 5 minutes with an electric drill. Remaining mixing water was then added as needed to obtain the desired consistency. The next step was to remove the excess water from the substrate and apply a scrub coat of EMACO S88 Cl. A scrub coat consists of working the fresh patch material into the pores of the existing concrete with a stiff bristle brush. Scrub coats are necessary to provide a strong bond between the existing concrete and the patch material.

The mixed EMACO S88 Cl was installed immediately following the application of the scrub coat. Formwork was used to restore the original flange profile of the P/C beam. The formwork was installed in three sections while the patch was being placed. Each piece of the formwork consisted of a piece of 3/4 in. plywood and a 2x4 stiffener. Vertical shoring was not required to hold the formwork in place since it was anchored to the beam with concrete screws. All of the holes for the screws were predrilled at the appropriate locations with an electric hammerdrill. A side form was also used to form the patch on the starting side of the bottom flange.

A photograph and an elevation view of the completed patch formwork in the laboratory are shown in Figures 4.1 and 4.2. Once the patch material was placed, the opening on the side of the flange was finished with a hand trowel. Approximately four 55-lb bags of EMACO S88 Cl were required to fill each patch (≈ 2.0 ft^3).

All of the patches on the field bridges were installed using standard industry practice. The flange shapes were restored with greased wood formwork, and the patch was installed. The major difference between laboratory and field was the use of epoxy injections. Epoxy was injected into all cracks of the bridge beams, while no epoxy was used in the laboratory repair.

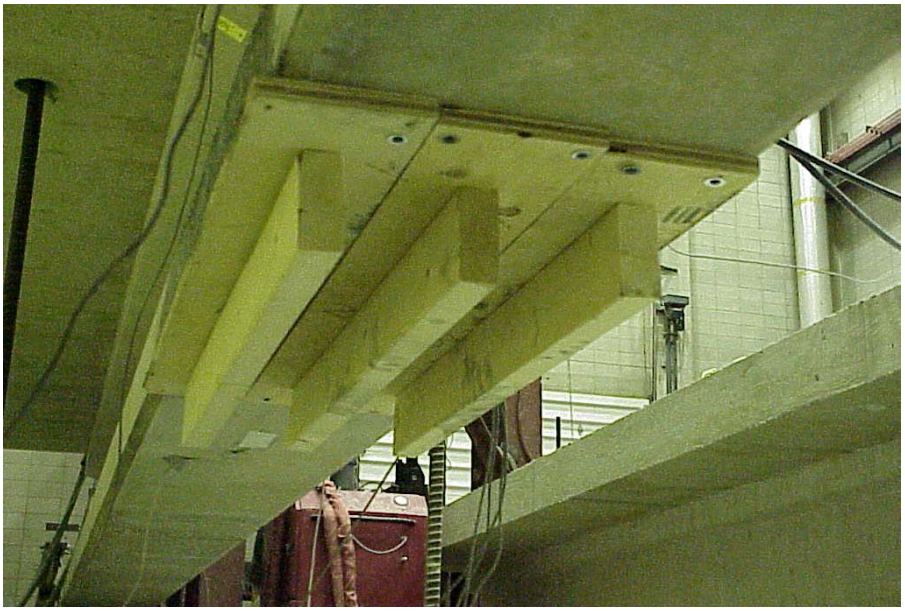

Figure 4.1. Completed patch formwork.

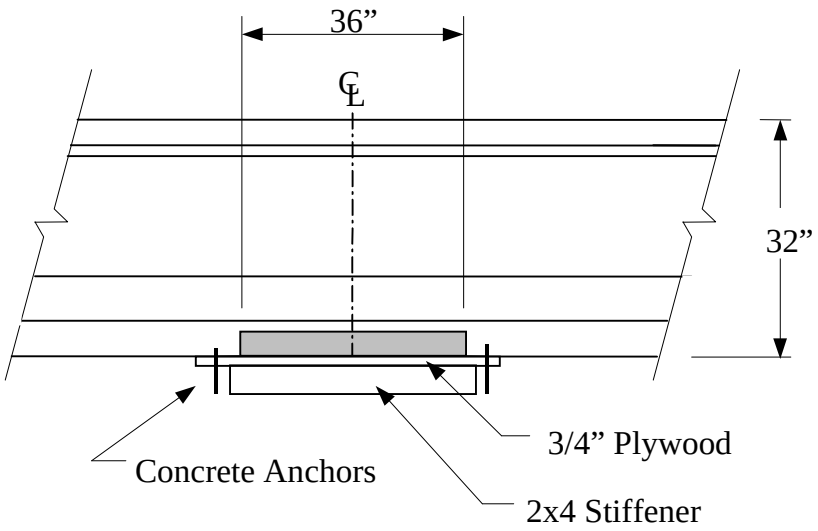

Figure 4.2. Elevation view of patch and patch formwork.

4.2. CFRP Components

The CFRP product selected for the laboratory part of the project was the MBrace Composite Strengthening System (www.mbrace.com). This proprietary system is currently being produced by Master Builders Inc. of Cleveland, Ohio. The MBrace system uses unidirectional carbon fiber sheets bonded to concrete surfaces to strengthen existing concrete structures. The system is comprised of the follow five individual components:

- Primer
- Putty (optional)
- Saturant
- Carbon fibers sheets
- Topcoat (optional)

These individual components and their material properties are discussed in Section 4.3.

4.2.1. CFRP Sheet Installation – Laboratory and Field

The procedure described is for laboratory and field beams requiring CFRP sheets. CFRP plates are installed in a similar manner that is discussed in section 4.2.2. The bridge near Altoona was the only bridge to have CFRP plates installed as well as CFRP sheets.

As specified by the manufacturer, the concrete surface was prepared to provide a strong bond between the CFRP sheets and the concrete substrate. Concrete/masonry grinding wheels were used with a hand grinder to roughen the surface of the existing concrete and the patch in the laboratory. The bridges in the field were sand blasted to prepare the concrete. Other approved surface preparation methods include abrasive and water blasting. Surface preparation is necessary to open the pore structure of the concrete to create a strong epoxy bond. The concrete surface should also be free of unsound material, dust, dirt, and/or oil. Shown in Figure 4.3 is the grinding process along with the dust collection unit used in the laboratory. A damp rag was used to remove any dust from the surface after the grinding was completed.

All of the CFRP sheets were precut to the required dimensions. The sheets were supplied in a roll with a nominal width of 20 in. along with backing paper. Specialize cutting equipment was not required to size the individual sheets as they can be cut with standard hand scissors (see Figure 4.4). To keep the sheets clean and free of dust, they were covered

with a plastic tarp until they were ready to be installed. The design of the CFRP sheets used in the laboratory (dimensions, layout, etc.) is presented in detail in Section 4.5.

As shown in Figure 4.5, the primer coat was quickly applied to the entire bottom surface of the P/C beam using a medium nap roller. See Appendix C for photos of field priming. The primer coat is designed to penetrate the concrete pores and provide a strong bond between the concrete and the carbon fibers. This first layer is a two-part epoxy system with a Part A and B. As specified by the manufacturer, the primer was mixed with a 3/1 ratio by volume with an electric mixer. The primer has a 20-minute working time at room temperature. At 90 °F, the working time of the primer is reduced to approximately 10 minutes. However, it is possible to extend the working time of the epoxies in extreme heat by cooling the unopened containers in ice water.

Figure 4.3. Grinding the bottom surface of the P/C beam.

Figure 4.4. Precutting the CFRP sheets to desired dimensions.

Figure 4.5. Application of primer coat with medium nap roller.

Epoxy putty filler was not required for the laboratory part of this project. The putty is designed to fill holes or defects up to 1/4 in. deep. Putty is not required when the concrete surface is in good condition and does not contain surface defects or "bug holes". In cases were it is necessary, putty is applied directly over the wet primer with a hand trowel. Putty was used on the Osceola and De Soto bridges. See Appendix C for putty installation photos of the Osceola Bridge.

The next step in the application process was to apply a single layer of saturant. The saturant was approximately three times more viscous than the primer and was dark blue in color. The purpose of the saturant was to impregnate the dry fibers and hold them in place while the epoxy cures. Saturant was mixed and applied using the exact same steps as the previous primer coat. The working time of the saturant is 45 minutes at room temperature and is reduced to 15 minutes at 90 °F.

The precut CFRP sheets were applied directly onto the single layer of saturant. The sheets were pressed against the concrete surface with the backing paper still in place. Air pockets/wrinkles were removed by pushing them out by hand as shown in Figure 4.6. Once the sheet was securely in place, the protective backing paper was removed. A ribbed roller was then used to work the carbon fibers into the layer of saturant. The ribbed roller was only run in the direction of the carbon fibers. Running the ribbed roller across the sheets can potentially damage the fibers. The next layer of saturant was applied 30-45 minutes after the first layer of carbon fiber had been installed. After another 30-45 minutes, the epoxy was re-saturated (i.e. 2 layers of saturant applied to the first layer of carbon fiber) and the second layer of CFRP was applied as previously described. See Appendix C for saturant and sheet installation pictures.

4.2.2 . CFRP Plate Installation – Field

Due to the amount of damage the second beam (see Figure 3.22) of the Altoona Bridge sustained, CFRP plates were included in the design. The four 75 ft long, Sika S1012 plates were attached to the bottom flange after the damaged concrete area had been patched. To attach a plate to the beam, an epoxy was spread on the underside of the beam with putty knives, while the same epoxy was also spread on the topside of the plate. The plate was then lifted into place, pressed tightly, and held for a short time. This process was repeated three

more times for a total of four plates. A roller was then used to press the plates tightly into the epoxy along the length of the beam. After the epoxy dried, transverse CFRP sheets were installed near the center and ends to help prevent any plate debonding. The sheets were also installed at the damage points of the other beams to help contain the patches.

Figure 4.6. Applying the CFRP sheets to the bottom the beam.

4.3. Design of CFRP Strengthening System for Laboratory Beams

The purpose of the CFRP sheets was to restore the ultimate flexural capacity of impact damaged prestressed beams. The sheets obviously do not restore prestressing force lost due to the severed strands. Strain compatibility concepts were used to determine the amount of CFRP necessary to strengthen the beams and an analytical procedure was developed to estimate the flexural strength of P/C beams strengthened with CFRP sheets. The results indicate that it is feasible to restore the original ultimate strength of damaged P/C beams with CFRP sheets.

4.3.1. CFRP Material Properties

The material properties of the unidirectional CFRP sheets used in the laboratory are shown in Table 4.2 (56). As shown, the CFRP sheets have an ultimate tensile strength of 620 ksi. However, a design strength of 550 ksi is suggested by the manufacturer. This value was determined by reducing the ultimate stress of the material by three standard deviations.

The design modulus of the bonded sheets is slightly higher than the value of structural steel. However, it is difficult to add significant stiffness to P/C beams with CFRP sheets. CFRP sheets are generally very thin and therefore they do not increase the cross-sectional area in relation to a composite P/C beam. The CFRP sheets used were extremely thin and flexible. CF 130 sheets have a design thickness of 0.0065 in. For this reason, these types of carbon fiber sheets obviously do not increase the stiffness of typical P/C composite beams. The stress-strain behavior of the CFRP sheets used in the design is shown in Figure 4.7. Carbon fiber is a linearly elastic material until failure. Unlike typical structural steels, carbon fibers experience sudden brittle failures without yielding.

Table 4.2. Material properties of CFRP sheets.

CFRP Sheet Designation	Ultimate Strength (ksi)	Design Strength (ksi)	Design Tensile Modulus (ksi)
CF 130 High Tensile Carbon	620	550	33,000

4.4. Analytical Procedure

An analytical procedure was developed to determine the amount of CFRP material necessary to restore the original strength of the damaged P/C beams in the laboratory. It is important to determine which mode of failure will govern under ultimate strength conditions. When repairing damaged P/C girders, the following flexural failure modes are possible:

- Concrete crushing
- Rupture of CFRP sheet(s)

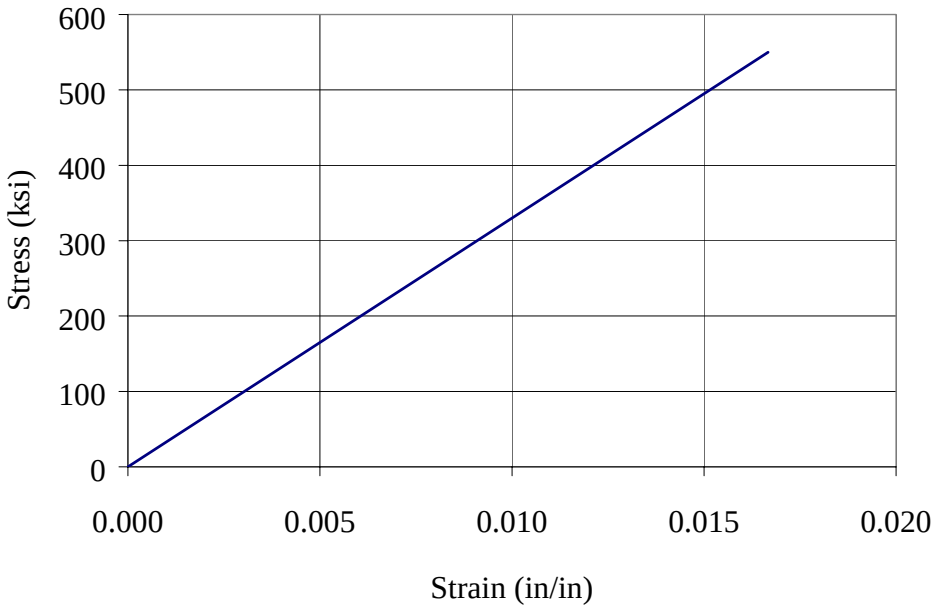

Figure 4.7. Stress-strain behavior of CFRP.

Due to the high ductility of prestressing steel, rupture of the stands will generally not control. In most cases involving the repair of P/C beams, debonding or rupture of the CFRP sheets will define failure under ultimate strength conditions.

Strain compatibility and equilibrium concepts were used to calculate the ultimate capacity of a strengthened P/C beam. The design procedure consisted of limiting the strain in the CFRP sheets to 16,667 MII based on the design stress/modulus and by assuming a neutral axis depth as shown in Figure 4.8. Once a neutral axis depth was determined, the magnitude of the respective forces in the CFRP sheets, prestressing steel, and concrete slab were calculated. For equilibrium, the sum of the tensile forces in the CFRP and prestressing steel must equal the compressive force in the slab.

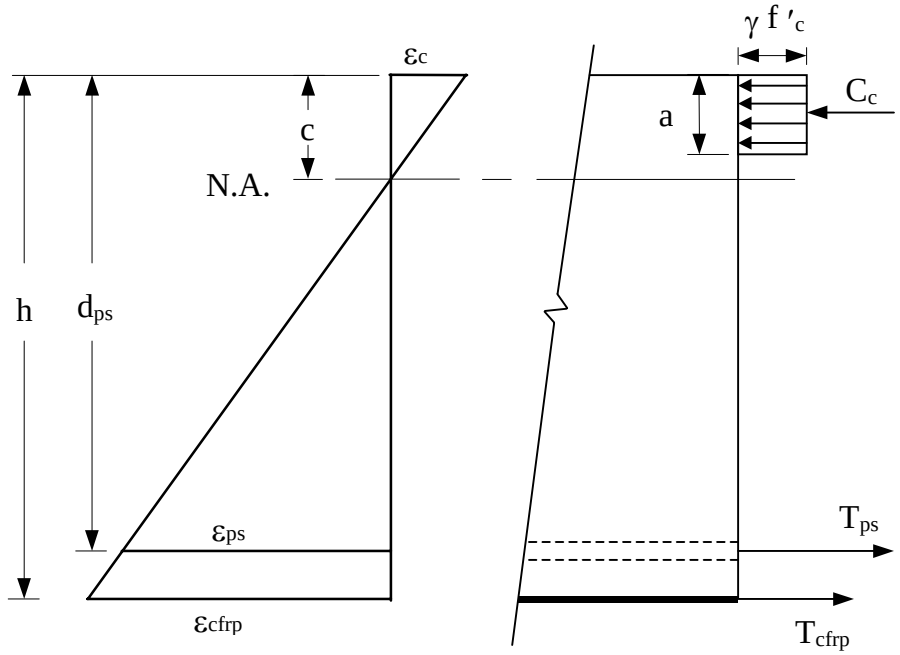

Figure 4.8. Strain distribution with corresponding forces at failure.

Where:

a = depth of the rectangular stress block = $\beta_1 c$
c = depth to the neutral axis.
C_c = compressive force in the concrete.
d_{ps} = depth to the centroid of the prestressing steel.
f'_c = compressive strength of the concrete.
h = total depth of the composite section.
T_{cfrp} = tensile force in the CFRP sheets.
T_{ps} = tensile force in the prestressing strands.
β_1 = factor to determine the depth of the rectangular stress block.
γ = factor to determine the intensity of the rectangular stress block.
ε_c = strain in the top concrete fiber.
ε_{cfrp} = strain in the CFRP sheets.
ε_{ps} = strain in the prestressing steel.

If the sum is not zero, the assumed neutral axis location is revised as necessary and the process is repeated. This iterative process generally converged after three or four trials. A set of sample calculations is presented in Appendix B. Once equilibrium was reached, the ultimate moment capacity of the section was calculated by summing moments about the

compressive force in the concrete slab. The live load moment was then found by subtracting the moment due to the self-weight of the composite beam.

It is important to remember that at the time of testing, the CIP concrete slab and the CFRP sheets were free of stress. This was not true for the prestressing strands. The total strain in the prestressing steel consisted of the effective prestressing strain (ε_1), decompression strain (ε_2), and the strain due to the applied load (ε_3). The first two strains (ε_1 and ε_2) were added to the live load strain to determine the total force in the prestressing strands.

For this particular case, the ultimate strain of the concrete slab ($\varepsilon_c = 0.003$ in/in) was not reached when the design strain of the CFRP sheets was exceeded. The standard Whitney stress block is only valid when the outermost fiber reaches ultimate strain conditions. The following equations were used to calculate equivalent factors for a modified concrete stress block (57):

$$\beta_1 = 2 - \frac{4\left[\left(\frac{\varepsilon_c}{\varepsilon'_c}\right) - \arctan\left(\frac{\varepsilon_c}{\varepsilon'_c}\right)\right]}{\left(\frac{\varepsilon_c}{\varepsilon'_c}\right)\ln\left(1+\left(\frac{\varepsilon_c}{\varepsilon'_c}\right)^2\right)} \tag{4.1}$$

$$\gamma = \frac{0.90\ln\left(1+\left(\frac{\varepsilon_c}{\varepsilon'_c}\right)^2\right)}{\beta_1\left(\frac{\varepsilon_c}{\varepsilon'_c}\right)} \tag{4.2}$$

$$\varepsilon'_c = \frac{1.71 f'_c}{E_c} \tag{4.3}$$

Where:

E_c = elastic modulus of the concrete in compression.
f'_c = compressive strength of the concrete.
ε_c = maximum compressive strain in the concrete.

The force in the prestressing strands was determined using the equations for stress/strain behavior published in the PCI Design Handbook (58). The strain at the level of the prestressing steel centroid was then converted from a stress to a force.

4.5. CFRP Sheet Details

In order to develop their full flexural strength, externally bonded CFRP sheets must also satisfy development and cutoff requirements. These checks are analogous to those in traditional R/C design for steel reinforcement where the larger of the two values determines the reinforcement length. When strengthening full size beams with CFRP, the cutoff requirement will usually control. Under normal situations, the development criteria for CFRP sheets will only control on short span beams. These guidelines are intended to prevent premature debonding type failures similar to those discussed in Section 2.5.1.

4.5.1. Cutoff Points

For simply supported beams, the manufacturer suggests that all of the CFRP sheets extend beyond the location of the theoretical factored cracking moment for the section. The outermost layer of CFRP should extend 6 in. past this calculated cutoff point. Additional layers should also be terminated at 6 in. intervals on both sides of the strengthened beam (Figure 4.9). Staggering the termination points in this manner helps to avoid large stress concentrations at the ends of the CFRP sheets. For this project, the required length of CFRP was calculated to be 28 ft (72% of the span length). Including the staggered termination points increased the total length of the first layer of CFRP to 30 ft (78% of the span length).

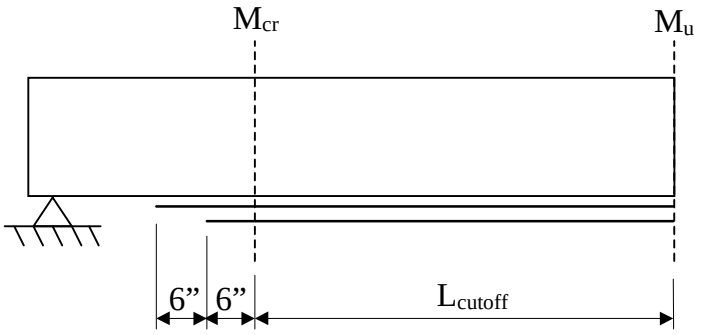

Figure 4.9. Termination points for beam strengthened with 2 layers of CFRP.

4.5.2. Development Length

The development length of the CFRP sheets also needs to be checked when determining the total amount of material required. Development length is a function of fiber strength, sheet thickness, and strength of the concrete substrate. The manufacturer suggests using the following formula for calculating the development length of bonded CFRP sheets:

$$l_{df} = \frac{f_{fu} t_u n}{3\sqrt{f'_c}} \tag{4.4}$$

Where:

l_{df} = development length (in.)
f_{fu} = design strength of the CFRP fibers (psi)
t_u = thickness of one CFRP sheet (in.)
n = number of CFRP sheets
f'_c = compressive strength of the concrete (psi)

Using this relationship, the development length with 2-layer of CFRP can be calculated to be 30 in. The total length of the sheet required would then be twice this or 60 in. Therefore, in this case the cutoff requirement clearly is the controlling factor when determining the lengths of CFRP required.

4.5.3. CFRP Sheet Splices

Splices were required in the final design of the CFRP sheets. It would not be practical to install 30 ft long sheets on the flanges of damaged girders in the field. With this in mind, the maximum individual sheet length was limited to 8 ft. According to the manufacturer, the full tensile capacity of a CFRP sheet can be developed in a 2 in. lap splice. However, in the laboratory a 6 in. lap splice was used to simplify the installation process and to ensure the full strength of the material would be reached. As recommended, the splices of the two different CFRP layers were staggered. The final design of the CFRP sheets is shown in Figure 4.10. Sheet dimensions were selected so that only two standard sheet lengths would be required (marked A & B). Sheets given the designation A were 94.5 in. long and the two end sheets marked B in the second layer were 44.25 in. long. Therefore, the total

length of layer 1 and layer 2 including the 6 in. lap splices were 30 ft and 29 ft, respectively. All of the sheets in layers one and two were 14 in. wide which is 1.5 in. less than the bottom flange width.

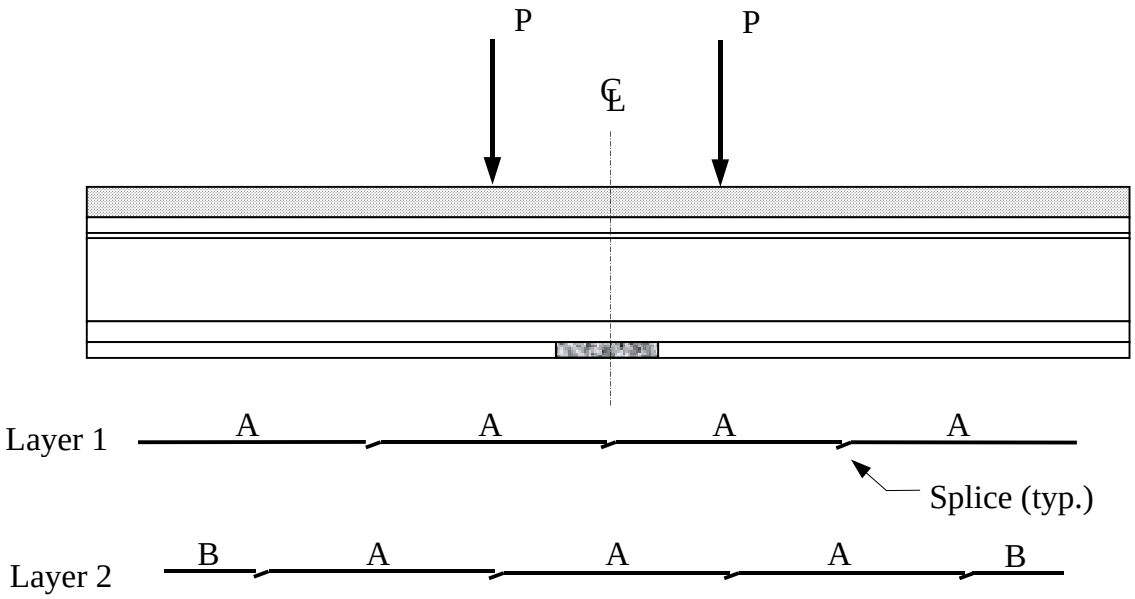

Figure 4.10. Layout and dimensions of CFRP sheets on laboratory beam with 6 in. splices.

4.6. CFRP Jackets

In addition to the longitudinal CFRP sheets, Beams 2,3, and 4 were strengthened with transverse CFRP sheets or jackets. The intended purpose of the jackets was to prevent longitudinal sheet debonding and to confine the patch material. The three jacket configurations used in the laboratory are discussed in the following sections. The CFRP jackets used in the field most closely resembled the jacket used on beam 3 in the laboratory. They varied in length depending on the bridge, but all of them went well up the web near the bottom of the top flange.

4.6.1. CFRP Jacket Installation – Beam 2

Installation of the CFRP jacket around the bottom flange of Beam 2 is presented in Figure 4.11. The same type of CFRP sheet that was used for the longitudinal fibers was also used in the transverse direction. The longitudinal fibers were allowed to cure for one day before the jacket was installed. As with the longitudinal fibers, a hand-held grinder was used

to prepare the sides of the beam. The continuous CFRP sheets completely wrapped the entire bottom flange of the P/C beam as shown in Figure 4.12. A gap of approximately 1/4 in. was provided between the individual jacket pieces to avoid disturbing adjacent jacket pieces during installation. Four individual CFRP sheets 14 in. wide were required to complete the jacket. After sheets were positioned in the proper location, a topcoat of epoxy was added to encase the jacket.

The CFRP jacket was design to prevent debonding of the longitudinal sheets and to confine the patch material. With these factors in mind, the width of the jacket in the longitudinal direction was 6 ft (Figure 4.13), which is 3 ft longer than the patch. This was exactly twice the width of the damaged region. The jacket was designed to terminate on the inclined portion of the bottom flange on both sides of the beam

4.6.1.1. CFRP Jacket Strain Gages

Four strain gages were placed on the CFRP jacket to monitor the strain levels in the transverse fibers. These gages were positioned on the vertical portion of the bottom flange. Each gage was oriented in the vertical direction, i.e. the same direction as the fibers in the jacket. Two gages were placed on each side of the beam approximately 10 in. from the end of the jacket (Figure 4.13). The results from these strain gages are discussed in Section 5.2.2.2.

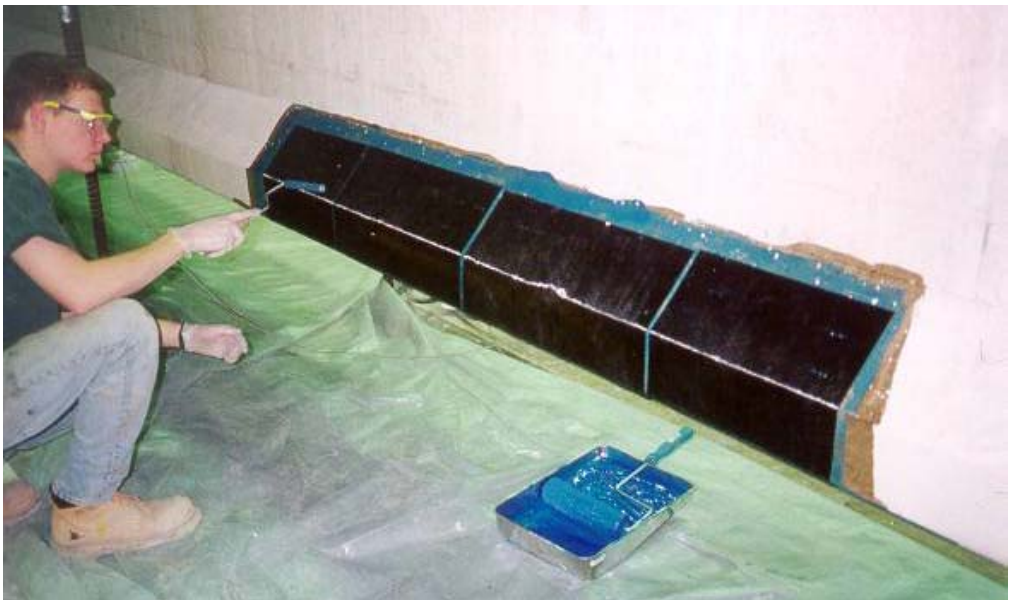

Figure 4.11. Installation of transverse CFRP jacket on Beam 2.

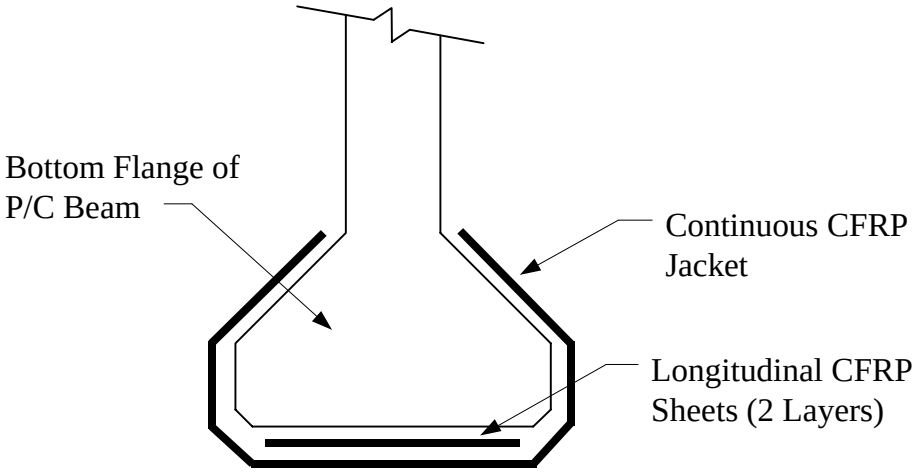

Figure 4.12. Cross-section showing CFRP jacket used on Beam 2.

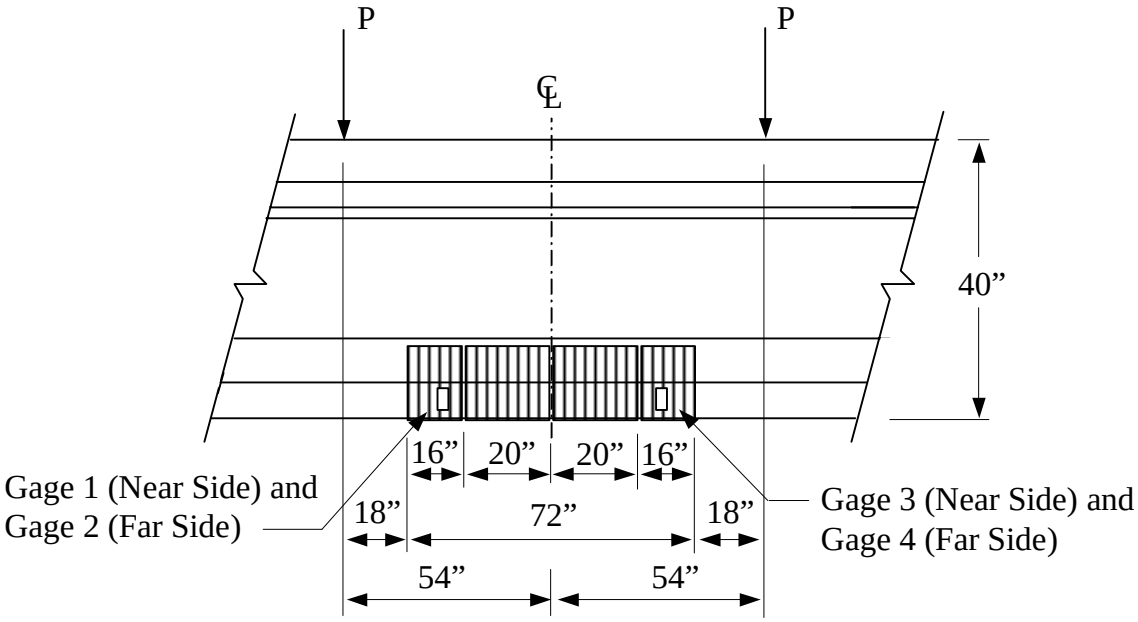

Figure 4.13. Profile of CFRP jacket used on Beam 2.

4.6.2. CFRP Jacket Installation – Beam 3

As with Beam 2, a CFRP jacket was also installed on Beam 3 to help contain the patch material and to prevent longitudinal sheet debonding. A typical cross-section of the CFRP jacket used on Beam 3 is shown in Figure 4.14. This jacket was designed and

positioned on both sides of the concrete web terminating approximately 1 in. from the top flange. Recall that the jacket used for Beam 2 stopped on the inclined portion of the bottom flange (Section 4.6.1). The jacket used for Beam 3 was also longer than the jacket used for Beam 2. The jacket had a total length of 14 ft. and is illustrated in Figure 4.15. The increased length allowed the jacket to extend 2 ft – 6 in. beyond the load points on each side of the beam to allow for complete web coverage in the constant moment region. Results from the first two beam tests indicated that the large increases in shear at the load points contributed to the debonding action.

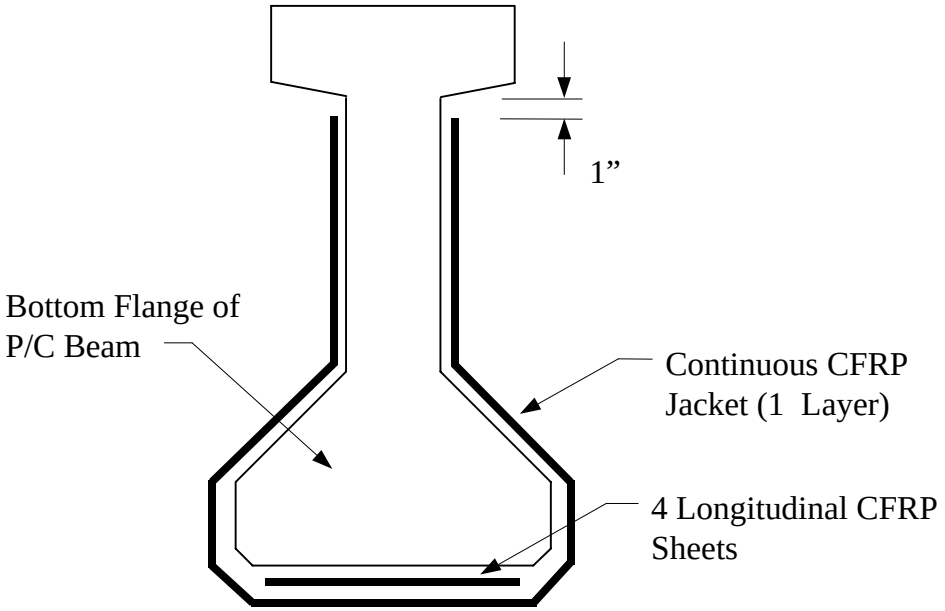

Figure 4.14. Cross-section of CFRP jacket used on Beam 3.

4.6.3. CFRP Jacket Installation – Beam 4

Figure 4.16 shows a cross section of the jacket, and Figure 4.17 shows the layout and dimensions of the jacket. The jacket on beam 4 extended 40 in. both ways from the center of the beam, which was the entire length of the patched area, similar to beam 2. Five strips were cut to cover this area; three were left their nominal 20 in. wide, and two were cut down to 10 in. The sizes were chosen to avoid the wires from the prestressed strand gages that stuck out from the patch. All of the strips were approximately 6 ft. long to allow them to cover the entire bottom flange and reach up to cover the entire web leaving only an inch from the bottom of the top flange, which was similar to beam 3.

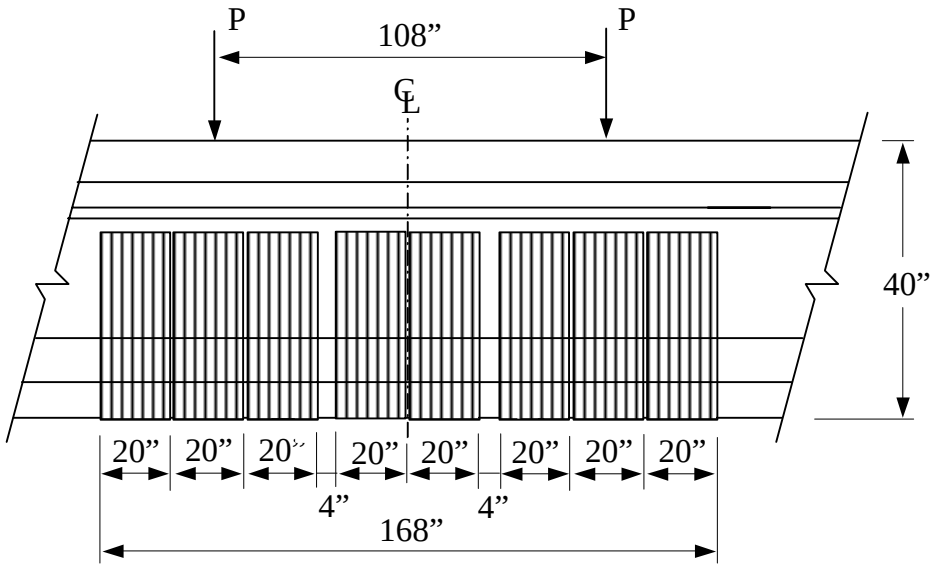

Figure 4.15. Profile of CFRP jacket used on Beam 3.

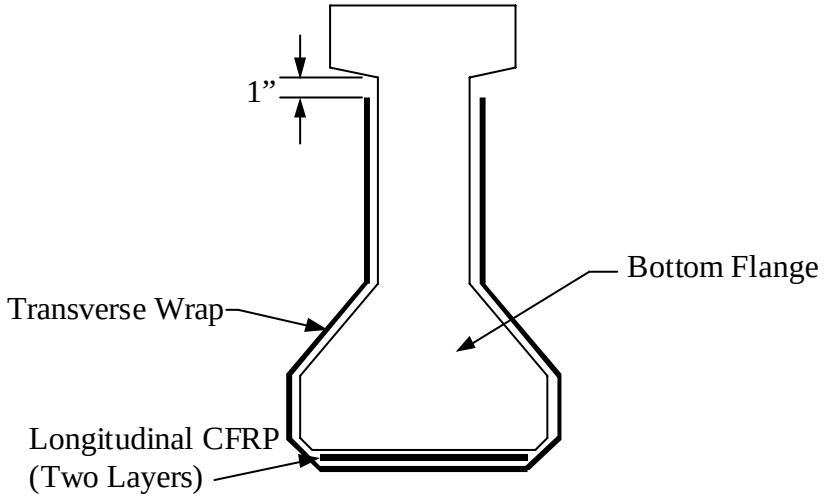

Figure 4.16. Cross-section of CFRP jacket used on Beam 4

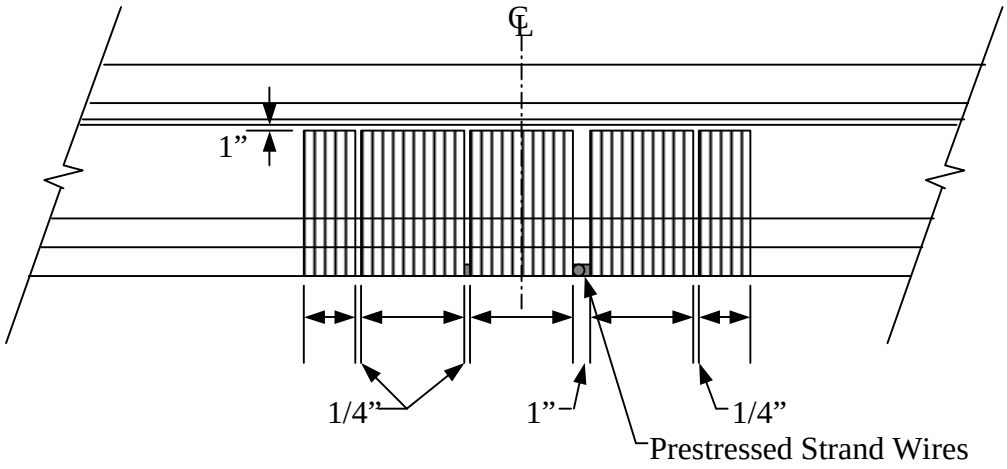

Figure 4.17. Profile of CFRP jacket used on Beam 4.

4.7. Modulus of Rupture Beams

Durability and long-term behavior are major concerns associated with using CFRP products to repair and strengthen concrete structures in Iowa. The CFRP strengthening systems must be able to withstand prolonged exposure to moisture, freeze-thaw cycles, chlorides, and ultraviolet radiation. To address these problems, a number of small-scale environmental test specimens were built. This test was designed to rate the epoxy bond performance over a period of years.

4.7.1. Test Specimens

The small-scale test specimens consisted of standard modulus of rupture beams with dimensions of 30 in. x 6 in. x 6 in. A total of fifteen beams were cast in June, 1999. Due to a limited number of steel forms, it was necessary to cast the specimens in two separate concrete pours. The concrete used was a standard Iowa DOT mix design (C4) with 6% entrained air. The two pours took place within a week of each other. The average 28-day compressive cylinder strength of pours 1 and 2 were 4,850 and 4,750 psi, respectively. As a result, an average concrete strength of 4,800 psi was assumed for all of the small-scale specimens.

The CFRP sheets were applied to one side of the modulus beams on January 6, 2000. Three control beams were left unreinforced. The same CFRP application procedure (described in Section 4.2.1) was used as on the P/C beams except all of the beams were

rotated to an upright position to simplify the process. As before, a hand grinder was used roughen the concrete surface. The next step was to apply a coat of primer and a coat of epoxy. As shown in Figure 4.16, a single layer of CFRP 5 in. wide and 25 in. long was applied to the remaining beams. This CFRP sheet was worked into the epoxy with the ribbed roller as shown in Figure 4.17 and allowed to cure for 30 minutes. The final step was to apply a second layer or topcoat of epoxy to seal in the CFRP sheet. Once completed, the strengthened modulus beams were not moved for a period of seven days. Three unreinforced beams and three reinforced modulus beams were then tested.

The remaining modulus beams were dated and placed in an exterior storage area. They were positioned so the CFRP side was facing down. This was done to avoid any directed exposure to ultraviolet radiation. This orientation represents the exposure a repaired girder would experience in the field. CFRP sheets bonded to girders in the field would be protected by an ultraviolet blocking paint. A timetable has been proposed for the testing schedule of the remaining modulus beams. Three beams will be tested every three years in the same manner to determine if any bond degradation occurs. Thus, the total test time is 9 years.

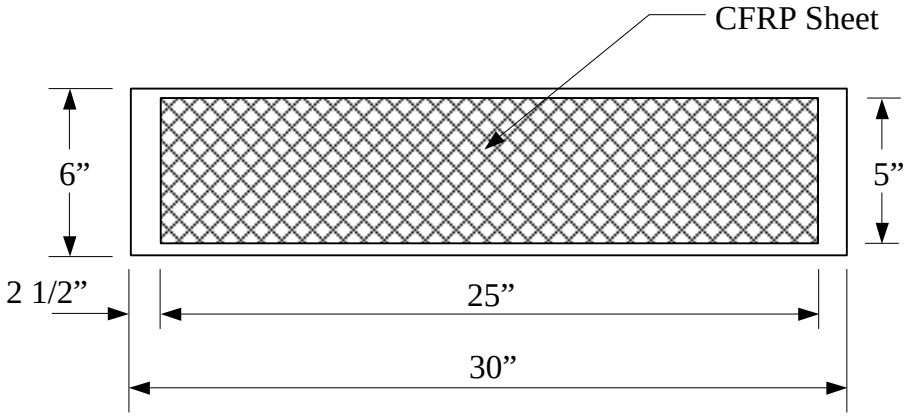

Figure 4.18. Location of CFRP sheet on bottom of modulus of rupture beam.

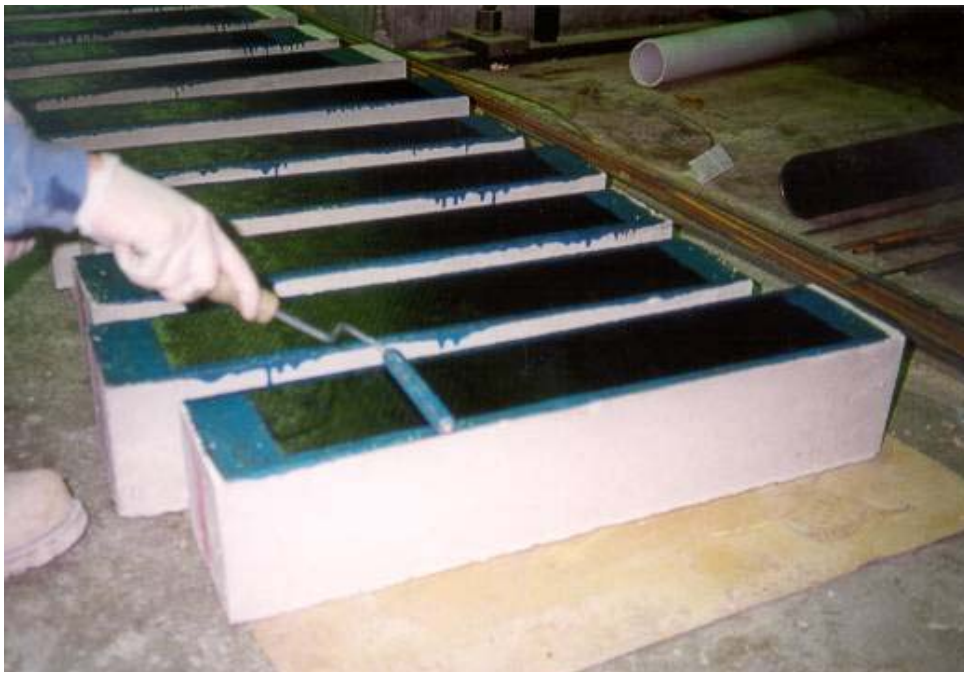

Figure 4.19. Application of CFRP sheet to modulus beam.

4.7.2. Test Setup

The modulus beams were tested to failure under two-point loading as shown in Figure 4.18. The loads were applied to the concrete beams though a series of steel pins and rollers. The rollers consisted of 1/2 in. diameter steel rods that extended across the entire width of the modulus beams. All load points in contact with concrete surfaces were distributed with steel plates to avoid stress concentration problems. Neoprene bearing pads were also placed underneath the top two load points to ensure an evenly distributed pressure. A strengthened modulus beam in the testing machine is presented in Figure 4.19. Readings taken during the test included applied load, centerline displacement measured with a DCDT, and centerline CFRP strains. A small piece of angle was glued to the side of the beam to provide a reference point for the DCDT shown in the foreground.

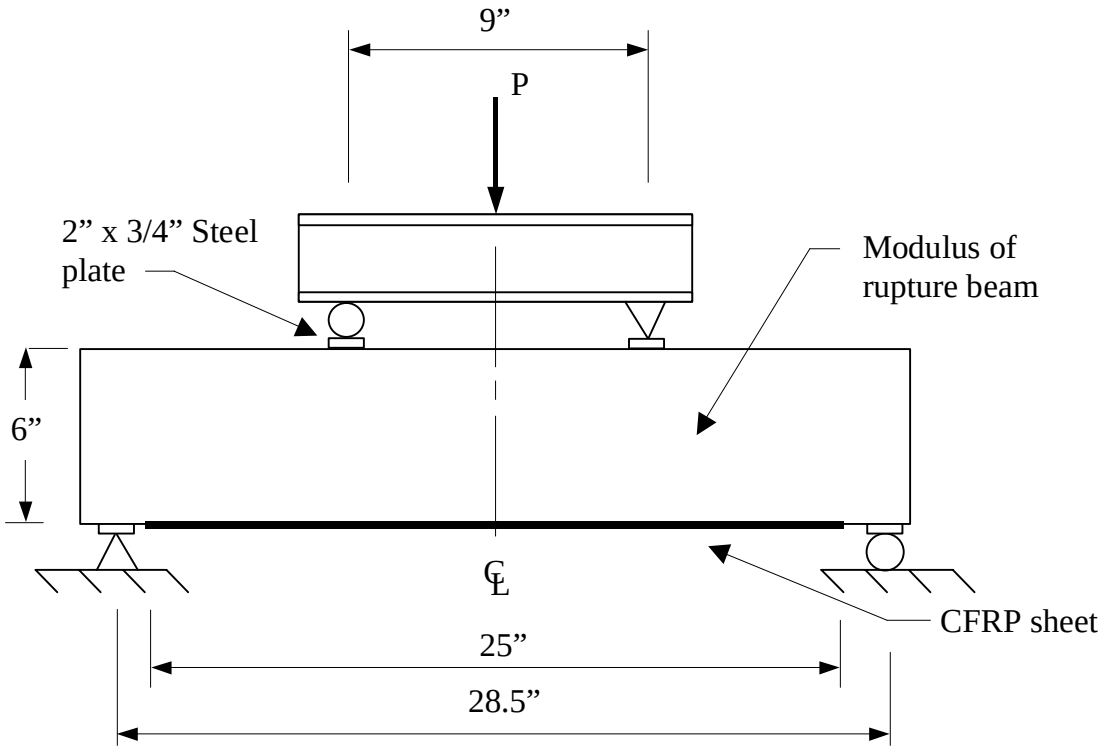

Figure 4.20. Modulus of rupture beam test setup.

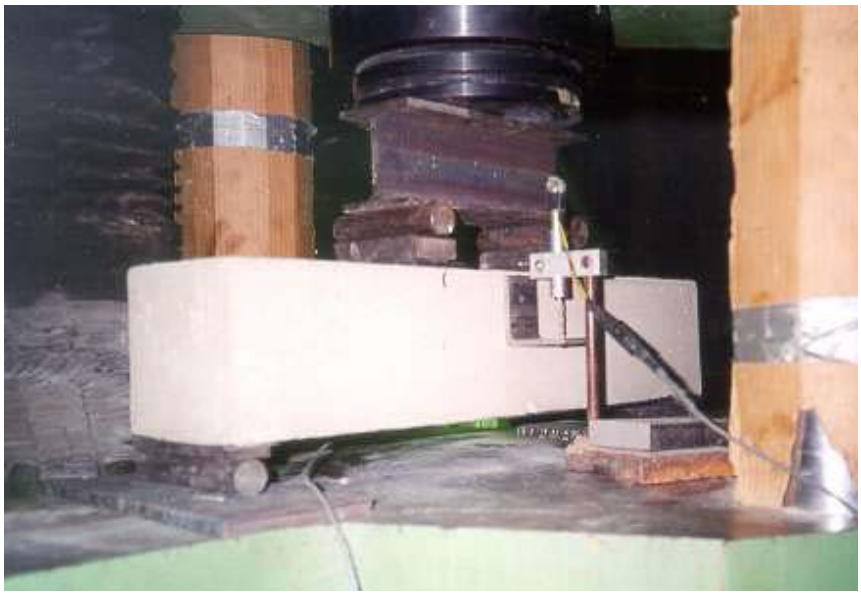

Figure 4.21. Modulus of rupture beam in testing machine.

5. LABORATORY AND FIELD TEST RESULTS

All of the repaired prestressed laboratory beam specimens were tested to failure in two-point bending as previously discussed in Chapter 3. Impact damage was simulated by removing concrete from the bottom flange and severing either two or four prestressing strands. The beams were than patched and strengthened by applying multiple layers of CFRP sheets. The fourth beam was subjected to cyclic loading. The typical failure mode of the strengthened beams was delamination of the CFRP sheets at the CFRP/concrete interface. Delamination was initiated by flexural cracks near the midspan of the beams. However, the majority of the flexural strength was restored before delamination occurred. In the upcoming discussion, the term "failure" represents the premature delamination of the CFRP sheets.

Three bridges that had sustained damage were load tested in the field, one near Altoona, IA, another near Osceola, IA, and one near De Soto, IA. All of the bridges were subsequently repaired, and the Altoona bridge was tested again. All of the repairs consisted of concrete patches followed by attachment of some CFRP, either plates and/or fabric.

5.1. Beam 1

Beam 1 was damaged and then strengthened using the procedures previously discussed in Chapters 3 and 4. A section of the bottom flange 36 in. long and 4 in. deep was removed from the beam at the centerline. Two prestressing strands were also severed (17% of the flexural reinforcement). The beam was then patched and strengthened with two layers of CFRP.

5.1.1. Service Load Tests – Beam 1

Service load tests were conducted at various stages of beam damage. The maximum service load applied to the beam was 25 kips at each load point. This service load was large enough to obtain general elastic behavior and was less than the estimated cracking load. Instrument readings were taken by the computer controlled DAS at 2.5 kip intervals. Centerline load deflection plots for Beam 1 at various stages of damage are presented in Figure 5.1. The initial undamaged beam stiffness was 138.2 kips/in. Beam stiffness was determined by using the secant modulus definition at the maximum service load for each

damage case (Load P = 25 kips). The final damaged beam stiffness was 125.5 kips/in, resulting in a 9.2% reduction in stiffness (the removed concrete and two prestressing strands accounted for 58% and 42% of that reduction, respectively). Calculation of accurate stiffnesses after the application of the CFRP material could not be done for Beam 1. It was necessary to move the entire beam before the repair process which resulted in slightly different bearing conditions that changed the beam stiffness. The remaining specimens were not moved during the repairs. It will be shown in later sections that the CFRP sheets have very little, if any, affect on beam stiffness.

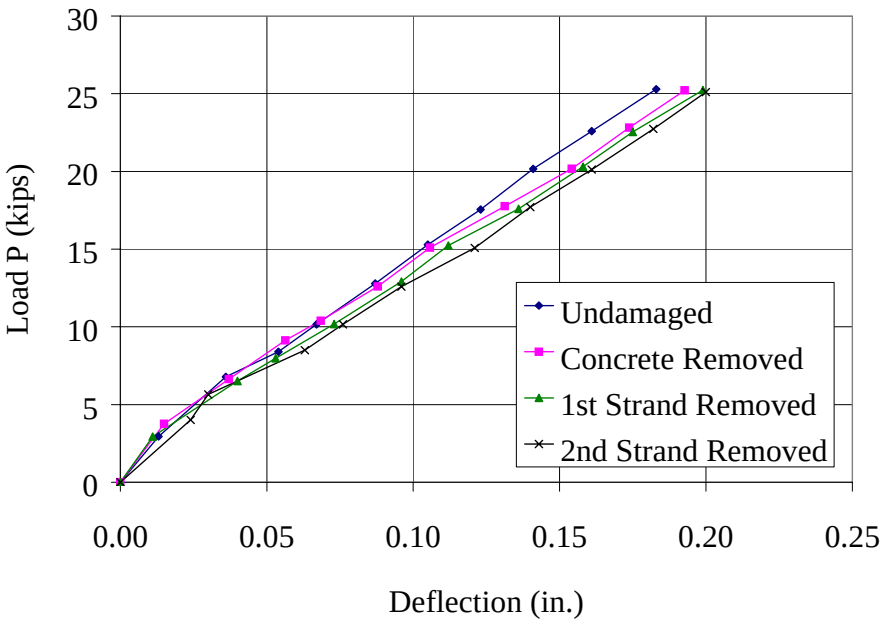

Figure 5.1. Load vs. centerline deflection for Beam 1 at different stages of damage.

5.1.2. Ultimate Strength Test – Beam 1

Beam 1 was damaged and repaired with two sheets of CFRP. A plot of the load/deflection behavior to failure is shown in Figure 5.2. Sheet debonding occurred at a load of 80.6 kips with a centerline deflection of 2.65 in. Note that the load P shown only represents one-half of the total load applied to the beam. Cracking occurred at a load of approximately 40 kips. This was about 31% higher than the predicted cracking load of 30.4 kips. The CFRP sheets and the epoxy tended to confine the concrete and increase the cracking load. After the section cracked, the behavior remained linear until a load of 55 kips. At this point, the prestressing strands began to yield. The CFRP sheets began to make small

popping noises at a load of approximately 75 kips. Vertical displacements along the length of Beam 1 at the centerline and quarterpoints are presented in Figure 5.3. The quarterpoint deflections remained symmetric up until debonding.

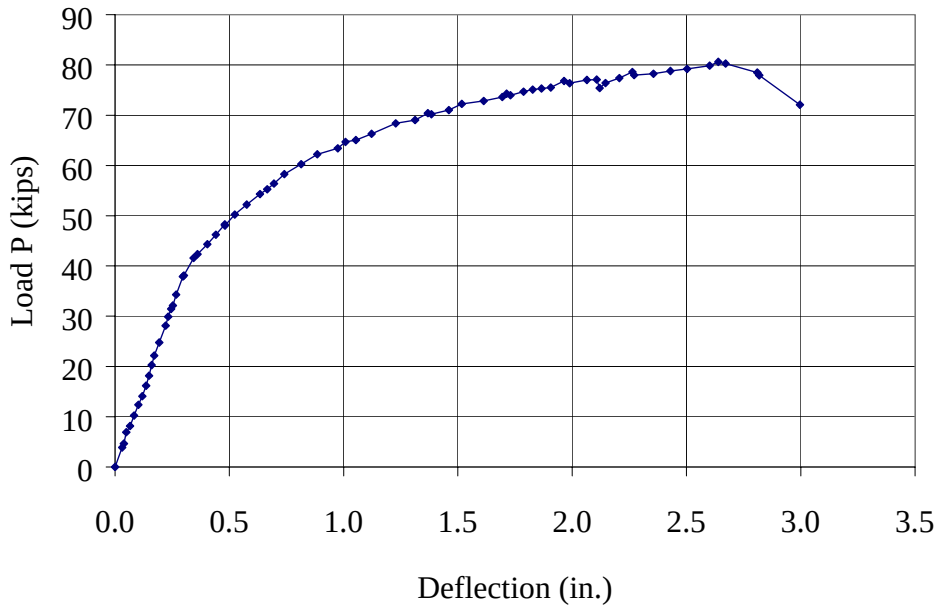

Figure 5.2. Centerline deflection of Beam 1 during the ultimate strength test.

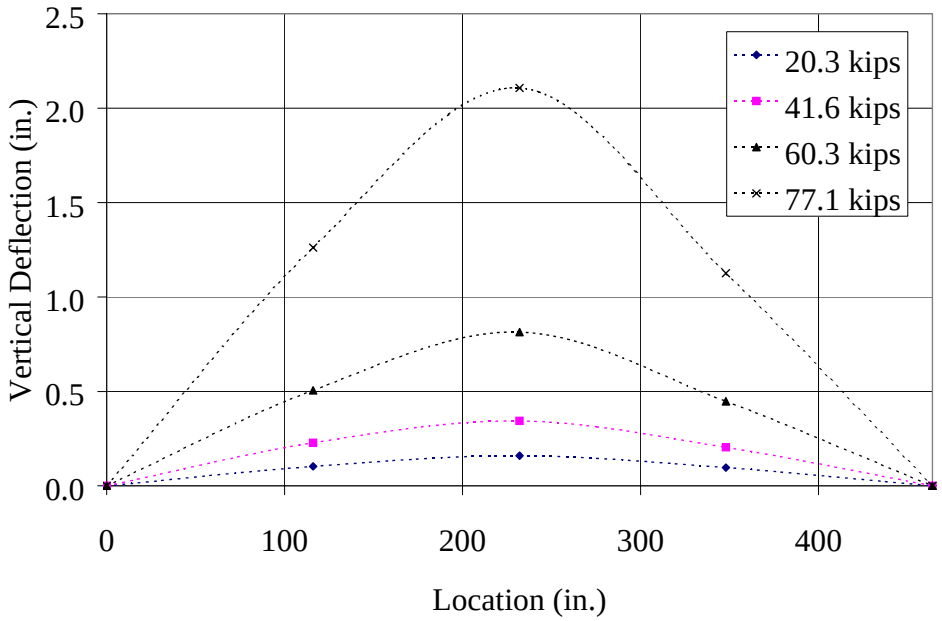

Figure 5.3. Vertical displacements along the length of Beam 1.

5.1.2.1. Sheet Debonding – Beam 1

As previously mentioned, failure was initiated by the debonding of the CFRP sheets which occurred at the CFRP/concrete interface. The debonding action started near the center of the beam and then quickly propagated to one of the ends. The large flexural cracks were likely the source of the sheet debonding. This sheet debonding process is idealized in Figure 5.4; it should be noted that the crack width and the relative vertical displacements were exaggerated in this figure to illustrate the behavior. As these vertical cracks opened in the P/C beam near the ultimate load, they produced small vertical displacements at each end of the crack (Δ_{tip}). These crack tip displacements resulted in a normal force or stress being applied to the CFRP sheets which caused the CFRP sheets pull away or "unzip" from the P/C beam. It is also possible that the patch contributed to the debonding problem as well. At failure, the beam curvature may have resulted in the patch material also producing a normal force on the CFRP.

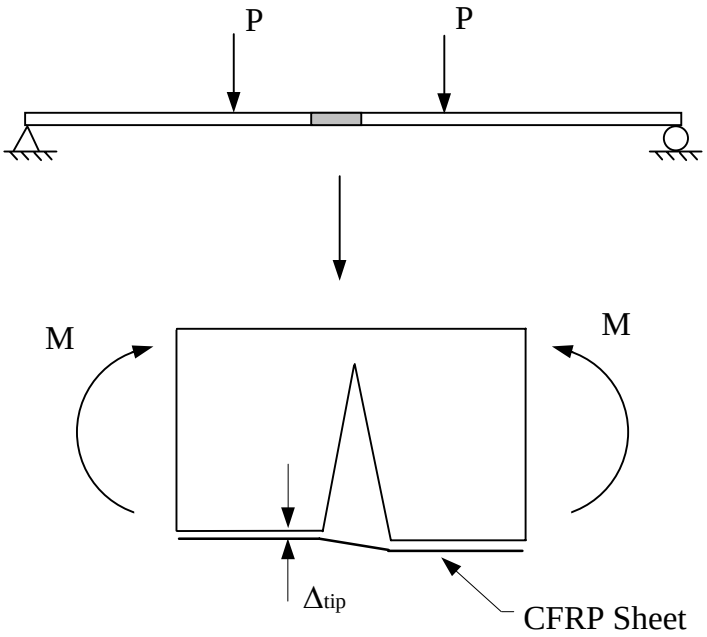

Figure 5.4. Idealized flexural crack with relative crack tip displacement.

The north side of Beam 1 after the debonding failure is shown in Figure 5.5. One-half of the CFRP material has completely debonded from the beam and is lying on the floor. The sheet debonding was characterized by a sudden failure. Almost instantaneously, one-

half of the CFRP material pulled away from the P/C beam. The only warning was small popping noises coming from the CFRP located at the center of the beam approximately 5 kips before failure. A large horizontal crack also formed in the patch material approximately 2 in. from the bottom edge of the beam. This horizontal crack did not become visible until after the debonding took place.

A small piece of patch material fell away from the beam at the end of the patch when the sheet debonded. A close-up of this section is shown in Figure 5.6. From this photograph, the flexural cracks can be followed through the patch material into the P/C beam. Large cracks developed around the entire perimeter of the patch and the bond between the patch and the beam was clearly broken. The piece of patch material that fell out was approximately 3 in. x 3 in. x 1 in. This piece did not fall out until the CFRP sheets debonded from the beam. The bottom side of Beam 1 after debonding is shown in Figure 5.7. Notice the large amount of concrete still bonded to the CFRP sheet (i.e. when the CFRP debonded, the sheet pulled a portion of the concrete substrate with it). This would indicate that the concrete was the weak link in the epoxy/concrete bond. The 6 in. lap splices in the CFRP sheets showed no sign of distress and performed well under the high loads.

Figure 5.5. North side of Beam 1 after sheet debonding.

Figure 5.6. Patch material after CFRP sheet debonding.

5.1.2.2. Strain Readings – Beam 1

Strain values along the CFRP sheets during various stages of loading are presented in Figure 5.8. Strain gages were placed at the centerline, quarter points, and termination points of the sheets (Section 3.1.2). The strain in the bottom of the beam was assumed to be zero at the ends. As shown in the figure, the strain values at the sheet termination points were very small. Even at the ultimate load, the strain at the end of the sheets did not exceed 200 MII. This is an indication that the sheets were properly detailed and installed thus avoiding debonding at the ends. The maximum-recorded strain value was approximately 4,300 MII at the beam centerline. The design strain specified by the manufacturer for the CFRP sheets was 16,700 MII. Therefore, the sheets only developed 26% of their design strength when failure occurred. Also, the strain values at the left quarter point (116 in. from left support) were considerably higher than those at the right quarter point. These values should have been equal due to beam symmetry. At failure, the strain values at the left quarter point were three times higher than the right quarter point. The theoretical strain at the quarterpoint with a load P of 41.6 kips was 230 MII ($M_{1/4}$=4,826 in - kips, c_b=24.88 in., E=4,800 ksi, and I_c=109,775 in^4), which agrees with the values measured at the right quarterpoint.

Figure 5.7. CFRP/concrete interface of Beam 1 after sheet debonding.

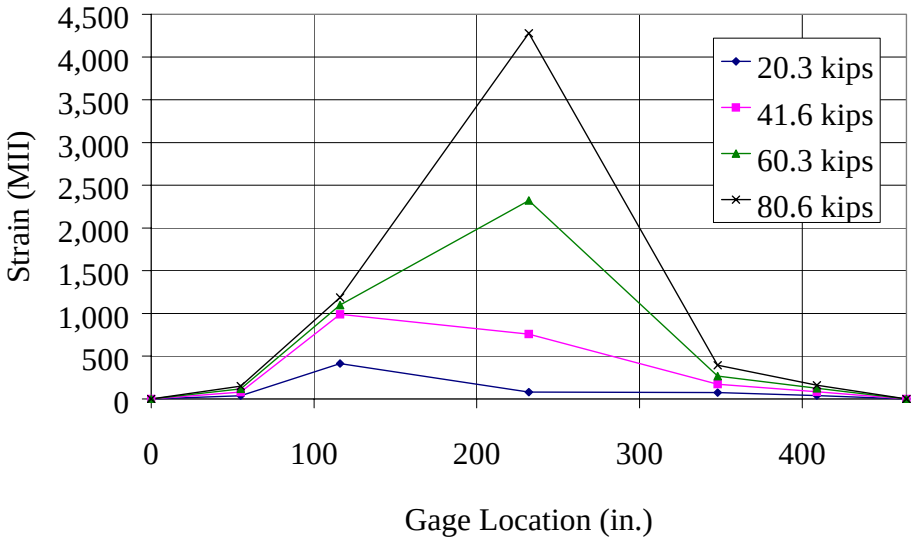

Figure 5.8. Tensile strains along the CFRP sheets in Beam 1.

These larger values at the left quarterpoint indicate some type of stress concentration in this area. As expected from these results, the debonding action initiated just left of the patch material.

Strain distributions at the centerline of Beam 1 are shown in Figure 5.9. The vertical axis represents the depth of the composite section with zero being the bottom or tension side of the beam. The strain values for all of the data points shown were obtained by averaging the readings from the strain gages at that location. Strain gage locations were shown in Section 3.3. As expected, the location of the neutral axis moved upward as the applied load was increased. At the failure load of 80.4 kips, the neutral axis was 8 in. from the top of the composite beam (bottom of the slab). Also, the average compressive strain in the extreme fiber was approximately 1,000 MII. This indicates that the full capacity of the concrete slab had not been reached at the time of debonding. The uncracked neutral axis was determined from experimental strain readings to be 22.6 in. from the bottom of the beam.

Strain distributions for Beam 1 at the left and right ends of the CFRP sheets are presented in Figures 5.10 and 5.11, respectively. At these two locations, strain gages were positioned on the top of the CIP concrete deck and on the CFRP sheets. A straight line was drawn between these points to obtain the strain distribution at these sections. Figures 5.10 and 5.11 are useful in verifying the location of the uncracked neutral axis. The neutral axis for Beam 1 was determined from the strain readings to be 23.7 in. from the bottom of the beam compared to the calculated neutral axis of 24.9 in. for the uncracked beam.

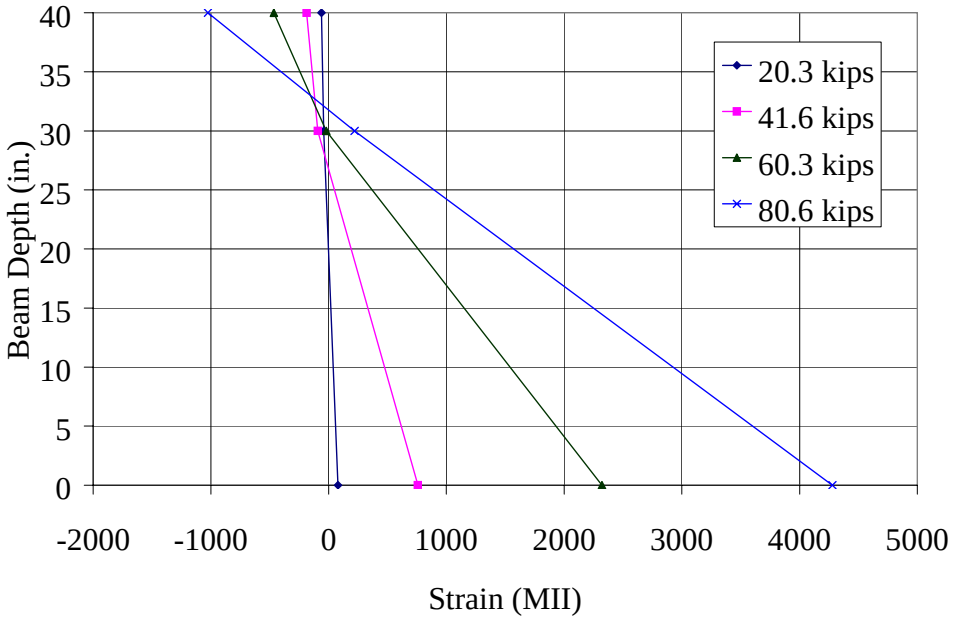

Figure 5.9. Strain distribution at the centerline of Beam 1.

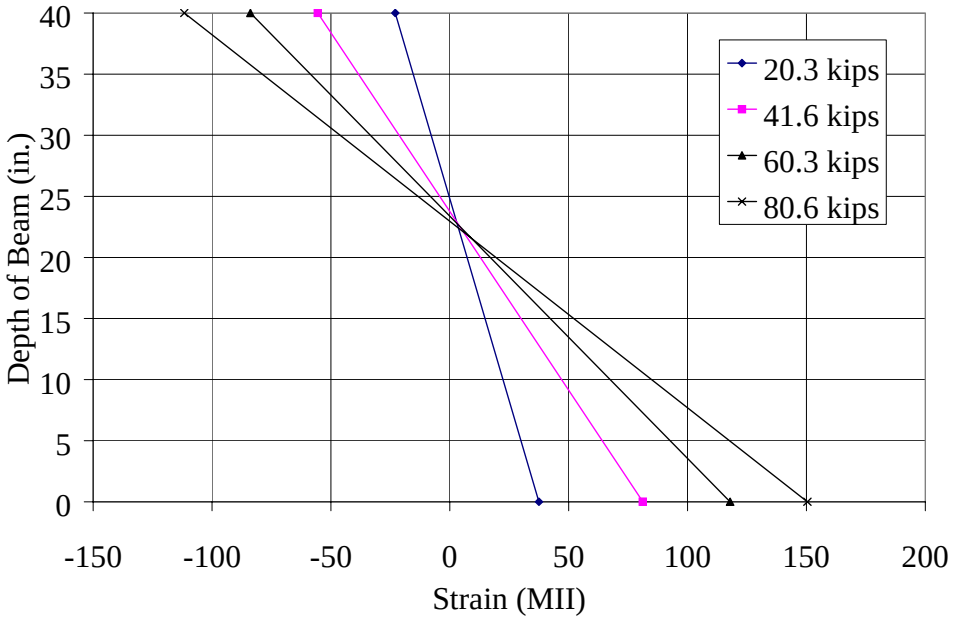

Figure 5.10. Strain distribution at left end of CFRP sheets in Beam 1.

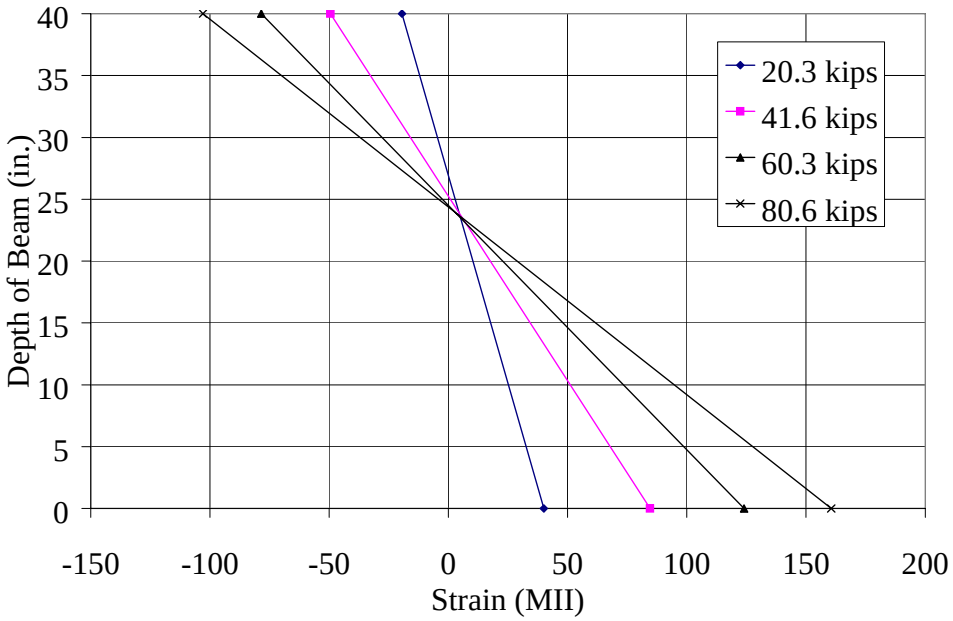

Figure 5.11. Strain distribution at right end of CFRP sheets in Beam 1.

5.2. Beam 2

Beam 2 was damaged and repaired using the same procedures and materials that were used for Beam 1. However, a CFRP jacket was also installed (See Section 4.6) in the area of the patch around the bottom flange. The intended purpose of the transverse fibers or jacket was to help prevent debonding of the longitudinal sheets and to confine the patch material.

5.2.1. Service Load Tests – Beam 2

As with Beam 1, Beam 2 was subjected to a series of service level loads after each damage level. The results of these tests are shown in Figure 5.12. The initial undamaged stiffness was 145.0 kips/in, slightly higher than Beam 1. The difference in undamaged stiffness values was most likely the result of slight changes of the support conditions. As with Beam 1, the stiffness values were based on the secant definition. Removing the concrete and severing two prestressing strands resulted in a 15.6% loss in beam stiffness (122.4 kips/in). After the repairs were made (patch and CFRP) another service load test was completed. Readings indicated that 38% of the lost stiffness was returned to the beam (131.1 kips/in). This increase was due to the patch material and not the CFRP sheets. The high bond strength of the patch restored a portion of the beam stiffness.

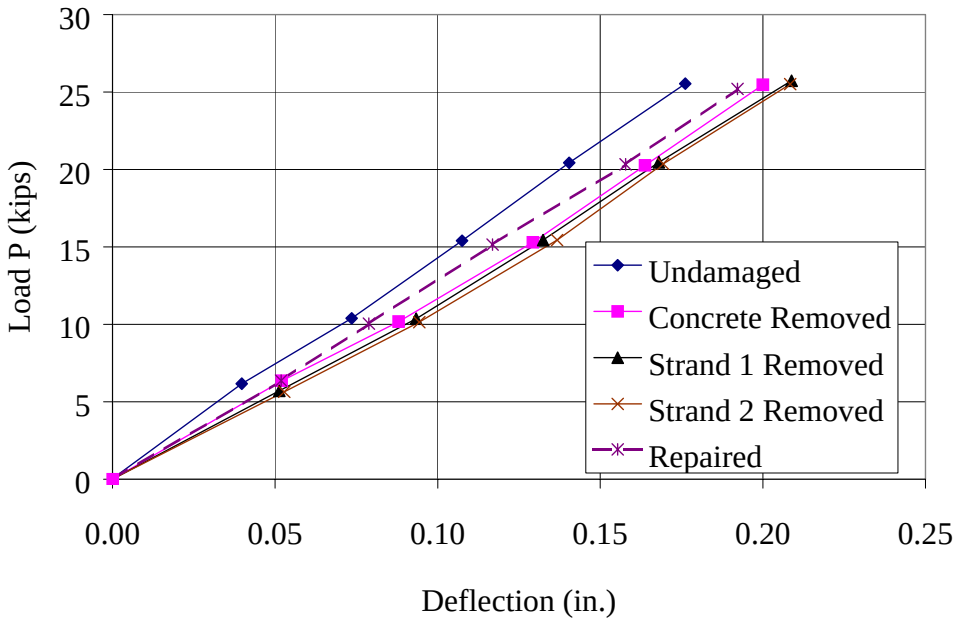

Figure 5.12. Load vs. centerline deflection of Beam 2 at various stages of damage.

5.2.2. Ultimate Strength Tests – Beam 2

Load/deflection results from the ultimate load test of Beam 2 are presented in Figure 5.13. For comparison the same results from Beam 1 are also plotted. Beam 2 reached a load of 83.6 kips before the longitudinal CFRP sheets debonded. This was a 3.7% increase in ultimate strength and a 13.1% increase in ductility compared to Beam 1. The CFRP jacket had only a moderate effect on the beam behavior. As shown in Figure 5.13, the curves for both beams were almost identical until approximately 75 kips. As with Beam 1, the load decreased suddenly when the CFRP sheets debonded. However, the jacket provided full containment to the patch at ultimate load. No patch material broke away from the beam at any stage of the loading.

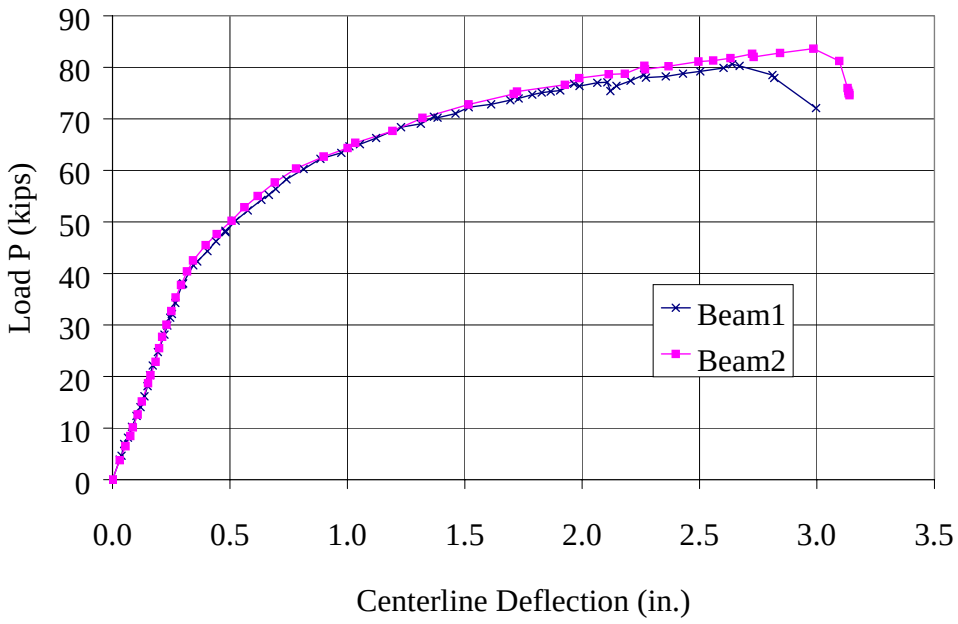

Figure 5.13. Load vs. deflection plots for Beam 1 and Beam 2.

5.2.2.1. Sheet Debonding – Beam 2

The CFRP sheet debonding exhibited by Beam 2 was very similar to Beam 1. Debonding was initiated by large flexure cracks near one of the load points and then quickly propagated to the left end of the beam. The location of these flexural cracks at a load P of 75 kips (90% of ultimate load) in relation to the CFRP jacket are presented in Figure 5.14.

At this level of load, the cracks extended half way through the top flange of the P/C beam. When failure occurred, the cracks were 2 to 3 in. into the 8 in. thick concrete slab. A close-up of the CFRP jacket after debonding occurred is presented in Figure 5.15. The debonded longitudinal fibers are clearly visible in the left-hand side of the photograph. Vertical flexural cracks extended through the CFRP jacket into the concrete web. The jacket obviously provided no strength to the beam in the longitudinal directions since the fibers were oriented in the transverse direction.

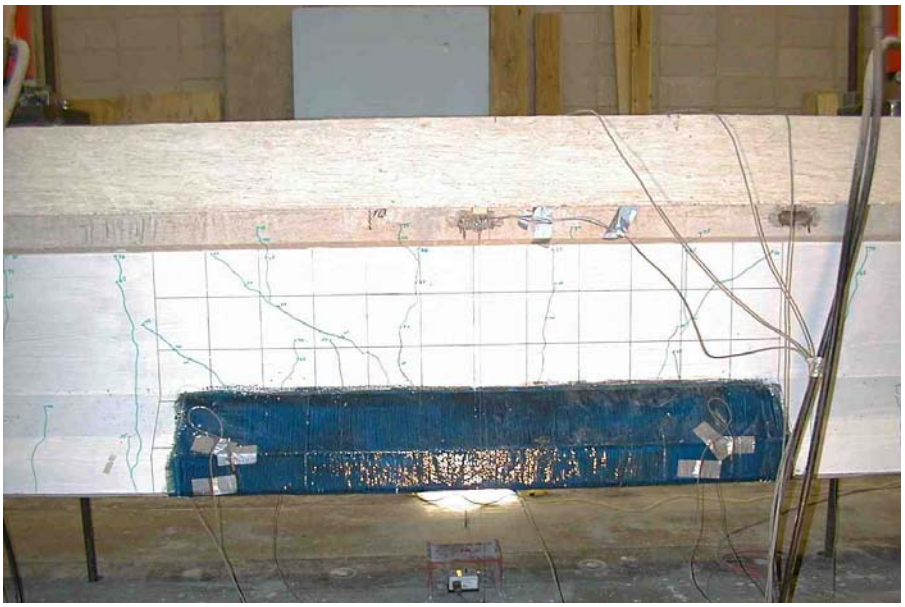

Figure 5.14. Crack pattern on the side of Beam 2 at 75 kips.

5.2.2.2. Strain Readings – Beam 2

The strain distribution at the centerline of Beam 2 at various depths in the ultimate load test are presented in Figure 5.16. The maximum tensile strain in the CFRP sheets at debonding was 5,500 MII (33% of the ultimate design strain). This represents a 28% increase in maximum tensile strain compared to the Beam 1 results. Another point of interest is the relatively low level of strain in the CFRP sheets at 60.4 kips. As shown in the graph, a large increase in tensile strains takes place between 60.4 kips and the ultimate load of 83.6 kips. This difference is evident when comparing the strains in Figure 5.16 with the strain

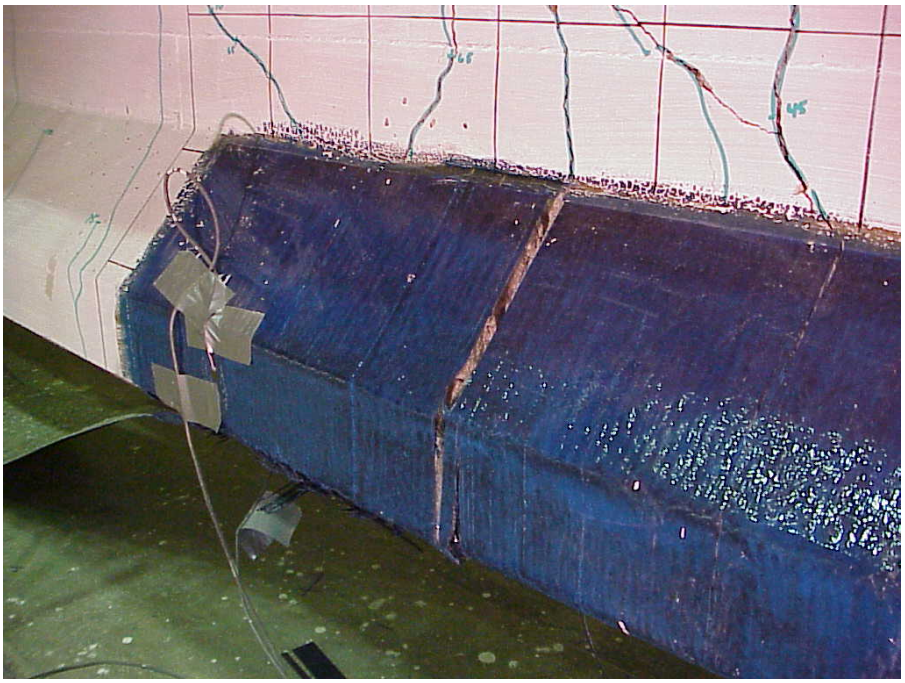

Figure 5.15. Close-up of cracks in CFRP jacket after failure of Beam 2.

distribution of Beam 1 in Figure 5.9. This rapid increase in tensile strain indicates that the CFRP sheets were not fully bonded with the P/C beam at 60.4 kips. The tensile strains along the CFRP sheets are shown in Figure 5.17. Again, the increase in midspan strains between the loads of 60.4 kips and 83.6 kips is apparent. However, the strain levels at the quarter points and the CFRP sheet termination points were symmetric for Beam 2.

The purpose of the CFRP jacket was to confine the patch material and to help prevent premature debonding of the longitudinal CFRP sheets. Strain readings from the strain gages placed on the CFRP jacket are presented in Figure 5.18. The four strain gages were oriented in the vertical direction with two gages on each side of the bottom flange of the P/C beam (Section 4.6.1.1). All of these gages clearly went into compression as the applied load was increased. This decrease in strain is due to the Poisson's ratio effect. Using the corresponding longitudinal strain results, the Poisson's ratio of the test specimen was found to be –0.22 at 30 kips (Note: Poisson's ratio for concrete is commonly taken to be –0.20). The jacket strains remained linear until the beam cracked at a load of 40 kips. Gages 1 and 3

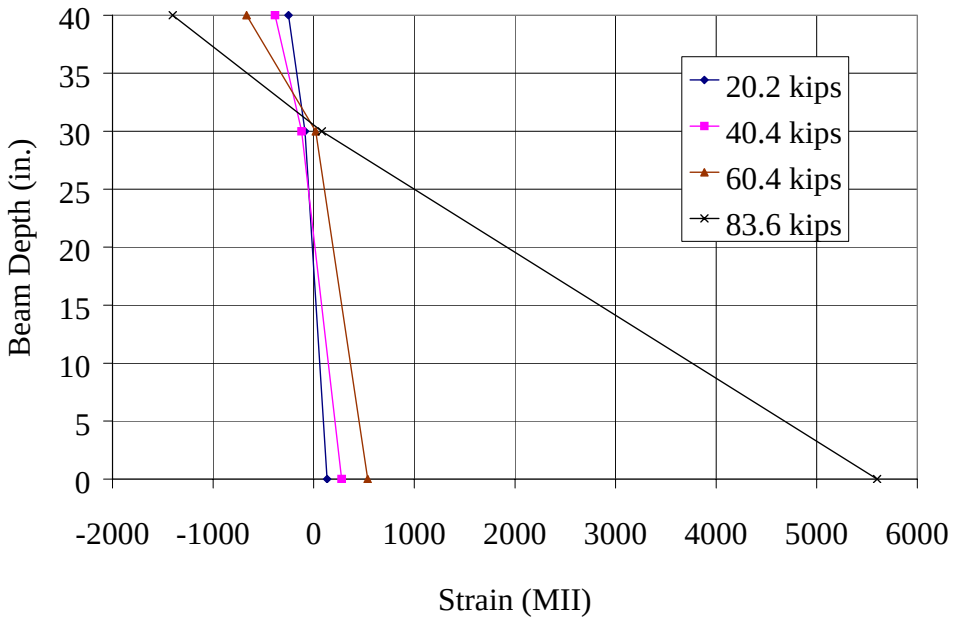

Figure 5.16. Strain distribution at the centerline of Beam 2.

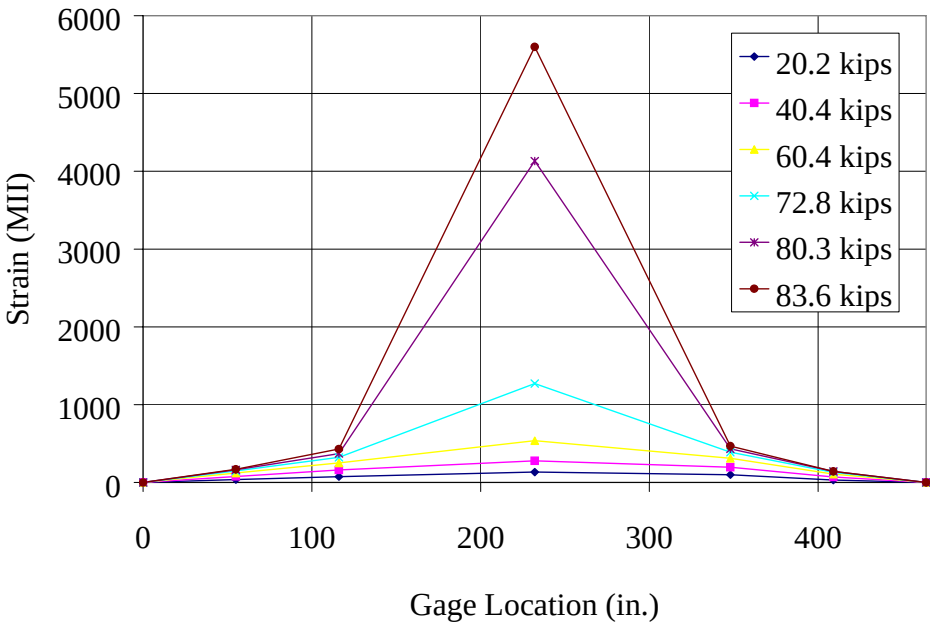

Figure 5.17. Tensile strains along the bottom of Beam 2.

were on the side of the beam with the two severed strands. Gages 2 and 4 were on the opposite side. It is interesting to note that in the linear range, the strain readings from the

undamaged side of the beam were slightly higher. This difference would indicate that a small amount of out-of-plane bending was taking place because of the simulated impact damage. Strain levels remained constant with small fluctuations between loads of 40 and 80 kips. However, rapid increases in jacket strains were present immediately before the longitudinal sheets debonded (83.6 kips). This would indicate that the jacket was carrying tension and resisting a portion of the normal force from the patch and/or longitudinal sheets. The maximum CFRP jacket strain at failure was close to 140 MII.

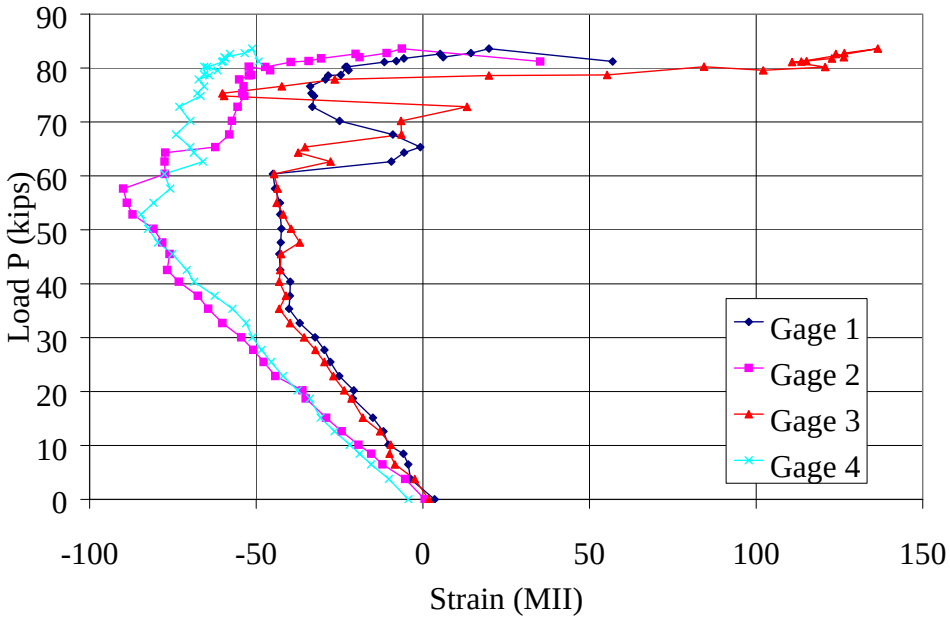

Figure 5.18. Strains on the CFRP jacket on Beam 2.

5.3. Beam 3

Beam 3 was designed to represent a bridge girder with a more severe level of impact damage than the first two beams. The beam was initially loaded on the bottom flange to produce cracking similar to a vehicle impact. Four prestressing strands were also severed (33% of the original flexural reinforcement). Beam 3 was then repaired using the same procedures used for Beams 1 and 2 except four layers of CFRP were required to restore the original flexural strength to the beam. A modified CFRP jacket was also used to prevent debonding of the longitudinal sheets at the load points.

5.3.1. Lateral Load

A lateral load was applied to the bottom flange of Beam 3 with the intention of creating the diagonal cracks typically found on the webs of impact damaged girders. The beam was rotated 90 degrees, and the load was applied at the bottom flange as illustrated in Figure 5.19. This test was completed before the composite slab was added because the overhead crane did not have the capacity to rotate the entire section. As shown in this figure, the applied force produced an equivalent weak-axis bending force and a torsional component.

The weak-axis test setup is shown in Figure 5.20. Each support was moved in 9 ft at the ends to produce an effective span of 21 ft – 4 in. This reduction in span length was done to minimize the vertical bending and amplify the torsional component of the applied force. A single hydraulic jack was used to apply the force at midspan. Steel plates were placed on the both sides of the top flange at the supports to support the beam. The steel plates were necessary because the width of the top flange was 4 in. narrower than the bottom flange. Unfortunately, this test setup did not produce the desired cracking pattern in the web. The weak-axis beam dominated the beam behavior and only vertical flexural cracks were visible. These flexural cracks extended to the mid-depth of the beam at the final load of 35 kips. There was also a 1/4 in. of permanent deformation at midspan indicating that the strands opposite the applied load had yielded.

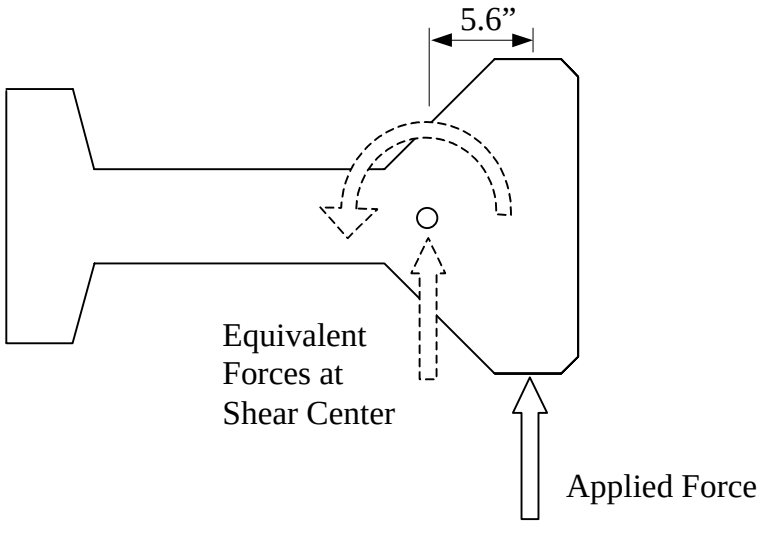

Figure 5.19. Location of the applied force and the corresponding equivalent forces.

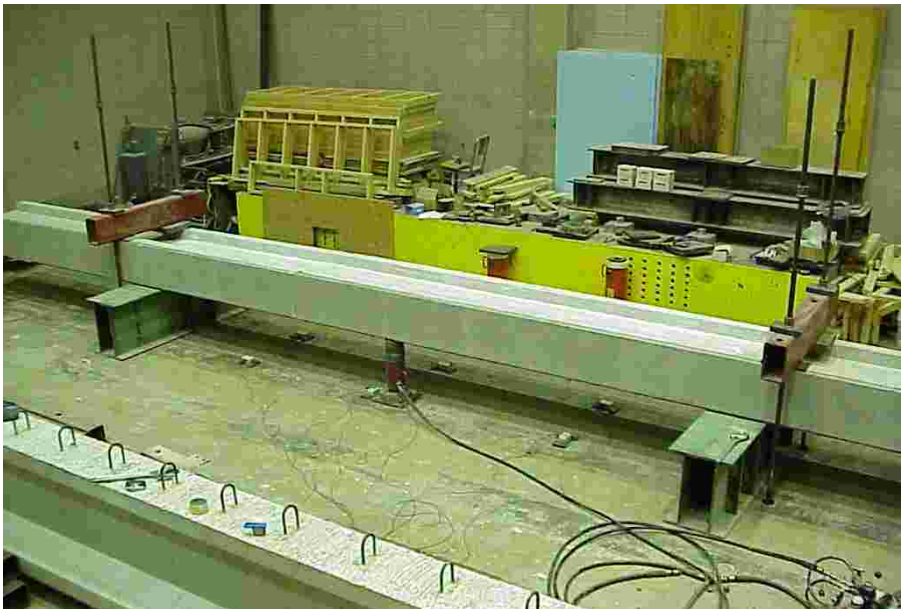

Figure 5.20. Weak-axis test setup for Beam 3.

5.3.1.1. Beam 3 Damage

After the lateral load was removed, the P/C beam was rotated back to the original upright position and a composite concrete slab was cast as described in Section 3.1.1. The portion of concrete removed from the bottom flange is shown in Figure 5.21. The damage shape was slightly different from Beams 1 and 2 (Section 3.4) and was intended to take the shape of a typical vehicle impact. As before, this profile was maintained for 3 ft along the length of the beam (1 1/2 ft on each side of the centerline). Four prestressing strands (33% of the original flexural reinforcement) were severed to represent a more severe vehicle impact.

5.3.2. Service Load Tests – Beam 3

The results for the Beam 3 service levels tests with the varying amount of damage is shown in Figure 5.22. As with the previous two tests, a service load of 25 kips was applied to the beam after each damage stage. An undamaged load case was not available for Beam 3 because the lateral load was applied to the bottom flange before the composite slab cast. The initial beam stiffness after the concrete was removed was measured to be 159.9 kips/in. As

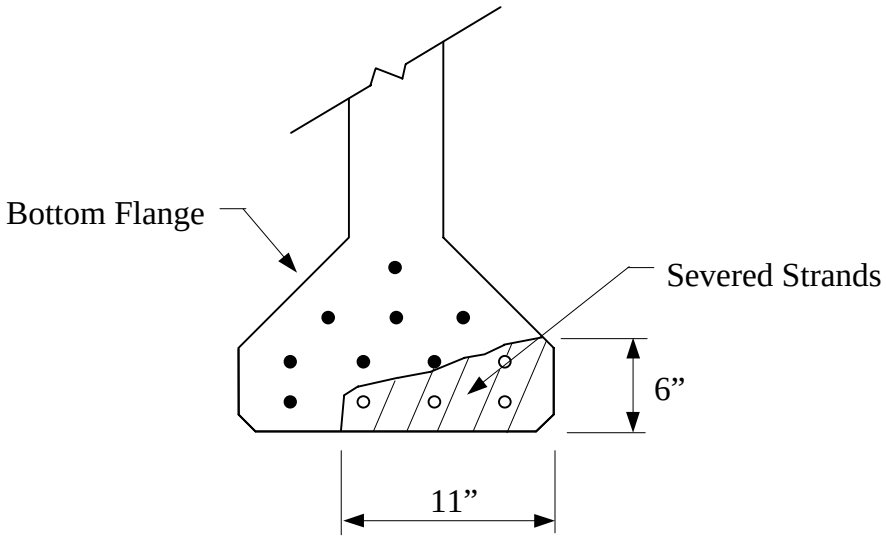

Figure 5.21. Beam 3 damage, four prestressing strands removed.

expected, the beam stiffness decreased slightly after severing each of the four prestressing strands. The beam stiffness decreased incrementally to 141.9 kips/in (11.3% from 159 kips/in) after all of the prestressing strands were severed. Only two of these four service level tests are shown in Figure 5.22 for clarity. The beam stiffness increased to 151.4 kips/in after the damaged beam was patched and strengthened with four layers of CFRP. This increase in stiffness was similar to the response of Beam 1 and 2 after strengthening. As previously discussed, this increase in stiffness was attributed the patch material and not the CFRP.

5.3.3. Ultimate Strength Test – Beam 3

Load/deflection results from the ultimate load test of Beam 3 are presented in Figure 5.23. The load/deflection curves for Beams 1 and 2 are also included to show the relative behavior of beams with two prestressing strands severed. Beam 3 cracked at a load of 32 kips (8 kips less than Beams 1 and 2). This was 46% higher than the predicted value for a composite beam with four severed strands. The increase in the calculated cracking load was consistent with the results from Beams 1 and 2. After the beam cracked, the behavior remained linear until the prestressing steel began to yield at a load of approximately 58 kips. The ultimate capacity of Beam 3 was 75.5 kips with a centerline deflection of 2.59 in. This

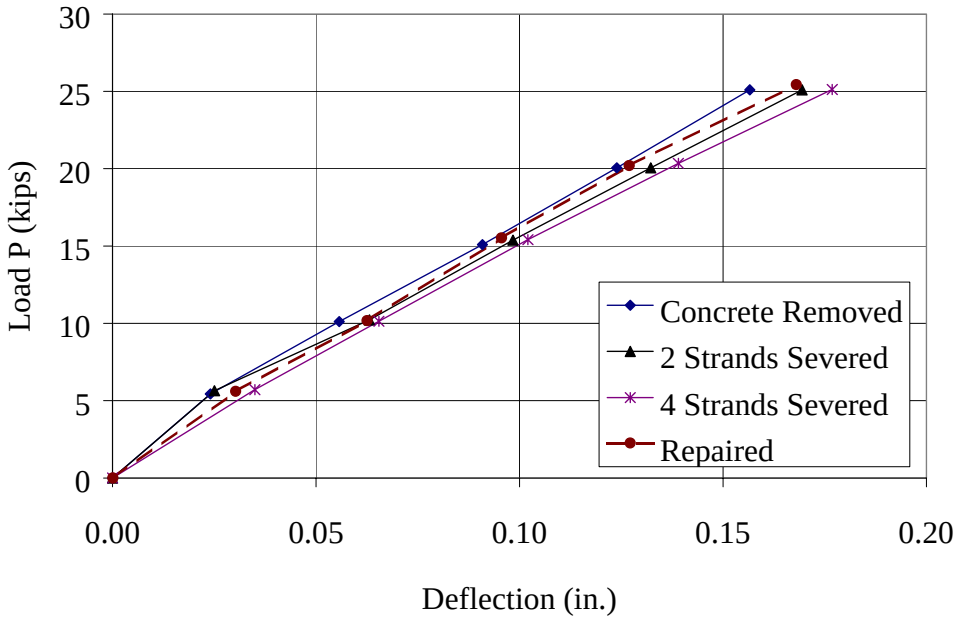

Figure 5.22. Load vs. centerline deflection of Beam 3 at various stages of damage.

ultimate capacity was 22.4% higher than the predicted strength (54.0 kips) for an unstrengthened beam with four severed strands but was still 11.7% under the original beam strength (86.7 kips). Approximately 66% of the lost beam strength was recovered by the carbon fiber sheets. As with Beams 1 and 2, failure was initiated by the longitudinal CFRP sheets debonding from the bottom of the beam. Cracking noises before the sheets debonded indicated that the debonding started at the load point and moved out towards the support.

5.3.3.1. Sheet Debonding – Beam 3

The four layers of CFRP after they had debonded from the bottom flange of the P/C beam are shown in Figure 5.24. The debonding process was very similar to that in the first two beams. CFRP pulled away from the beam suddenly at one end of the beam with very little warning. Soft cracking noises were the only indication that the sheet was going to debond. The 6 in. lap splices connecting the individual pieces making up each layer of longitudinal CFRP performed very well and did not show any signs of distress. Large amounts of concrete were also pulled away from the beam with the CFRP indicating the concrete was the controlling factor in the bond.

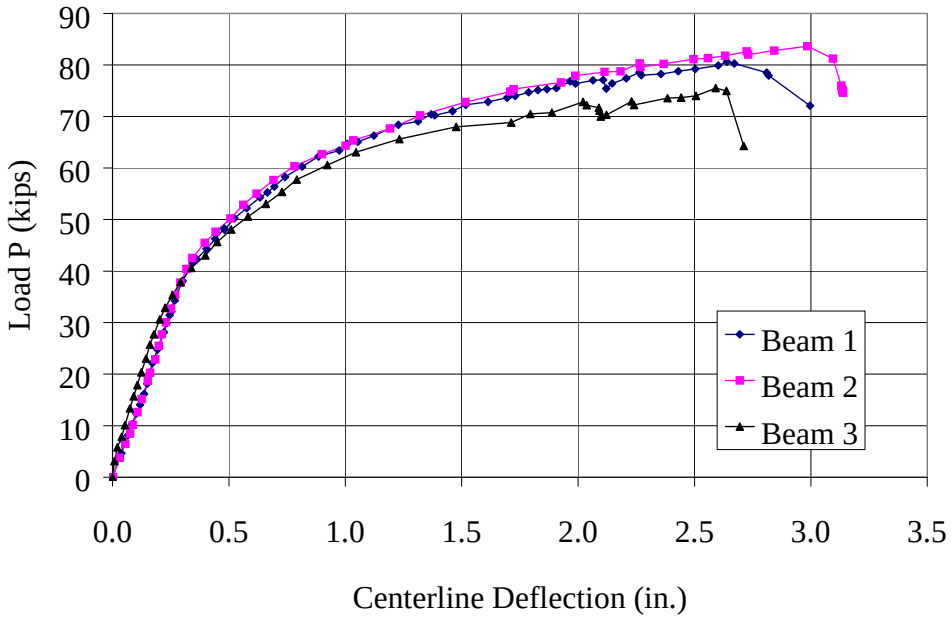

Figure 5.23. Load vs. deflection plots for Beams 1, 2, and 3.

Figure 5.24. Debonded longitudinal sheets on Beam 3.

The CFRP jacket near center span after the ultimate test was completed is shown in Figure 5.25. Flexural cracks and local delaminations were present on both sides of the web. These local delaminations developed at isolated locations near the web/bottom flange interface at approximately 70% of the ultimate capacity (60 kips). These types of local debonding problems did not occur in the Beam 2 CFRP jacket. The jacket on Beam 2 stopped 2 in. short of the web (Section 4.6.1). Tension in the jacket will result in a normal force between the CFRP and concrete at the bottom flange/web interface. The results from the second and third beams tests suggest that CFRP jackets should terminate short of the web unless the jacket is required to increase the shear strength of the section.

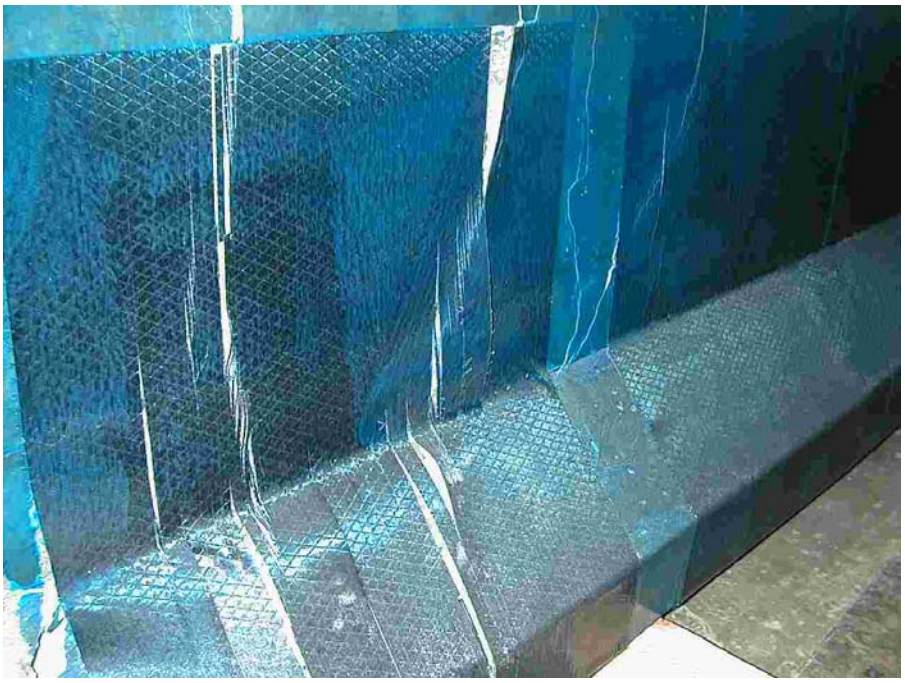

Figure 5.25. CFRP jacket cracks and local delaminations on the web in Beam 3.

5.3.3.2. Strain Readings – Beam 3

The strain distribution along the centerline of Beam 3 is shown in Figure 5.26. The elastic neutral axis was found to be 24.4 in. from the bottom fiber of the composite section using the strains compared to the theoretical value of 24.3 in. At failure, the neutral axis was at the bottom edge of the slab or approximately 8 in. from the top of the beam. The average

compressive strain in the top of the slab when the CFRP sheets debonded from the beam was 1,660 MII. The design procedure assumed that the CFRP rupture would be the controlling factor in the flexural design and predicted a maximum compressive strain of 1,800 MII. There was also a significant increase in the tensile strains at midspan between 40.6 kips and 60.6 kips indicating that the CFRP did not fully engage when a large portion of the live load was applied.

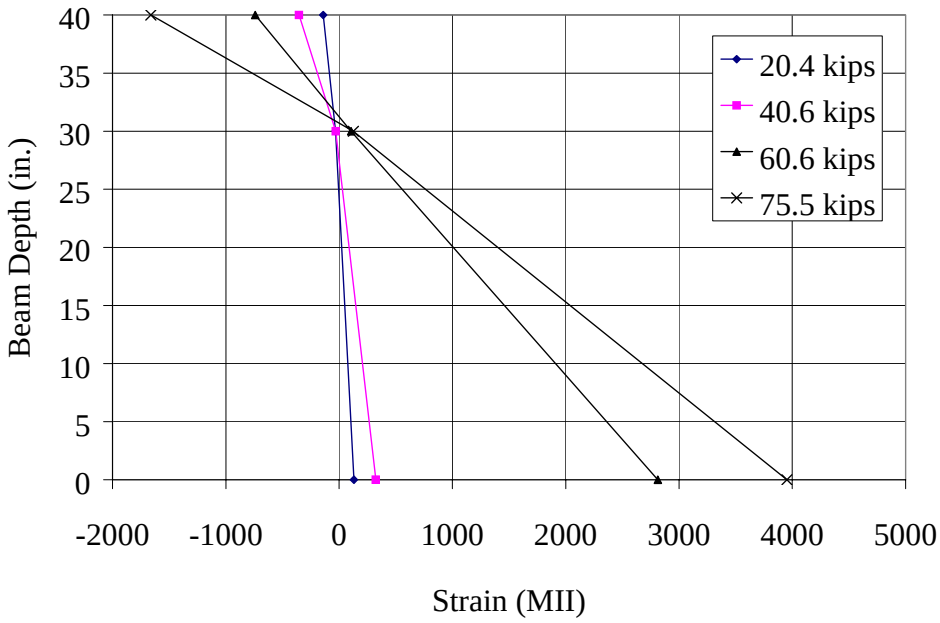

Figure 5.26. Strain distribution along the centerline of Beam 3.

Tensile strains in the CFRP sheets along the length of Beam 3 at various levels of loading are presented in Figure 5.27. The maximum-recorded tensile value was 4,150 MII, or 25% of the design strain specified by the manufacturer. For comparison, the maximum recorded values for Beams 1 and 2 were 4,300 and 5,300 MII, respectively. The CFRP sheets debonded to the right of the beam centerline and was consistent the first two beam failures. The spike in Figure 5.27 at the gage location marked 348 in. (circled) most likely created a stress concentration that initiated the debonding process.

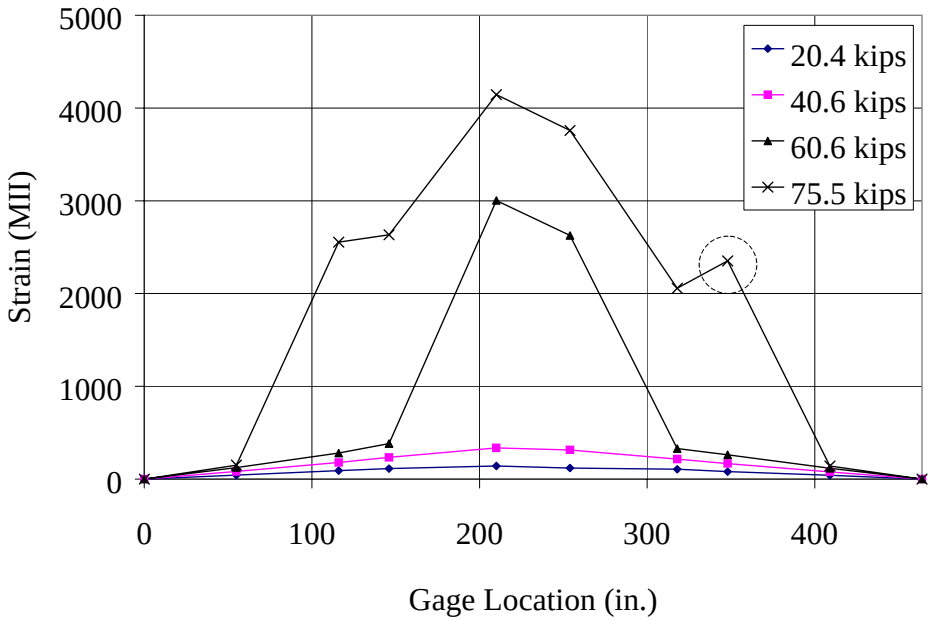

Figure 5.27. Tensile strain readings along the CFRP in Beam 3.

5.4. Beam 4

Beam 4 was damaged and repaired using CFRP. Two layers of longitudinal CFRP sheets, 30 ft long, were attached to the bottom flange with epoxy. A transverse wrap about half that length was then wrapped around the bottom; it extended from just under the top flange on one side to just under the top flange of the other side in the center portion (7.67 ft) of the beam.

5.4.1. Service Tests

Service tests were performed before and after the prestressing strands were cut. Two tests were performed on the undamaged beam, followed by another after two of the prestressing strands were cut. The service load was 25 kips which is lower than the cracking load. Data were taken at intervals of 1 kip. Once the concrete area was removed, it was difficult to get a good center deflection reading, thus the quarter point deflections are presented in Figure 5.28. The deflection increased slightly (0.002 in.) due to the cutting of the tendons and loss of concrete.

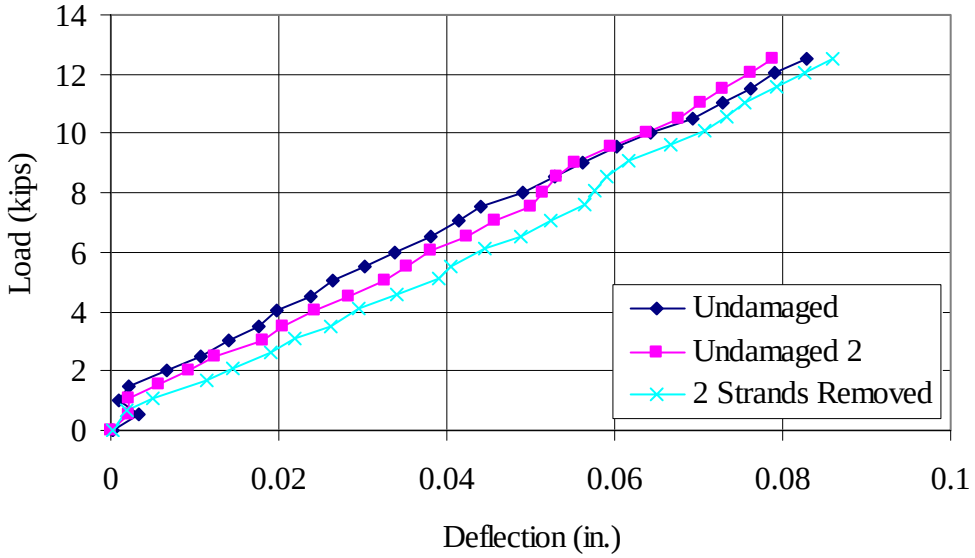

Figure 5.28. Load vs. center line deflection during strand removal.

The stiffness of the undamaged beam (as determined using the secant modulus definition at the highest service load of 25 kips) was 107.1 kips/in. The damaged beam had a stiffness of 103.7 kips/in, which shows some decrease, which can be attributed to the damage. The stiffness calculations appear to give smaller than normal results compared to the previous beams, and this is due to the steel tubing that was used as supports for the simply supported beam. During loading, the steel tubing deflected a small amount and altered the stiffness from the secant modulus definition. This deflection was measured during subsequent tests. Celescoes were later attached near the supports to measure this deflection so it could be subtracted from the mid-span deflection. The final stiffness with the patch and CFRP was 114.07 kips/in. that includes the support subtractions.

5.4.2. Degradation

The beam was cyclically loaded with a loading range of 2 to 58 kips at a rate of 0.7 cycles per second. The load range was not high enough to crack the beam. (The load range was based on information from previous static load tests that was misinterpreted, thus the load range was half of what it was supposed to be. The error was discovered after the cyclic loading was completed.) Cyclic loading was stopped and service tests were performed at various loading increments, approximately 150,000 cycles. The test was stopped after 2.2

million cycles. The centerline deflections from three of these service tests, approximately a million cycles apart, are shown in Figure 5.2. It was clear that there was no degradation due to the cyclic loading, also there was no noticeable debonding of the CFRP due to the loading.

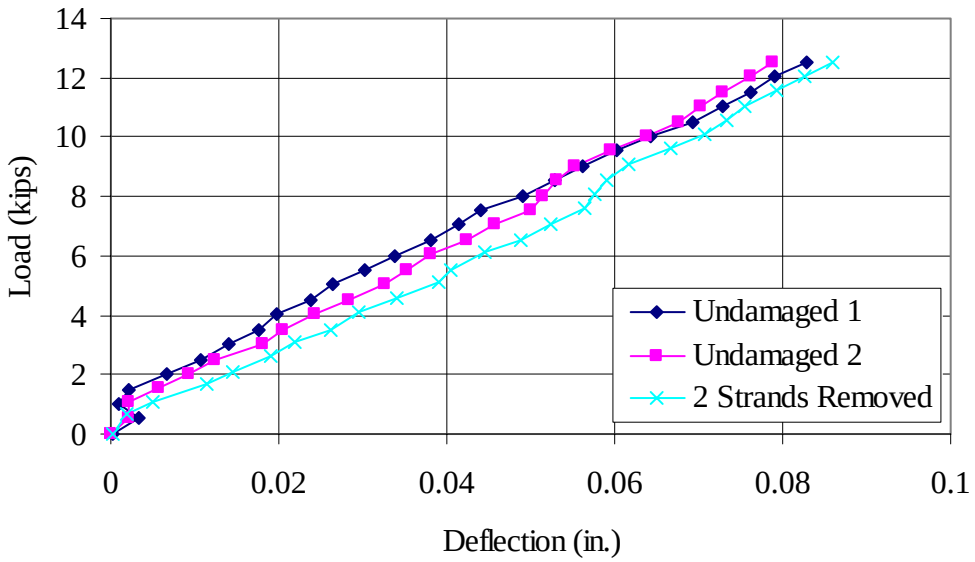

Figure 5.29. Load vs. centerline deflection in Beam 4 after 0,1, and 2 million cycles.

5.4.3. Ultimate Test

After completing the cyclic loading and the service tests, Beam 4 was statically loaded to failure. Figure 5.30 shows the ultimate load test deflection results. Cracking of the beam occurred at approximately 44 kips. With increased loading, the CFRP sheets began to make popping noises at approximately 75 kips. The load peaked once at 89.2 kips per actuator before it decreased slightly. The mid-span deflection at this point was 3.42 inches. The load then increased to 89.4 kips before major failure occurred. Failure resulted when the CFRP caused the concrete to delaminate. Concrete was still attached to the CFRP after failure indicating that the epoxy bond was not the cause of the failure.

The deflection just prior to failure was 3.61 inches. The total applied load of 178.8 kips was higher than previous tests of similar CFRP reinforced beams. A similar beam tested with the same longitudinal CFRP and a wrap only around the bottom flange of the beam reached 167.2 kips before failure. Thus, the additional wrap length up the entire web of the

beam more than likely helped reach this higher load. This repaired beam was more ductile than previously repaired beams as it reached a deflection of 3.61 in. before failure occurred. The largest failure deflection for the previous tests was approximately 3.0 in. As shown in Figure 5.31, the deflections were symmetrical about the centerline of the beam prior to failure, which reflects the symmetric loading conditions.

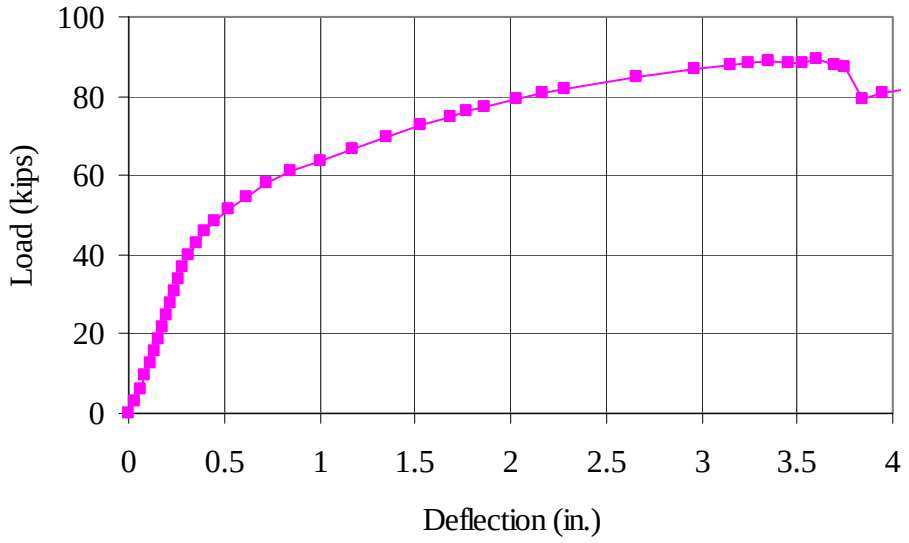

Figure 5.30. Load vs. centerline deflection for ultimate test of Beam 4.

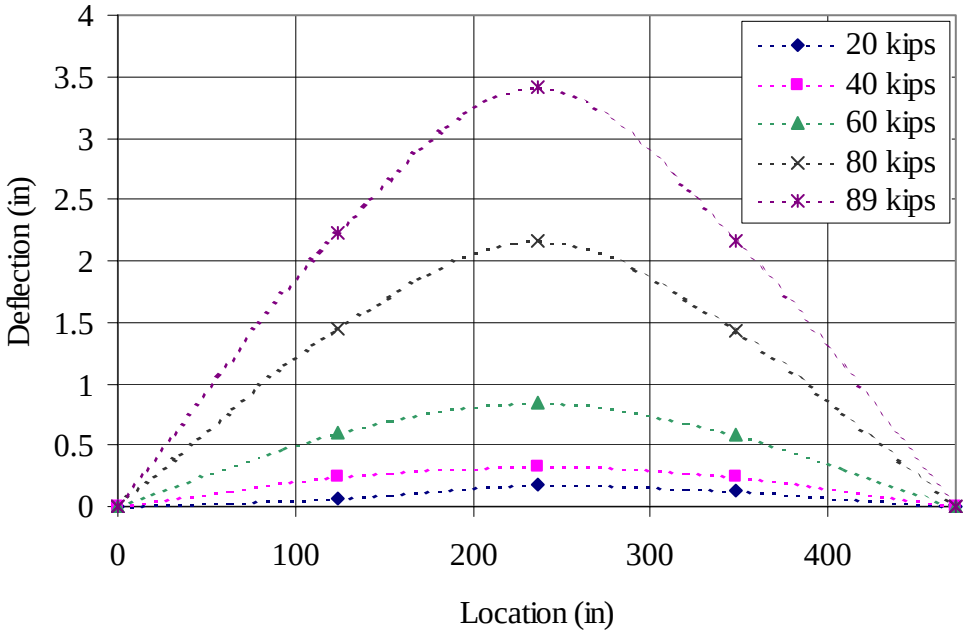

Figure 5.31. Vertical displacements along the length of Beam 4.

5.4.3.1. Strains

The strains in the longitudinal CFRP reached a maximum of 5,850 MII at the failure load. The maximum strains measured in previous laboratory beam ultimate tests were 5,300 MII or less. Perhaps the full web wrap again helped to prolong the delamination allowing the CFRP to carry higher strains. The design strain for the CFRP sheets as stated by the manufacturer was 16,700 MII. Obviously, with the CFRP only reaching 35% of its design tensile capacity, it was not the cause of failure. The longitudinal strains in the CFRP are shown in Figure 5.32.

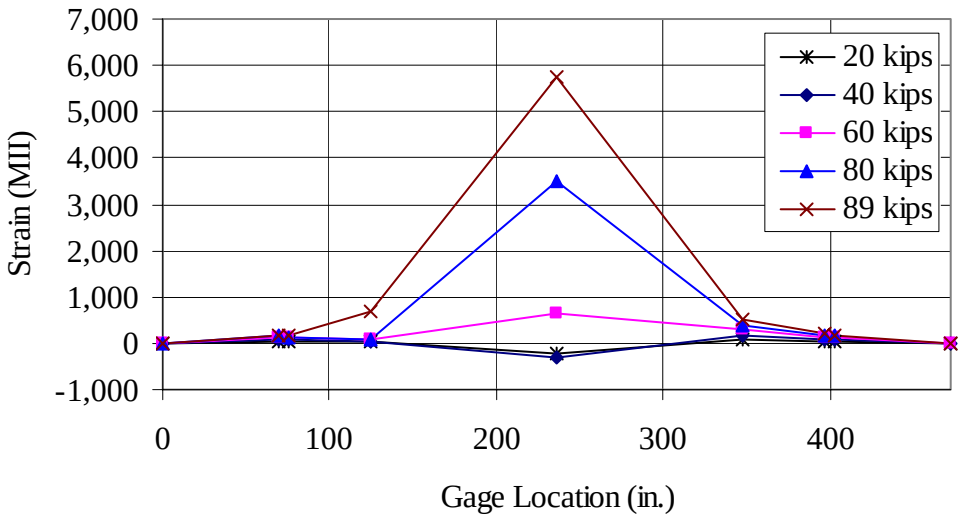

Figure 5.32. Tensile strains along the CFRP sheets in Beam 4.

The strains appear to be quite symmetric under the symmetric loading conditions. Although at one of the quarter points, the increase in strain from the 80 kip load to the 89 kip load looks larger than the increase at the other quarter point. This could be an indicator of an eventual failure mode. The strains near the termination points of the CFRP were still quite low, 194 MII at failure, therefore, debonding near the end of the CFRP was not a cause of failure.

Strain distribution through the depth of the composite beam is shown in Figures 5.33-35. The top of each graph is the top of the concrete deck. As seen in Figure 5.33, the neutral axis location at the center of the beam was 7 in. below the top of the deck during the final stages of loading, while the neutral axis location at the quarter points was approximately 15

in. from the deck top throughout the test. The extreme compression fiber at the centerline of the beam reached a strain of 1,350 MII indicating that the concrete's full compressive strength had not been reached.

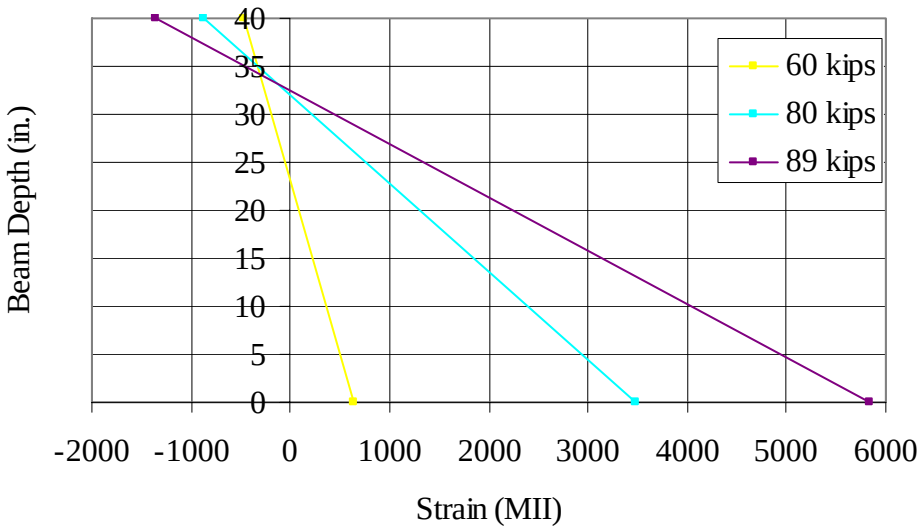

Figure 5.33. Strain distribution at centerline of Beam 4.

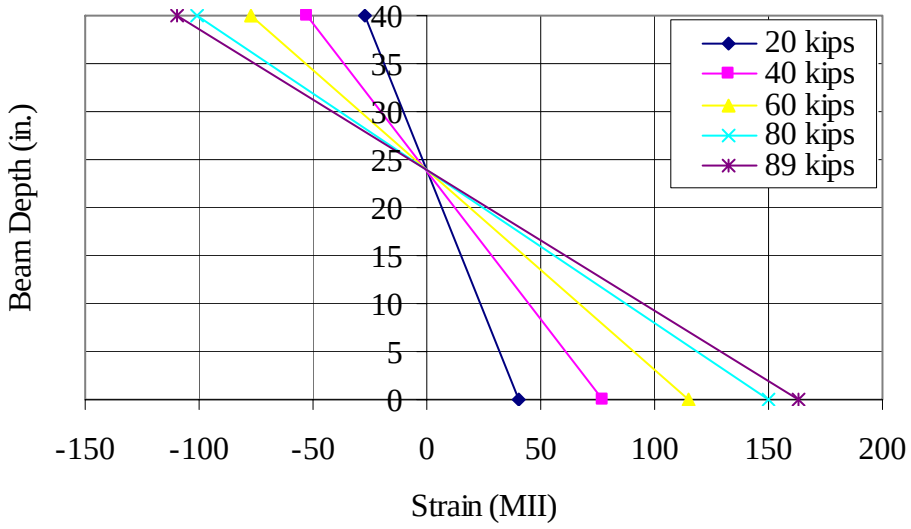

Figure 5.34. Strain distribution at left quarter point of Beam 4.

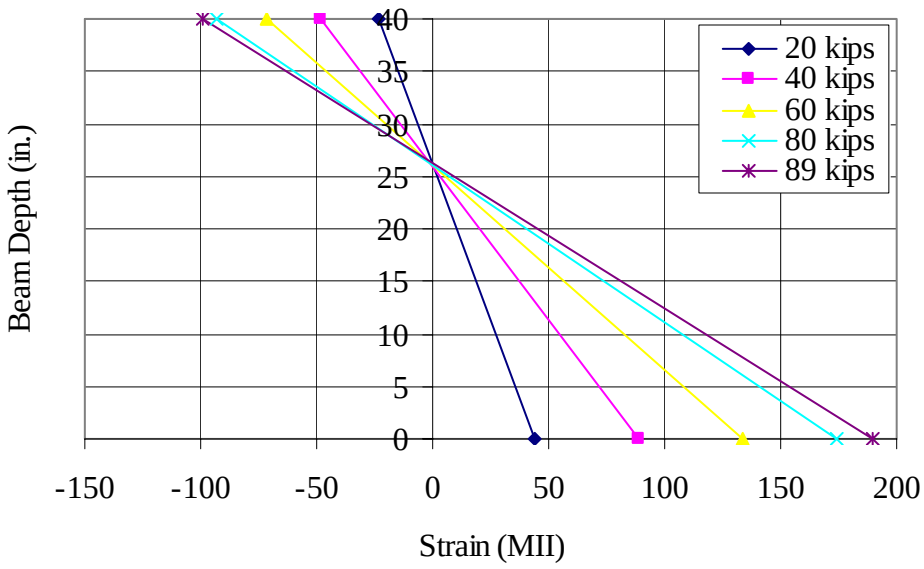

Figure 5.35. Strain distribution at right quarter point of Beam 4.

5.5. Prestressing Strands – Beams 1, 2, and 3

One concern with repairing impact damaged P/C girders is the possibility of increased stress levels in the remaining undamaged prestressing strands. Significant increases in service level stress range of prestressing strands can result in potential fatigue problems. Previous work involving conventional repair techniques (Section 2.2) has shown that a relatively small amount of strand damage can significantly decrease the expected fatigue life of the remaining prestressing strands. However, these findings were based on tests with precracked P/C beams. Fatigue of the prestressing strands is not a concern for uncracked girders (Overman, 1984; Muller, 1994; and Rao, 1996). The purpose of the following service tests was to verify that the stress ranges of the strands do not significantly increase in an uncracked beam with typical impact damage. The beams used for this project were uncracked at the time of the service load tests as they were new and in good condition. Furthermore, the cracking load of the composite beams was not exceeded at any time during the service load tests. This was later verified from the load/deflection data from the ultimate strength tests. During the ultimate load tests, all of the beams exhibited a change in the slope of the load/deflection curves.

In order to determine the magnitude of the strand stresses, strain gages were placed on exposed prestressing strands after the concrete was removed (Section 3.1.3.3). Two strain gages labeled A and B were placed on each of the four exposed bottom layer strands. Strain readings were taken at a service level load of 25 kips before any of the strands were severed to obtain initial readings. Strain readings were also taken after each subsequent severing of strands. The results from these tests are shown in Table 5.1. Strain levels in the initial tests were all fairly close to the average strain values indicating that live load was equally distributed to all of the prestressing strands. The average strain readings for the three beams under the full service load was 304 MII, which correlated well with the calculated strain value of 293 MII. The dash marks in the table indicate which strands were severed and in which order. The total change in the service level strain levels for Beams 1 through 3 were -20 MII, 7 MII, and 7 MII, respectively. Increases of these magnitudes do not represent a long-term fatigue problem for repaired P/C girders. These tests confirm that strand fatigue is not an issue for uncracked P/C girders in the field.

Strain readings in the prestressing strands were taken immediately after the individual strands were severed. Values shown in Table 5.2 are only due to the redistribution of internal forces after each strand was cut (i.e. no live load was applied to the beam). The average strain readings in the severed strands was 4,387 MII in compression. This value represents the effective prestressing strain in the strands at the time of the tests. Converting the axial strain to stress results in an effective stress of 125 ksi (MOE = 28,500 ksi) as the strain in the strands is in the elastic range. The “x” in this table denotes gages that were most likely lost due to excessive vibrations when the prestressing strands were severed. Beam 2 was the only specimen that displayed a significant change in strains after the strands were severed.

It is noted that the total average strain in the strands instrumented decreased as a result of cutting two strands (Beams 1 and 2). The total average strain slightly increased (9.3 MII) when four strands were severed. (Beam 3). The total change in strain in the prestressing strands at service loads was calculated by adding the changes in strain from Tables 5.1 and 5.2. Total percent changes in strain levels in the prestressing strands for the three beams were -0.7%, -2.2%, and 0.4%, respectively. The results from these tests indicated that no significant increases in strand stresses occurred when two strands were severed (i.e. a 17%

reduction in strand area) or four were strands severed (i.e. a 33% reduction in strand area). However, significant increases in strand stress would occur if the sections were cracked.

Table 5.1. Strains in prestressing strands under service load of 25 kips.

Beam 1	1A	1B	2A	2B	3A	3B	4A	4B	Average	Diff.
Initial	328	339	319	297	310	301	305	302	313	-
1st Strand	-	-	352	300	323	321	311	302	318	6
2nd Strand	-	-	-	-	313	243	314	302	293	-25

Total = -19 MII

Beam 2	1A	1B	2A	2B	3A	3B	4A	4B	Average	Diff.
Initial	332	265	323	324	300	290	314	292	305	-
1st Strand	-	-	325	324	307	272	326	332	315	10
2nd Strand	-	-	-	-	315	293	291	346	311	-3

Total = 7 MII

Beam 3	1A	1B	2A	2B	3A	3B	4A	4B	Average	Diff.
Initial	320	419	291	285	323	239	224	261	295	-
1st Strand	-	-	307	315	369	283	228	282	297	2
2nd Strand	-	-	-	-	309	338	215	311	293	-4
3rd Strand	-	-	-	-	-	-	298	307	302	9

Note: All strains are in MII. Total = 7 MII

Table 5.2. Strains readings in prestressing strands after severing.

Beam 1	1A	1B	2A	2B	3A	3B	4A	4B	Average
1st Strand	x	-5151	7	-27	-22	-85	-7	-11	-24
2nd Strand	-	-	-3823	-4598	8	19	13	13	13

Total = -11 MII

Beam 2	1A	1B	2A	2B	3A	3B	4A	4B	Average
1st Strand	-4015	x	-27	-30	-76	-69	-129	-68	-66
2nd Strand	-	-	-4802	x	-40	-44	-45	-16	-36

Total = -102 MII

Beam 3	1A	1B	2A	2B	3A	3B	4A	4B	Average
1st Strand	-4576	x	15	32	8	48	-10	11	17
2nd Strand	-	-	x	-3573	12	-11	-18	-78	-24
3rd Strand	-	-	-	-	-4806	-4491	0	32	16
4th Strand	-	-	-	-	-	-	-4032	x	-

Note: All strains are in MII. Total = 9 MII

5.6. Modulus Beams Results

The following section describes the results of the modulus beams tests described in Section 4.7. A total of six modulus beams were tested. Three of beams were left unreinforced and the other three were strengthened with a single layer of CFRP. The test results from one of the unreinforced modulus beams were disregarded due to poor correlation. Each beam was tested to failure at a static load rate of 200 lbs per second. Centerline deflection and applied load was recorded for all modulus specimens. A single DCDT was used to record the vertical deflections at midspan. Strain levels were also monitored for those beams strengthened with CFRP sheets. A single strain gage was positioned in the center of the each specimen directly on the CFRP. The distance from the centerline of a support to the centerline of a load point (i.e. shear span) was 9.75 in.

The load vs. deflection plot from the modulus beams is shown in Figure 5.36. The two unreinforced beams failed suddenly when the concrete cracked at an average load value of 2.02 kips. Using basic mechanics, the cracking load was estimated to take place at 1.92

kips. The beams strengthened with CFRP had a cracking load 35% higher than the unreinforced beams. The cracking load of the strengthened modulus beams was

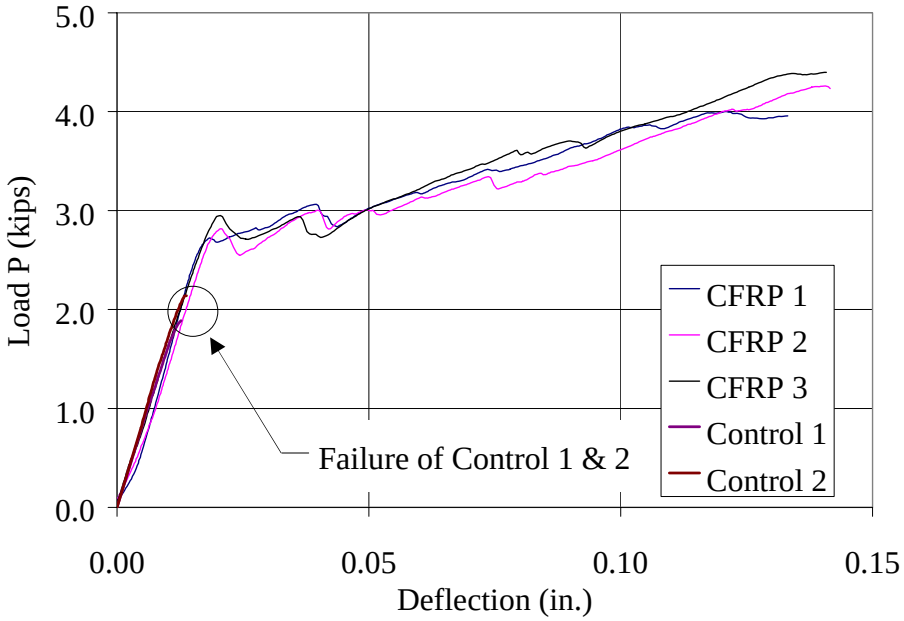

Figure 5.36. Load vs. deflection curves for modulus beam tests.

characterized by an abrupt change in slope. This increase in cracking load as a result of adding CFRP has also been reported by Shahawy and Beitelman (1996). They found that the cracking load tends to increase from 12 to 105% with the number of CFRP sheets. There was also no significant difference in the initial stiffness of the strengthened and unreinforced beams. Both groups had an initial stiffness of approximately 160 kips/in using the secant modulus definition. The CFRP sheets used to strengthened the beams were so thin (0.0065 in.) that they would not have a significant influence on the moment of inertia of the section. However, the average ultimate capacity of the strengthen beams was a 110% more than that of the unstrengthened beams (i.e. those not reinforced). Debonding at the CFRP/concrete interface was the mode of failure for all of the beams.

The load vs. strain behavior for the three modulus beams strengthened with CFRP is shown in Figure 5.37. All three of the beams cracked at approximately 300 MII. After cracking, the tensile strains increase rapidly until the average failure strain of 4,460 MII was reached. This corresponds to only 27% of the specified ultimate strain of the CFRP sheets.

It is interesting to note that the average ultimate strains in the CFRP on the P/C beams is also 27% of the ultimate specified design strain. Therefore, it may not be possible to reach the design rupture strength specified by the manufacturer. The maximum values for load, deflection, and CFRP strains occurring in the modulus of rupture tests are summarized in Table 5.3. The beams labeled Control 1 and 2 were not strengthened with CFRP, therefore no strain data was available for these two beams.

Table 5.3. Maximum values from modulus beam tests.

Beam Designation	Load P (kips)	Deflection (in.)	Strain (MII)
CFRP 1	3.96	0.133	3,706
CFRP 2	4.24	0.142	5,546
CFRP 3	4.40	0.141	4,632
Control 1	1.89	0.013	-
Control 2	2.14	0.014	-

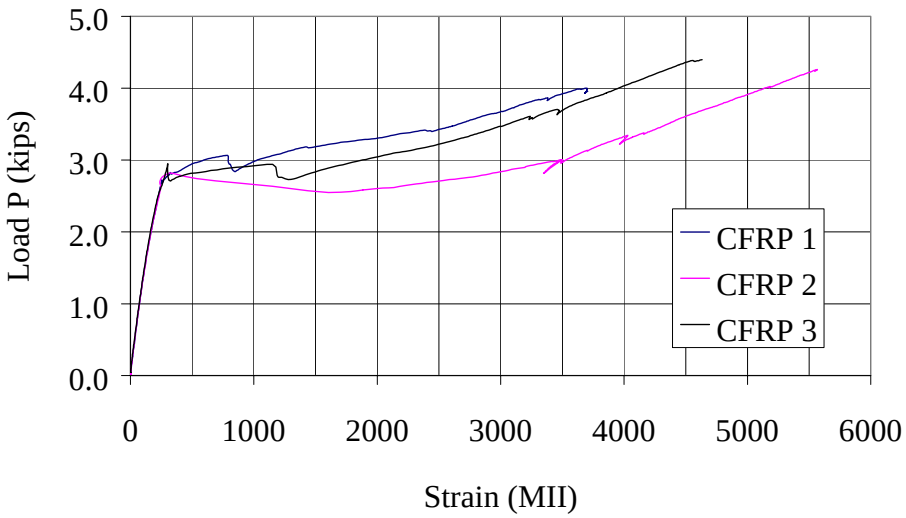

Figure 5.37. Load vs. strain for modulus of rupture beams strengthened with CFRP.

Photographs of a failed modulus of rupture beam strengthened with CFRP are presented in Figures 5.38 and 5.39. The photographs shown are representative of all of the

beams strengthened with CFRP sheets. The failure planes for all of the beams started at a point outside the constant moment region and traveled at an angle to one of the load points. The angled failure plane indicates that shear a factor in the beam failure. For comparison, the modulus beams not strengthened with CFRP failed on a nearly vertical plane. The CFRP sheets also pulled off a layer of concrete from the bottom of the beams when they debonded. As mentioned before, this is an indication that the concrete was the controlling factor in the bond strength.

5.7. P/C Beam Summary

A summary of the results from the ultimate load tests of the beams strengthened with CFRP is presented in Table 5.4. In this table, the column labeled P_{live} is the maximum live load applied to the beams at each of the two load points. This load was converted to a live load moment (M_{live}) and added to the dead load moment (M_{dead}) of the composite beam to determine the ultimate capacity of the section (M_n). Recall that four strands were severed on Beam 3 instead of the two strands severed on Beams 1, 2, and 4. The increased level of damage explains the reduced moment capacity of Beam 3, although with more CFRP sheets

Figure 5.38. Strengthened modulus of rupture beam immediately after failure.

Figure 5.39. Modulus of rupture beam positioned to show the debonding surface.

the capacity should have been higher. The debonding of the CFRP sheets prior to reaching their ultimate capacity was a factor that led to the lower capacity. As shown in Table 5.5, these experimental capacities were compared to the theoretical capacities for both the damaged and the strengthened beams. The predicted ultimate flexural capacity of an undamaged beam was 1,421 ft-kips.

As shown in Table 5.5, the predicted strength of all of the strengthened beams exceeded the flexural strength of an undamaged beam. Premature debonding of the longitudinal CFRP sheets prevented the beams from developing their full repaired design strengths. However, the majority of the undamaged beam strength was restored in Beams 2 and 4. The transverse CFRP jacket helped to increase the capacity and ductility of the section. The jacket also provided full patch containment at service and ultimate loads. For the more severely damaged Beam 3, approximately 65% of the lost flexural strength was recovered by the CFRP sheets.

Table 5.4. Moment results from beam tests.

Beam Description	P^*_{live} (kips)	M_{live} (ft-kips)	M_{dead} (ft-kips)	M_n (ft-kips)	% of Undamaged Beam Strength
Beam 1 (2 Sheets) 2 strands cut	80.6	1,195	135	1,330	93.6%

Beam 2 (2 Sheets & Jacket 1) 2 strands cut	83.6	1,240	135	1,375	96.7%
Beam 3 (4 Sheets & Jacket 2) 4 strands cut	75.5	1,120	135	1,255	88.3%
Beam 4 (2 Sheets & Jacket 3) 2 strands cut	89.0	1,320	135	1,455	102.3%

* The total load is twice this value.

Table 5.5. Predicted nominal moment strengths.

Beam Description	P_{live} (kips)	M_{live} (ft-kips)	M_{dead} (ft-kips)	M_n (ft-kips)	% of Undamaged Beam Strength
Undamaged Beam	86.7	1,286	135	1,421	100.0%
Damaged Beam 1, 2 & 4	70.3	1,042	135	1,177	82.8%
Strengthened Beam 1, 2 & 4	90.7	1,345	135	1,480	104.2%
Damaged Beam 3	54.0	801	135	936	65.9%
Strengthened Beam 3	96.0	1,423	135	1,558	109.6%

5.8. Altoona Bridge Test Results

Two tests were performed on the damaged bridge over Highway 6. The first test (Fall, 2000) was conducted after an over-height vehicle had damaged the bridge. The second test (Spring, 2001) was performed after the damaged area had been repaired with a mortar patch, epoxy injections, carbon fiber plates, and a carbon fiber wrap described in Chapter 4. The tests consisted of a static portion, with 32 different load cases, and a dynamic portion.

5.8.1. Damaged Bridge Test

The initial testing was performed weeks after the bridge had been damaged. No repair, retrofit, or epoxy injections had taken place prior to this testing. The results from these tests are compared to results of the following test, which was performed after the bridge had been repaired.

5.8.1.1. Load Distribution Behavior

Figures 5.40 through 5.42 show strains and deflections at mid-span of the damaged bridge for Load Cases 13, 19, and 23 (see Table 3.5). Two loaded trucks were placed at various locations along the bridge to measure the strain and corresponding deflection in the beams prior to the CFRP repair. The trucks weighed a combined 102,200 lbs (see Table 3.4). The plots reference the static load cases shown in Table 3.5. These load cases were chosen

because they caused the largest strains and deflections at mid-span from two truck loading. The data plots in all three cases show a nearly normal distribution of load among all the beams, except for jump or dip in strain visible on all three strain graphs. Several factors were considered when trying to explain the behavior of the structure but no conclusion was finally settled upon. Initially a faulty strain gage was suspected, but an extra strain gage was placed near the existing gage on Beam 5 and it gave similar results, so the abnormal strain curve was left without a logical explanation. The bridge must have been distributing the load in an unusual fashion.

A distribution factor (based on design assumptions) of 0.66 was calculated for the bridge using the 1996 AASHTO LFD Bridge Design Specification with one lane loaded. A value of 0.31 was computed in Beam 2 from the strain readings of the damaged bridge test, and a value of 0.27 was computed from the deflection data for the same beam. These values were taken from load case 13, which caused the highest strains in Beam 2. The actual load distribution factor of the bridge was lower than the design distribution factor. The maximum strain Beam 2 reached was 49 MII which is much less than the 185 MII that was calculated using the AASHTO distribution factor. It appears that the other beams could be assuming some of the load or that the distribution factor is quite conservative.

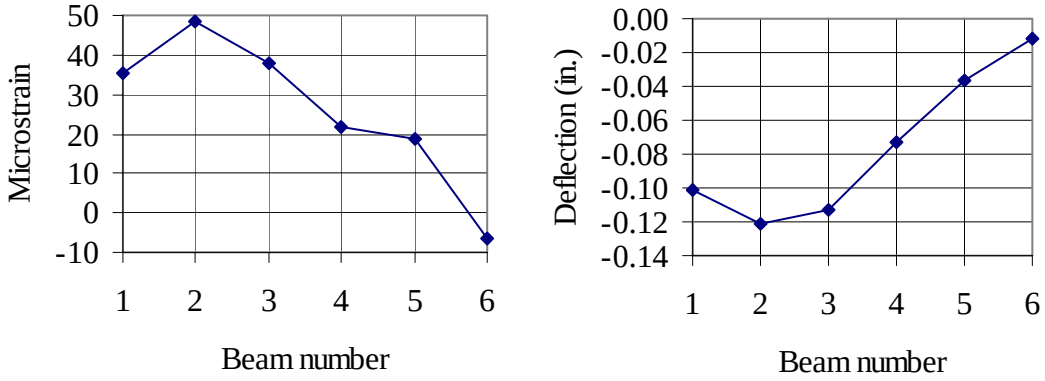

Figure 5.40. Strain and deflection in the Altoona Bridge for Load Case 13.

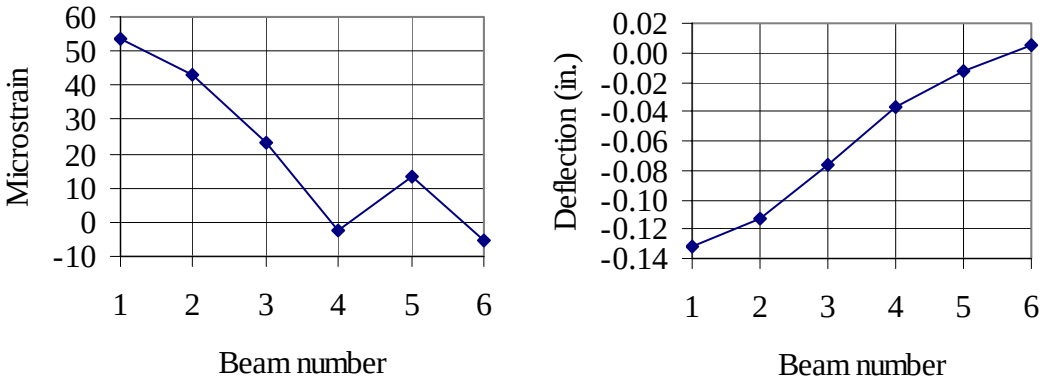

Figure 5.41. Strain and deflection in the Altoona Bridge for Load Case 19.

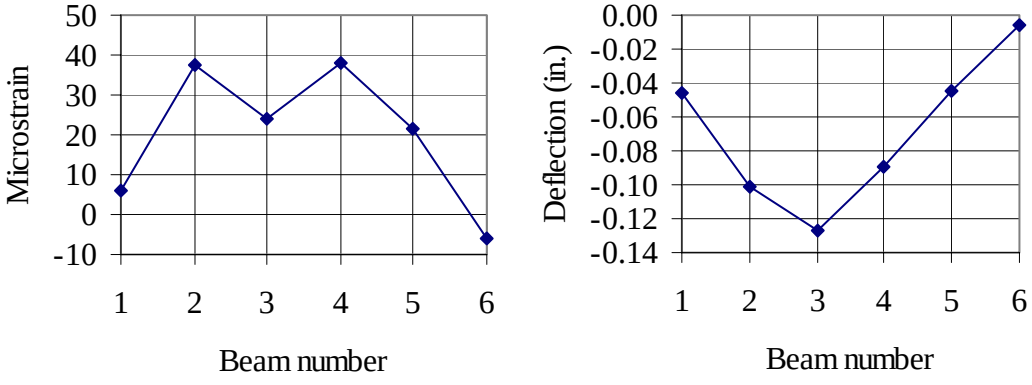

Figure 5.42. Strain and deflection in the Altoona Bridge for Load Case 23.

5.8.1.2. Longitudinal Behavior

Figure 5.43 through 5.45 show the strain at the center of span 2 as a function of truck position for a single truck was placed at five locations along the length of the bridge, and when both trucks were side-by-side at the same five locations. By doing this, the behavior of the more heavily damaged girder can be compared with two girders that only incurred concrete damaged. The positions were the midpoint of span 1; ¼, ½, ¾ points of span 2; and midpoint of span 3. For all three girders, the strains are either zero or negative when the truck was positioned in span 1 or 3, showing some moment continuity in the girders. The strains were the largest in the most heavily damaged girder (Beam 2), reaching almost 50 MII, but this can be attributed to the location of the wheel load, which was almost directly over Beam 2, and not the damage.

5.8.2. Comparison Plots

When both tests were completed, a comparison was made of the data from each test to observe the changes in the behavior of the bridge due to the addition of CFRP. The plots for the transverse behavior were used for the comparison. These plots were made from the second bridge test.

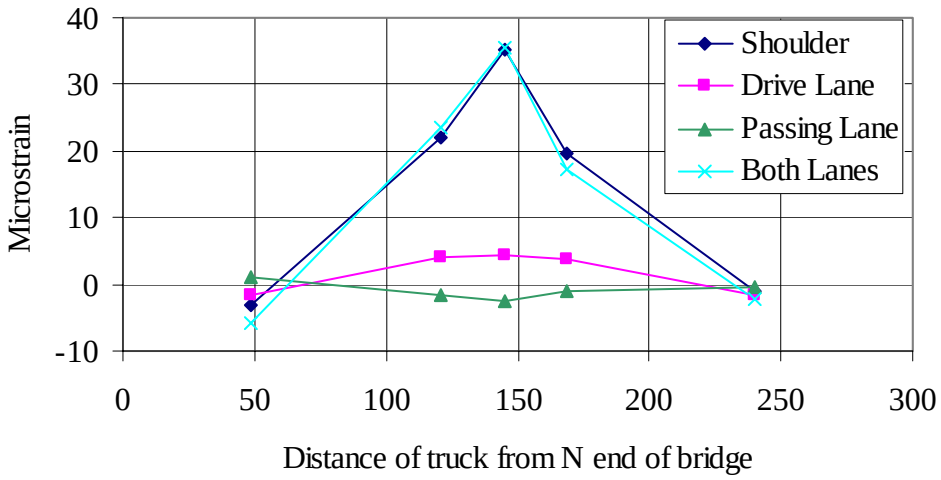

Figure 5.43. Strains in Beam 1 at the center of Span 2 in the Altoona Bridge.

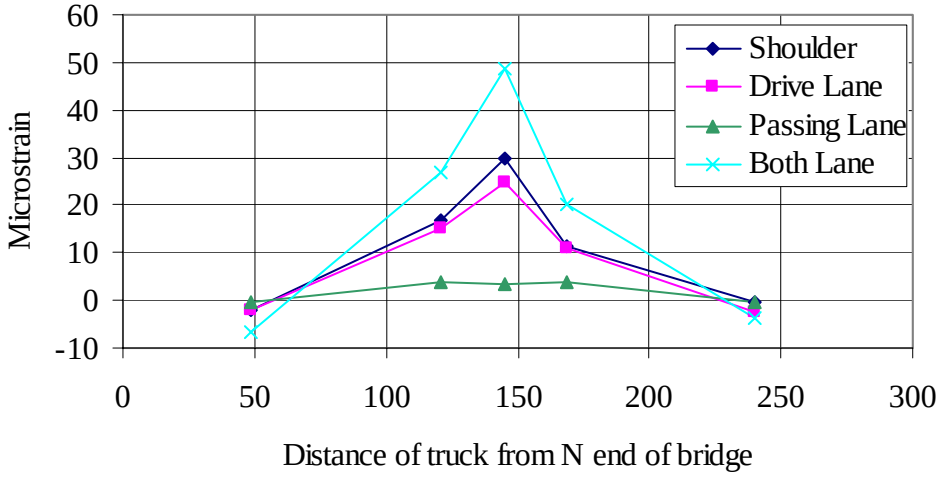

Figure 5.44. Strains in Beam 2 at the center of Span 2 in the Altoona Bridge.

Figure 5.45. Strains in Beam 3 at the center of Span 2 in the Altoona Bridge.

5.8.2.1. Transverse Behavior

Figures 5.46 through 5.48 show the strains and deflections for the damaged and repaired tests for the three load cases mentioned in section 5.8.1.1, cases 13, 19, and 23. Since the trucks used for the repaired bridge test weighed slightly less than the trucks used for the damaged bridge test, it was necessary to normalize the strain and deflection data. The normalization was based on the truck loads. For plotting comparisons, all the strains and

deflections of the repaired bridge test were multiplied by 1.0942 to represent a 9.42% difference in total weight.

As shown in Figures 5.46 through 5.48, the deflection in some of the beams decreased by up to 20%. This could be due to the repair or the positioning of the load trucks. The strain distribution also appears to have changed slightly, although the unusual jumps and dips evident in the first test are still observed in the repaired bridge test. In all three strain plots, the repaired Beam 2 has slightly higher strains than in the damaged tests, while Beam 3 has slightly lower strains. The addition of the CFRP plates slightly increased the stiffness of the repaired beam possibly causing it to attract more of the load than in the first test. The plates slightly increased the moment of inertia approximately 5%, but the decrease in strain due to this increase was only calculated to be approximately 1%. The load factor computed from the strains of the bridge test was 0.32, and the load factor computed from the deflections was 0.27. The load factor computed from the strain increased with the addition of the CFRP, while the load factor computed from the deflection data stayed the same.

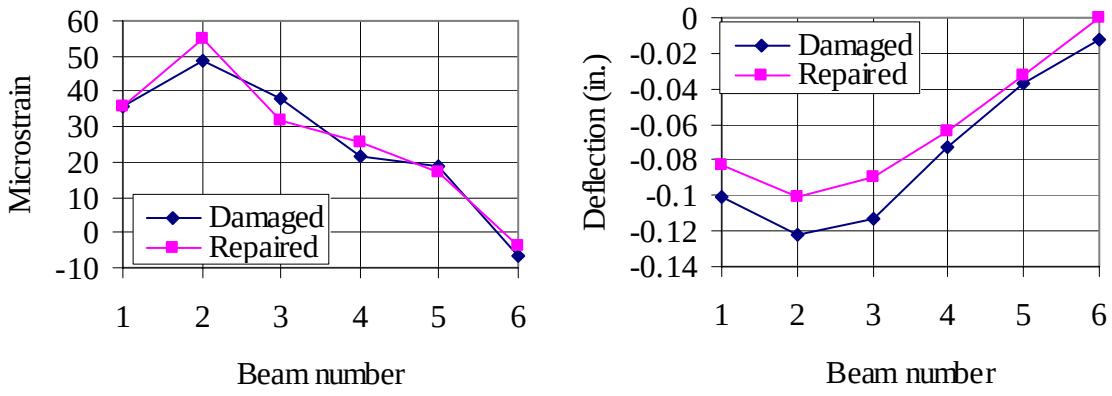

Figure 5.46. Strain and deflection comparison in the Altoona Bridge for Load Case 13.

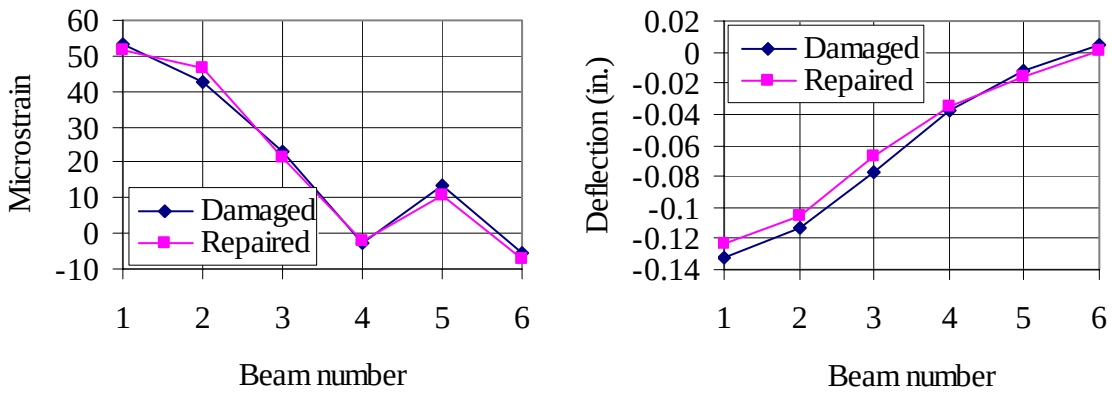

Figure 5.47. Strain and deflection comparison in the Altoona Bridge for Load Case 19.

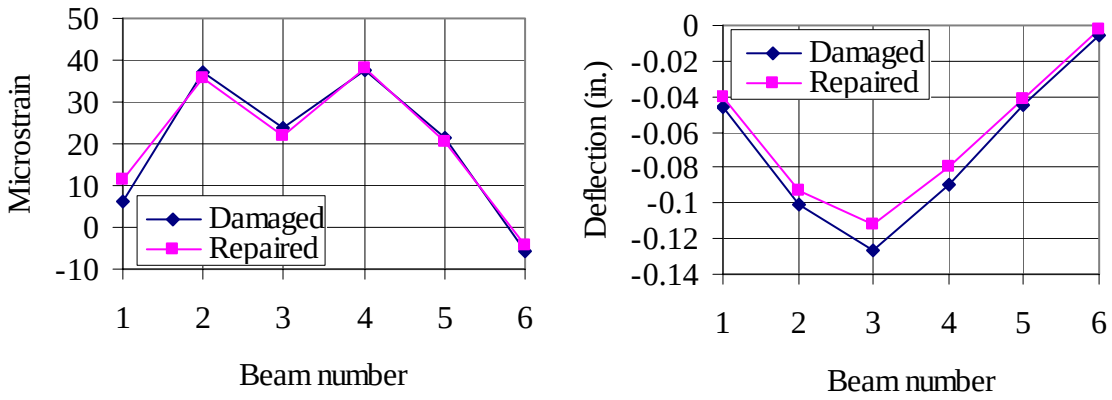

Figure 5.48. Strain and deflection comparison in the Altoona Bridge for Load Case 23.

5.9. Osceola Bridge Test Results

The damaged bridge carrying IA Highway 34 over US 35 was tested in a series of rolling tests using a standard IA DOT tandem axle truck. Strains were measured using the BDI-STS system of gages. One strand on Beam 1 was completely severed.

5.9.1. Transverse Behavior

Figures 5.49 through 5.51 show the transverse behavior during the loading for load lanes 1, 3, and 5; the two outside lanes and the center lane. The loaded truck traveled five different loading lanes for the test, making each pass twice. Using the auto-clicker of the BDI system, the center of the bridge could be found. The BDI gage on Beam 4 was giving

consistently high strain readings about 1.75 times higher than it should, indicating that it may have been placed on a microscopic crack or there was a problem with the gage. Thus the readings from that gage were left off the plots. Both trials of each load position are shown on the plots to show the consistency.

The strains in the extreme outside beams for the center load case, Load Lane 3, were quite small ranging from 3 to 7 MII. The damaged beam did not appear to exhibit any abnormal behavior, as it appeared to behave almost symmetrically to the beams on the opposite side of the bridge, which were undamaged. The strains in the beams at the center of the bridge only reached a maximum of 23 MII actually recorded and 25 MII estimated at the faulty gage. The highest measured strain in the bridge was 30 MII. This level of strain is extremely small for beams this large and is nothing that should cause any worry. The bridge is in no danger of failure.

A distribution factor of 0.39 was calculated for this bridge using the 1996 AASHTO LFD Bridge Design Specification manual. A value of 0.28 was computed in Beam 1 from the strain readings of the damaged bridge test for the northernmost truck loading. This loading caused the largest strains in the damaged beam. The calculated factor is higher than the actual factor, which shows that the undamaged beams were assuming more of the load.

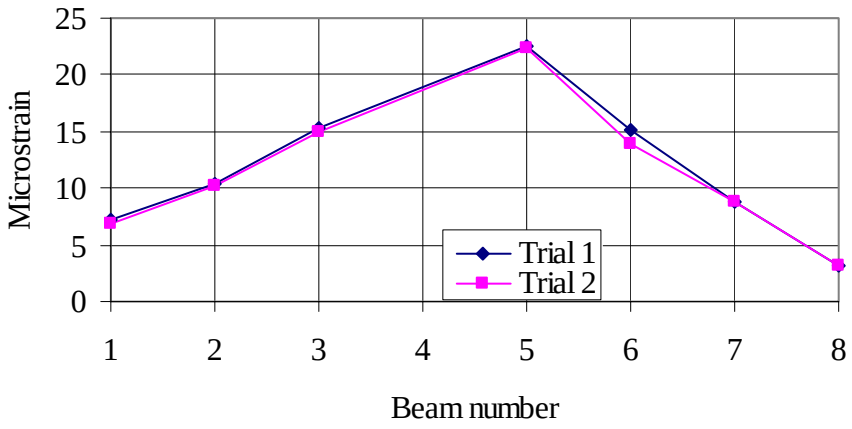

Figure 5.49. Strain at midspan for load position 3.

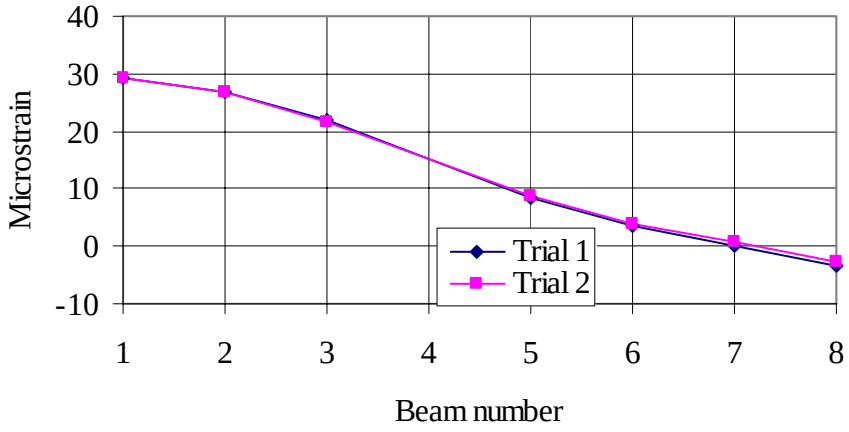

Figure 5.50. Strain at midspan for load position 1.

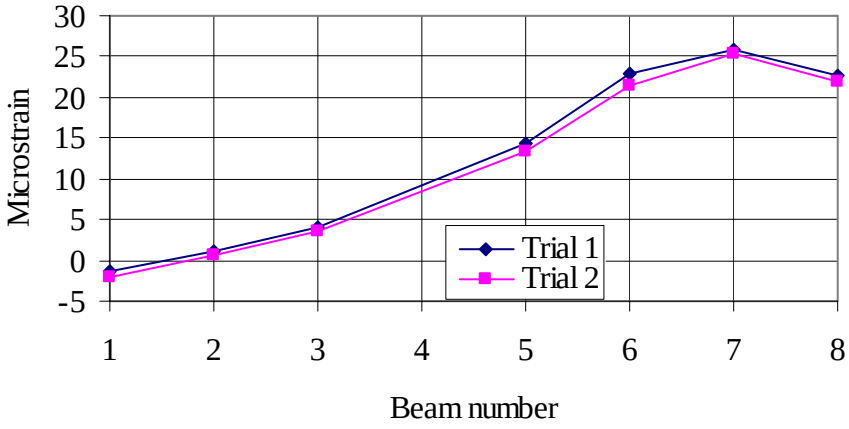

Figure 5.51. Strain at midspan for load position 5.

5.10. De Soto Bridge Test Results

The damaged bridge carrying Interstate 80 over Highway 169 was tested in a series of rolling truck tests using a standard IA DOT tandem axle truck. The test was very similar to the Osceola bridge test. Strains were measured using the BDI-STS system of gages. One strand of Beam 9 was completely severed.

5.10.1. Transverse Behavior

Figures 5.52 through 5.54 show the transverse strain behavior of the nine beams during the loading for all three load positions. The loaded truck traveled three different loading paths for the test, making each pass twice. The load lanes included the center of the driving lane, the center of the passing lane, and the shoulder on the passing lane side. Beam 1 was the damaged beam, which was on the south side under the passing lane shoulder.

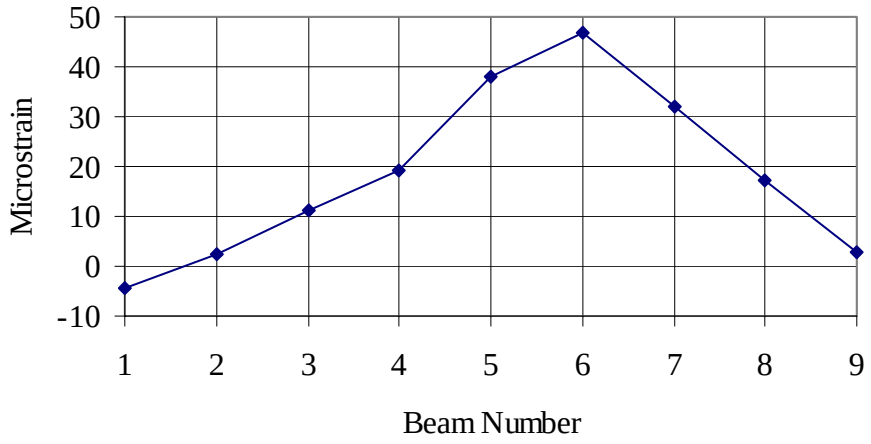

Figure 5.52. Strain at midspan in the De Soto bridge for Load Lane 1.

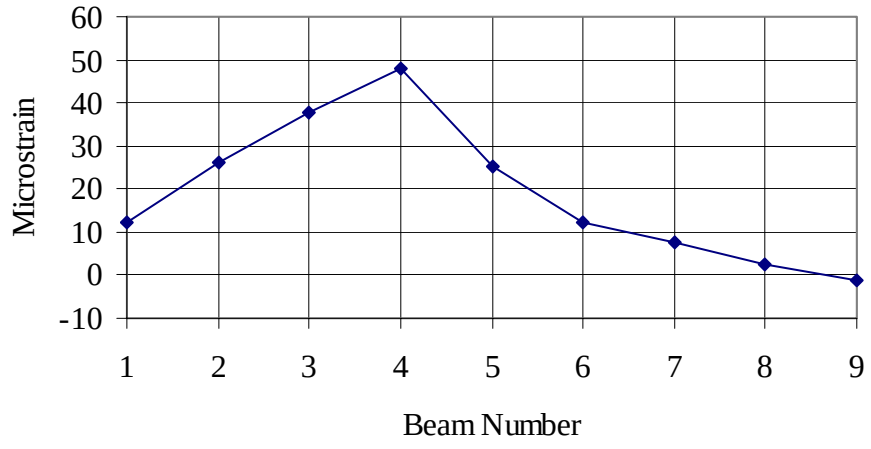

Figure 5.53. Strain at midspan in the De Soto bridge for Load Lane 2.

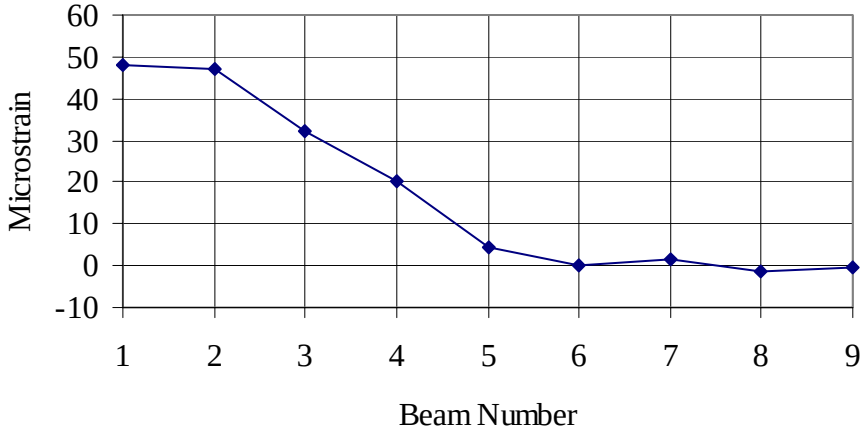

Figure 5.54. Strain at midspan in the De Soto bridge for Load Lane 3.

The highest strain recorded for any of the load cases was less than 50 MII. These high strains were always located in the beam directly below the lane of travel. The highest strain in the damaged beam for normal traveling lanes was less than 12 MII. The damaged beam did not appear to have higher strains than would be expected on an undamaged bridge. It can be concluded that the loss of only one strand out of nine beams is fairly insignificant for service loads.

A distribution factor (based on design assumptions) of 0.44 was calculated for this bridge using the 1996 AASHTO LFD Bridge Design Specification manual. A value of 0.30 was computed in Beam 1 from the strain readings of the damaged bridge test for the left shoulder loading, which caused the largest strains in the damaged beam.

5.10.2. Longitudinal Behavior

Figure 5.55 shows three different beams from three different trials. The beams plotted were the beams most directly beneath the left tire of the loaded truck. Beam 1 is plotted for the first shoulder run, S1, Beam 3 is plotted for the first pass lane run, P1, and Beam 5 is plotted for the first drive lane run, D1. The jaggedness of the figure was due to the truck bouncing somewhat on the bridge during the trial runs. Notice that all three beams achieve almost the same strain levels. The first beam had the highest strain, but it was on the outside where the strain distribution was not as good as the distribution is for the inside

beams. This can also be seen in the transverse plots, Figure 5.54, where only half of the bridge is taking the shoulder truck load.

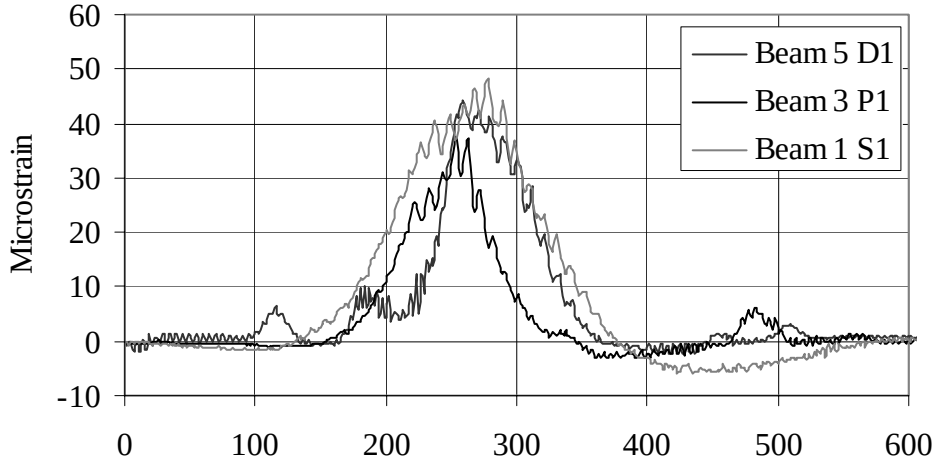

Figure 5.55. Strain at midspan of Beams 1, 3, and 5 in the De Soto Bridge.

5.11. Practical Design Implementation of CFRP

All of the P/C beams used for this project were LXA-38 sections (Section 3.1). However, larger sections make up the majority of the girders typically damaged in the field. These larger girders have more prestressing strands and therefore are less sensitive to the same amount of impact damage. The ultimate capacity of a LXA-38 as well as three other standard sections with different levels of damage is presented in Figure 5.56. This figure was normalized to show the ultimate strength of each girder as a percent of the undamaged strength. For these strength calculations, the composite slab dimensions were taken as 8 in. x 84 in. and the concrete strength was assumed to be 4,000 psi, which is a conservative concrete strength for typical slabs.

The LXA-38 composite beams used for this project are clearly more sensitive to severed strands than the larger “C” and “D” girders. For example, when two strands are severed in a LXA-38 the flexural design strength is reduced 28%. However, a LXD-105 composite beam still has 95% of its original flexural strength with the same amount of damage (two strands severed out of a total of 40). As illustrated in Figure 5.56, this difference becomes even more pronounced as the number of severed prestressing strands

increases. The results from the strengthening tests in this study indicate that CFRP is most effective when a damaged girder has at least 85% of the undamaged ultimate strength after the impact. With this limit in mind, CFRP systems should be considered as a strengthening option for impact damaged girders in the field. However, fatigue life of the remaining prestressing strands needs to be evaluated if the damaged girder has developed flexural cracks. For example as shown in Figure 5.56, CFRP sheets would be a viable strengthening option for an uncracked LXC-80 with up to four severed prestressing strands.

From the results of the load tests, it can be concluded that bridges with minor damage need not be closed to traffic prior to repairs. The load distribution exhibited by the damaged bridges was very similar to the distribution on an undamaged bridge. The strains reached on the damaged beams were also not large enough to cause concern prior to repair of the beams.

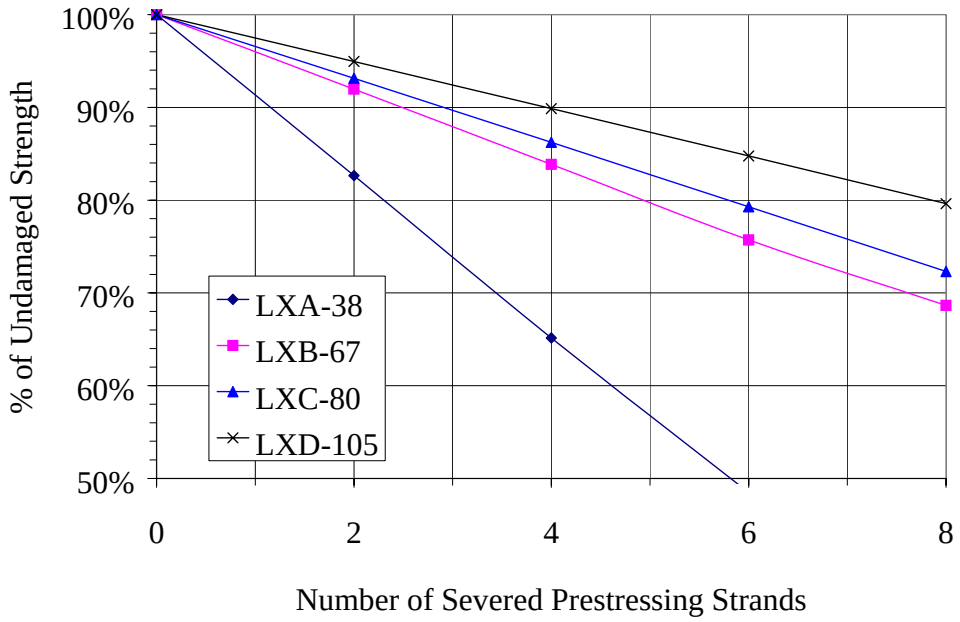

Figure 5.56. Comparison of damage to different size P/C girders.

6. SUMMARY AND CONCLUSIONS

6.1. Summary

In this study, isolated P/C beams were tested to static failure after creating damage to simulate vehicle impacts and then repaired/strengthened with CFRP. Several tasks were completed during the course of the investigation. A literature search was conducted to review research relevant to the project. In addition, a national survey was also conducted to help understand how other states are using CFRP materials to repair damaged P/C bridge girders.

Four full-sized P/C beams were intentionally damaged to simulate vehicle impacts. Damage consisted of removing concrete from the bottom flange and severing a number of prestressing strands. Beams 1, 2, and 4 were designed to represent moderate impact damage. Two prestressing strands were severed on each of these beams (17% of the total flexural reinforcement). Beam 3 was designed to represent more severe vehicle impact damage. Four of the prestressing strands were removed from Beam 3 (33% of the total flexural reinforcement). Beam 4 was subjected to cyclic loading prior to testing to static failure. All four of the beams were still uncracked flexural sections. Each beam was subjected to service load tests after each damage level to monitor changes in beam stiffness and the redistribution of forces in the remaining prestressing strands.

The beams were strengthened/repaired by patching the bottom flange and installing unidirectional CFRP sheets to restore the original flexural capacity. An analytical procedure was developed to calculate the ultimate flexural capacity of composite P/C beams strengthened with CFRP. All four beams were loaded to failure and compared with the analytical results. Premature debonding of the CFRP at the concrete interface was the failure mode for all of the beams. Two different CFRP jacket configurations were used to help prevent the debonding of the longitudinal fibers and to confine the patch material.

From the many bridges in Iowa that have been struck by overheight vehicles, three were repaired as part of this investigation. The southbound I-65 bridge near Altoona, the westbound IA-34 bridge near Osceola, and the westbound I-80 bridge near De Soto all had significant concrete loss on one or more beams, as well as at least one severed prestressing

strand. Repair strategies were developed so the moment capacity from the severed strand(s) could be restored by CFRP. CFRP also has the functional capacity of preventing the mortar patches from falling out onto the highways below. All three bridges were load tested using weighted DOT tandem axle trucks prior to repair. The Altoona bridge was also tested after the repair was complete to observe any differences in the bridge's behavior.

Photographic and written documentation were taken during the repair of the IA-34 bridge near Osceola. This documentation was used to create a CFRP application guide for any future bridge repairs. A design aid was also put together using manufacturer's suggested design guidelines as well as input from other sources. These materials were assimilated to assist other engineers in the design of similar repairs.

Environmental test specimens were constructed to evaluate the long-term performance of CFRP bonded to concrete. Modulus of rupture beams were strengthened with a single layer of CFRP and then placed in an outdoor storage area. These small-scale beams were periodically tested and the results compared to a set of control beams tested at the beginning of the project. The results from these tests help determine how prolonged exposure to moisture and freeze/thaw cycles influences the bond strength of the CFRP.

6.2. Conclusions

Carbon fiber repair/strengthening systems have a number of advantages over traditional repair/strengthening schemes for impact damaged prestressed girders. CFRP is lightweight and relatively simple to install in the field. In addition to its high tensile strength, CFRP sheets also have excellent corrosion/fatigue properties. However, CFRP sheets may have limitations. CFRP strengthening products are linear-elastic until failure (no yielding), can debond from concrete surfaces before the full design strength is obtained, and can be damaged by exposure to ultraviolet radiation. The results from this research indicate that flexural strengthening of impact damaged P/C girders is feasible when at least 85% of the prestressing strands are intact and undamaged. A typical repair strategy would consist of epoxy injecting any web cracks, removing loose material from the impact area, installing the concrete patch, and finally installing the CFRP. The following list is a summary of the conclusions from this investigation:

- Simulated damaged resulted in a 10 to 15% loss in elastic beam stiffness. This was determined from deflection measurements taken in isolated beam tests. Similar damage on a girder in the field would have a smaller effect because of larger girder spacings, slab/diaphragm continuity, and the support conditions.
- The CFRP increased the cracking load of the beams by 31 to 46%. This was confirmed in both the full-size beams and the modulus of rupture beam tests.
- The CFRP restored a portion of the lost flexural strength. However, debonding of the CFRP sheets was the mode of failure in all laboratory beams. The CFRP sheets debonded from the concrete surface at only 27% of the CFRP design rupture strength specified by the manufacturer.
- Transverse CFRP jackets helped develop the longitudinal CFRP sheets and prevented debonding. More importantly, the jackets helped to confine the patch material under service and ultimate loads. This is especially important for the field bridges where falling patch material can damage traveling vehicles.
- Beam deflections were reduced in the bridge tests as much as 20%. The deflections decreased up to 0.02 in. for the most heavily loaded beams. Deflection decreases although slight, were noticed in several of the load tests from the Altoona Bridge.
- Fatigue of the remaining prestressing strands in a damaged girder is not an issue as long as the damaged girder has not developed flexural cracks. If flexural cracks have developed, the fatigue life of the remaining prestressing strands needs to be evaluated.
- Distribution of loads among beams was always better than the AASHTO distribution factor predicted. The damaged beams carried a smaller percentage of the total load than predicted and were subjected to less stress than was predicted using the distribution factor.

APPENDIX A

QUESTIONNAIRE

Bridge Engineering Center
Iowa State University
Ames, Iowa

Iowa Department of Transportation
Research Project TR-428
"Effective Structural Concrete Repair"

Questionnaire completed by _____

Title _____

Address _____

City_____ State_____ Zip _____

Phone _____ Fax _____

Please return the completed questionnaire using the enclosed envelope (or fax your response) to:

Prof. F. Wayne Klaiber
Dept. of Civil and Construction Engineering
Iowa State University
Ames, IA 50011

Phone: (515) 294-8763
Fax: (515) 294-8216

---

1) Does your state currently have a strengthening/rehabilitation/repair program for impact damaged prestressed/reinforced concrete bridges?

YES **NO**

If yes, please list the types of repairs commonly made. If appropriate please provide repair guidelines, repair strategies, rehabilitation plans, etc...

2) What products do you use to patch impact damaged concrete bridge beams (prestressed and/or reinforced)? If possible, please list product brand names and manufacturers.

3) Has your state ever funded or planning to fund projects involving FRP strengthening/ rehabilitation/repair of prestressed concrete bridge structures? If so, who can we contact (name, address, phone number, etc…) for information.

YES **NO**

If yes, please describe project(s) and list any pertinent technical information.

4) Are you aware of other states that have experience with FRP strengthening/rehabilitation/ repair of prestressed concrete bridges?

YES **NO**

If yes, please provide the name, address, and phone number of the person who could be reached for more information.

5) If FRP technologies appear to be promising would you consider their use on strengthening/ rehabilitation/repair projects?

YES **NO**

If no, what additional information do you require?

Thank-you very much for your participation. If you would like to receive a copy of our final report, please mark the square below.

APPENDIX B

DAMAGE REPORTS

ALTOONA

Beam #1- At the impact point, concrete was spalled from the bottom flange for approximately 24 inches in the longitudinal direction, 7 inches in the vertical direction on the bottom flange west face, and 10 inches in the transverse direction. Approximately 2 ½ inches of concrete was missing at the deepest point. One prestressing strand was severed and there was one exposed stirrup. There was no evidence of cracking in the beam.

Beam #2- This was the most severely damaged beam. At the impact point, concrete was spalled from the bottom flange for approximately 48 inches in the longitudinal direction, the entire vertical face of the bottom flange and approximately 5 inches of the sloped west face, and transversely across the entire bottom of the bottom flange. Approximately 4 inches of concrete was missing at the deepest point. Five prestressing strands were exposed, and two more were severed. On the west face of the beam, one crack was located at the web and top flange interface and extended from approximately 8 ft. off of the face of the middle pier diaphragm to near the face of the centerline diaphragm. This crack was approximately 1/16th to 3/32nd inches wide at its widest point. Another crack extended from the bottom flange near the middle pier diaphragm, diagonally across the web, and met the top crack at approximately 23 ft. from the pier diaphragm. Four cracks extended diagonally across the bottom of the bottom flange and diagonally across the face of the bottom flange and along the web and bottom flange interface. These cracks were located at approximately 15, 18, 21, and 25 ft north of the centerline of the impact area. Sounding of the web in this area with a hammer produced a slightly different ring, indicating possible hollow areas. There were several other longitudinal cracks on the web of the west face. On the east face of the beam, one crack was located at the web and top flange interface and extended from the face of the centerline diaphragm to within 9 ft of the face of the middle diaphragm. There were a couple of other longitudinal cracks on the web of the east face.

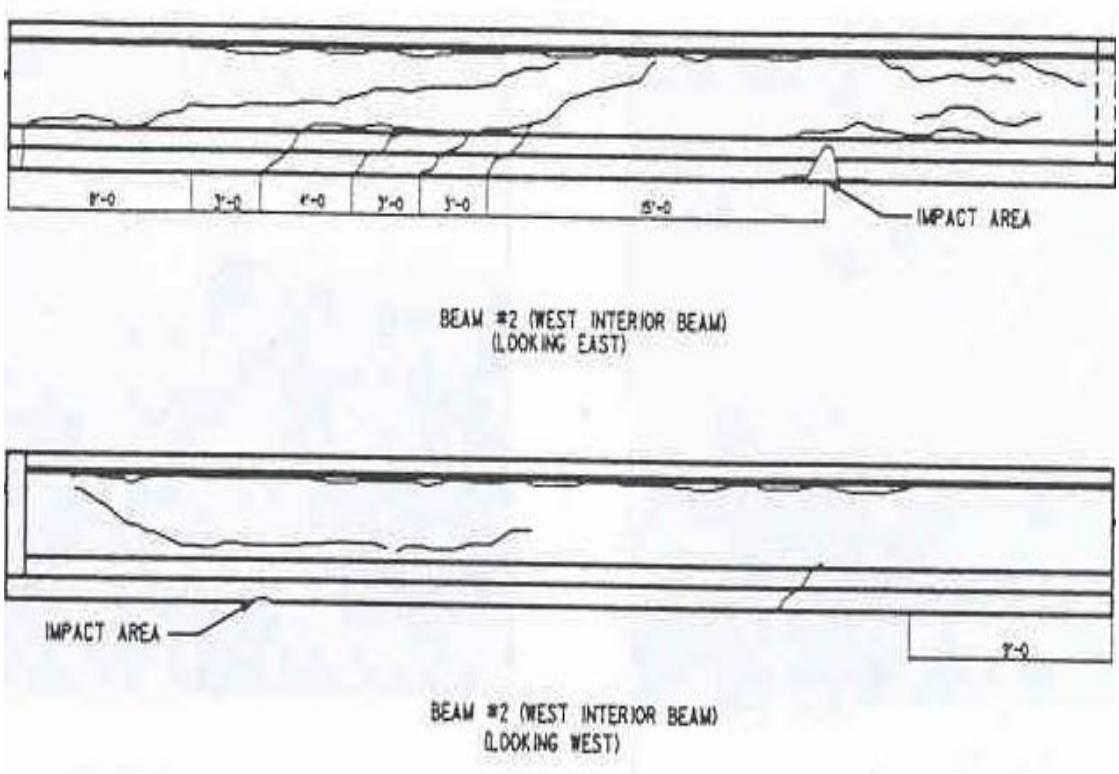

Figure B1. Altoona beam #2 damage drawings.

Beam #3- At the impact point, concrete was spalled from the bottom flange for approximately 26 inches in the longitudinal direction, 7 inches in the vertical direction on the bottom flange west face, and 10 inches in the transverse direction. Approximately 2 ½ inches of concrete was missing at the deepest point. One prestressing strand was severed and there was one exposed stirrup. On the west face of the beam a crack was located at the web and top flange interface and extended approximately 10 ft from the centerline of the collision area toward the middle pier.

Beam #4- At the impact point, concrete was spalled from the bottom flange for approximately 18 inches in the longitudinal direction, 6 inches in the vertical direction on the bottom flange west face, and 9 inches in the transverse direction. Approximately 2 inches of concrete was missing at the deepest point. One prestressing strand was partially exposed and it appeared gouged. There was no evidence of cracking in this beam.

Beam #5-At the impact point, concrete was spalled from the bottom flange for approximately 32 inches in the longitudinal direction, 6 inches in the vertical direction on the bottom flange west face, and 10 inches in the transverse direction. Approximately 2 ½

inches of concrete was missing at the deepest point. One prestressing strand was severed. There was a crack on both sides of the beam at the web and top flange interface that extended from approximately 10 ft. off of the middle pier diaphragm face to about 5 ft past the centerline of the impact point.

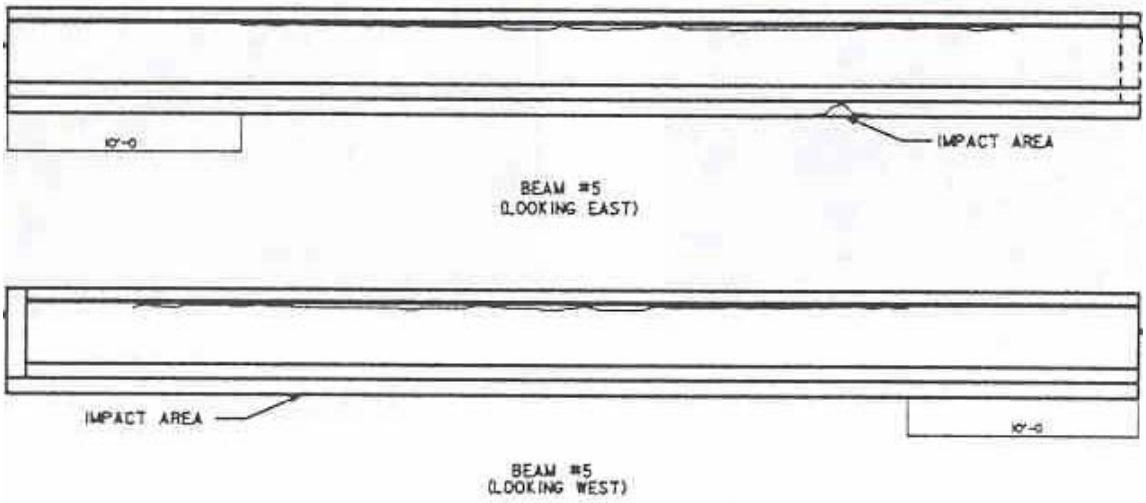

Figure B2. Altoona beam #5 damage drawing.

Beam #6-At the impact point, concrete was spalled from the bottom flange for approximately 45 inches in the longitudinal direction, 6 inches in the vertical direction on the bottom flange west face, and 10 inches in the transverse direction. Approximately 2 inches of concrete was missing at the deepest point. One prestressing strand was exposed and partially severed, and there were two exposed stirrups. There was also a crack starting at about 5 ft from the impact point, intersecting the top crack, and extending diagonally to the interface of the web and bottom flange at the centerline diaphragm.

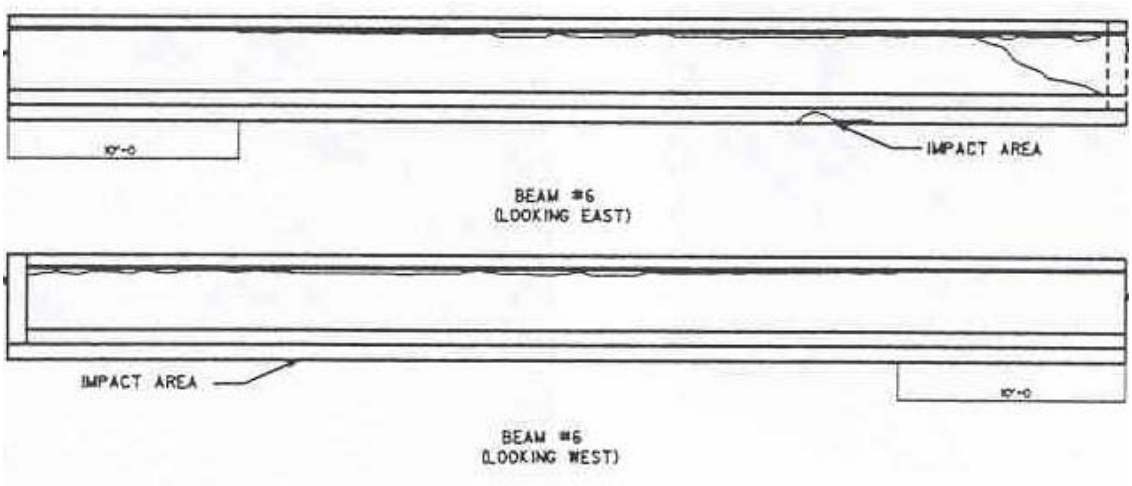

Figure B3. Altoona beam #6 damage drawing.

OSCEOLA

Beam #1- This beam was the most severely damaged of the two beams. Two strands were severed in the bottom layer of strands. There was a large hollow area in the bottom flange at the impact zone. A portion of the hollow area appeared to be cracked completely through from the top most edge to the bottom edge. This area was most likely being held in place by the strand that was running through it. The web was cracked along the top flange interface, on both sides of the beam, for a distance of approximately 25 ft over the impact zone. There was a hairline crack at the beam and diaphragm interface with a spall in the bottom of the diaphragm exposing the coil ties that connected the bottom flange to the diaphragm. On the north exterior face of the beam there was horizontal hairline cracking in the web at the impact zone. There was a diagonal crack staring in the bottom flange 12 ft from the east bearing, extending back towards the east bearing and stopping near the center of the web. The diagonal crack did not appear on the interior face of the beam.

Beam #2- Beam #2 had some minor spalls on the bottom flange and a large spall on the north side of the bottom flange. The large spall was approximately 2 ½ inches deep, partially exposing 2 to 3 strands and reinforcing steel. No cracking in the web was seen. Other spalls were ¾ to 1 inch deep with no reinforcing exposed. A drawing from the damage report is shown in Figure B4.

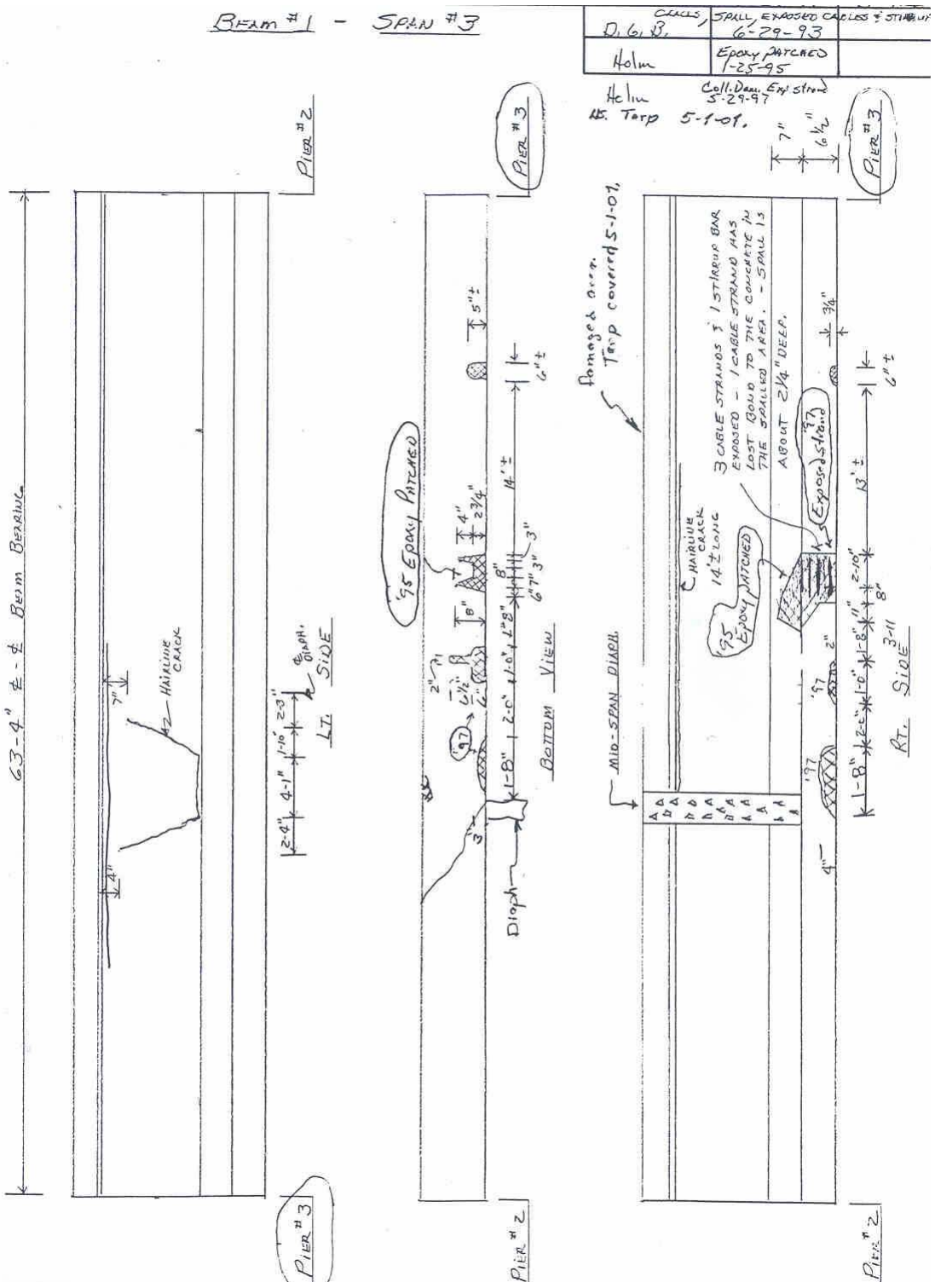

Figure B4. Osceola damaged beam drawing.

DE SOTO

Beam #1- This beam was the only beam to sustain major damage. A southbound vehicle struck the southernmost beam but virtually missed the other beams before it. The bottom strand on the north side of the beam was completely severed and another strand was almost totally visible. Three strands were also visible on the south side where concrete had broken away. There were several cracks along the bottom of the beam propagating from the impact zone. There was also a 1/8 inch crack that extended for several feet just below the top flange that was visible on both sides of the beam. A page from the damage report is shown in Figure B5.

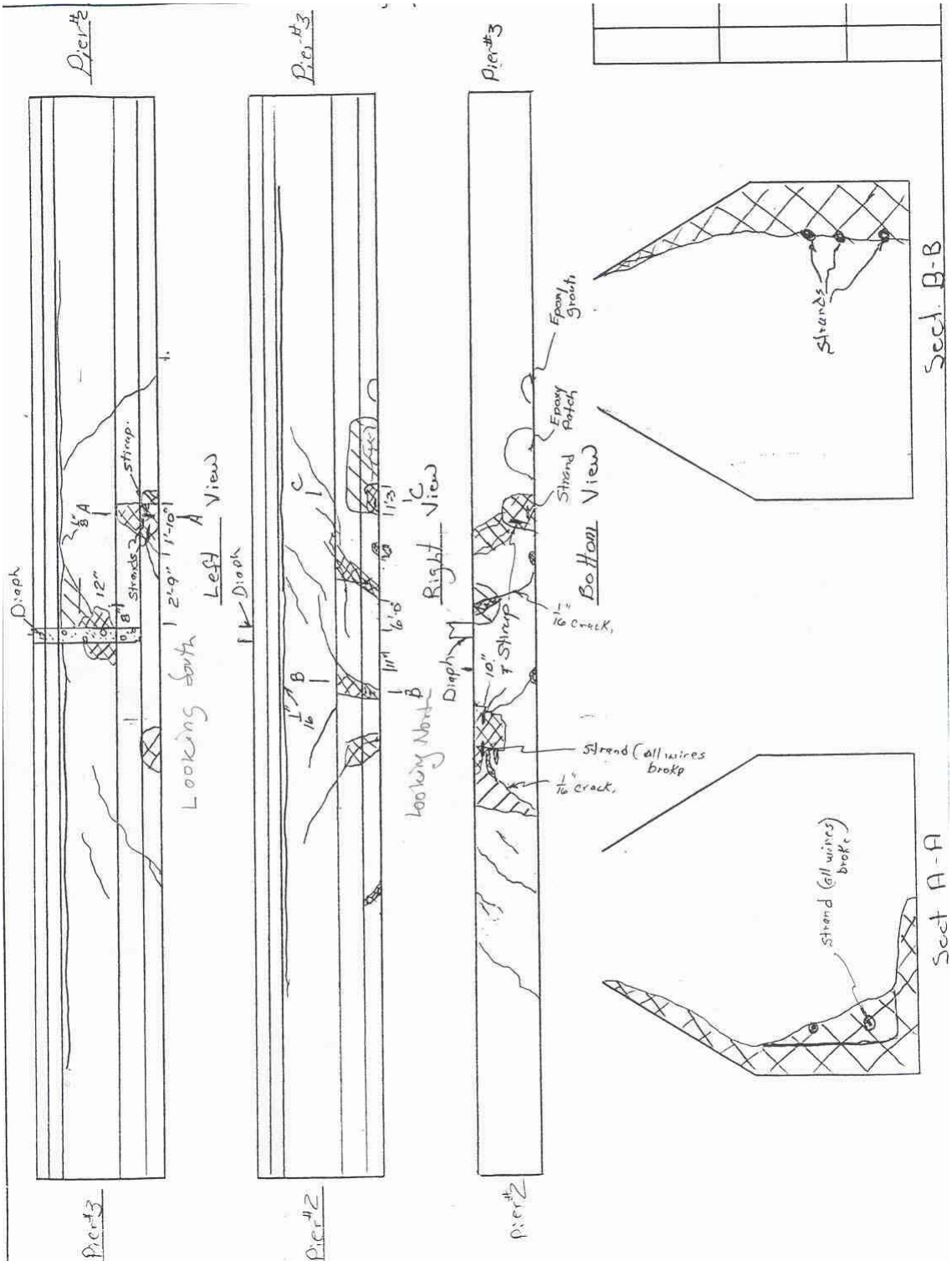

Figure B5. De Soto damaged beam drawing.

APPENDIX C

DESIGN/APPLICATION GUIDE

Design for Fiber Reinforced Plastic repair to a Prestressed Concrete Beam

Designing a CFRP repair system for a damaged prestressed beam can be somewhat confusing if the designer is not familiar with the design procedures This guide is intended to aid in the design process and will provide some step-by-step instructions as well as examples of previous designs.

1) Design is based on the Master Builders product CF 130 High Tensile Carbon

2) All highlighted values need to be entered manually

$kip := 1000 \cdot lbf$

$ksi := 1000 \cdot psi$

STEP 1: List all values needed for analysis of prestressed beam.

Area of beam.	$A_c := \_ \cdot in^2$
Height of beam.	$H := \_ \cdot in$
Area of prestressing steel.	$A_{ps} := \_ \cdot in^2$
Prestressing steel strength.	$f_u := \_ \cdot psi$
Distance from top of concrete that is in compression to centroid of prestressing steel in composite section.	$d := \_ \cdot in$
Distance from centroid of beam to bottom of non-composite section.	$Y_b := \_ \cdot in$
Slab thickness.	$t_s := \_ \cdot in$
Gross beam moment of inertia.	$I_g := \_ \cdot in^4$
Slab concrete strength.	$f'_c := \_ \cdot psi$
Beam concrete strength.	$f'_{cbeam} := \_ \cdot psi$
Distance from bottom to centroid of prestressing strands .	$Y_s := \_ \cdot in$
Moment on beam when FRP is installed. (100% Dead Load + 25% Live Load)	$M_{initial} := \_ \cdot ft \cdot kip$
Effective prestress force when FRP is installed.	$P_e := \_ \cdot lbf$
Modulus of elasticity of prestressing strand.	$E_p := \_ \cdot ksi$
Effective slab width.	$b := \_ \cdot in$

Transformed section modulus for the bottom of the beam only. $S_{beam} := \blacksquare \cdot in^3$

Section modulus for the composite beam and slab at the bottom of the beam, with the slab concrete transformed to equivalent beam concrete. (E_{slab}/E_{beam}) $S_n := \blacksquare \cdot in^3$

Section modulus for the composite beam and slab at the bottom of the beam, with the slab concrete transformed to equivalent beam concrete for long term loading. (E_{slab}/E_{beam})/3 $S_{3n} := \blacksquare \cdot in^3$

Section modulus for the composite beam and slab at the top of the beam, with the slab concrete transformed to equivalent beam concrete. (E_{slab}/E_{beam}) $S_{n\_top} := \blacksquare \cdot in^3$

Section modulus for the composite beam and slab at the top of the beam, with the slab concrete transformed to equivalent beam concrete for long term loading. (E_{slab}/E_{beam}) $S_{3n\_top} := \blacksquare \cdot in^3$

Transformed section modulus for the top of the beam only. $S_{top} := \blacksquare \cdot in^3$

FRP Material Properties

Thickness of fiber sheet $t_f := \blacksquare \cdot in$

Design strength $f_{fu} := \blacksquare \cdot psi$

Design strain $\varepsilon_{fu} := \blacksquare \cdot \frac{in}{in}$

Tensile Modulus $E_f := \blacksquare \cdot psi$

STEP 2: Determine the existing flexural capacity based on original section properties and determine the loss of capacity due to damage.

Determine Ultimate Moment capacity of beam before damage/deterioration using section properties.

$Mu_{original} := \blacksquare\ ft \cdot kip$

Determine Ultimate Moment capacity of beam after damage/deterioration.

$Mu_{existing} := \blacksquare\ ft \cdot kip$

Calculate loss in capacity :

$M_{loss} := Mu_{original} - Mu_{existing}$ $M_{loss} = \blacksquare\ ft \cdot kip$

STEP 3: Using the M_{loss}, estimate the number of sheets of FRP that will be needed based on the additional tensile force required to restore the original moment strength.

Tension to be recovered = T

$$T := \frac{M_{loss}}{0.9 \cdot d}$$

Area of FRP needed:

$$A_f := \frac{T}{0.9 \cdot 0.85 \cdot f_{fu}}$$

Nominal sheet width is 24 inches. The FRP is easy to cut into smaller widths such as 3, 4, 6, 8, or 12 inches.

Width of FRP sheet to be used:

$W_{FRP} :=$ ▮ $\cdot in$

Calculate the number of layers needed:

Layers required = n_p

$$n_p := \frac{A_f}{W_{FRP} \cdot t_f} \qquad n := ceil(n_p)$$

$n =$ ▮

Area of FRP to be used = A_{FRP}

$$A_{FRP} := n \cdot t_f \cdot W_{FRP}$$

STEP 4: Calculate the flexural capacity with the FRP. This is the beginning of the iteration process. Start by assuming an initial C value, which is the distance from the extreme compression fiber to neutral axis. An uncracked section is assumed.

Trial & Error Method

Initial "C" can be taken as 0.15(d)

For the initial iteration let $C = C_{initial}$, adjust C for subsequent iterations.

$C_{initial} := 0.15 \cdot d$ $\qquad C_{initial} =$ ▮ $\qquad C :=$ ▮ $\cdot in$

STEP 5: Determine the failure mode by reviewing the existing state of strain in the concrete Since FRP is usually installed unstressed, and the concrete surface to which it is attached is stressed from self-weight and prestressing, the strains will be different. In order to use strain compatibility, the existing state of strain in the concrete must be calculated This initial strain can then be added to the ultimate strain and used as shown below. As stated before, an uncracked section is assumed.

ε_{bi} = Strain in concrete substrate at time of FRP installation.

ε_{fu} = Ultimate strain of the FRP material. (given on page 1)

If $\varepsilon_{fu} + \varepsilon_{bi} < \varepsilon_{cu}(H + ts - C)/C$, Failure is controlled by concrete crushing.

If $\varepsilon_{fu} + \varepsilon_{bi} > \varepsilon_{cu}(H + ts - C)/C$, Failure is controlled by FRP rupture.

Maximum usable compressive strain in the concrete = ε_{cu}

$$\varepsilon_{cu} := 0.003$$

$$\varepsilon_{total} := \varepsilon_{cu} \cdot \frac{(H + t_s - C)}{C}$$

E_c = Approximate elastic modulus of concrete in compression (psi).

$$E_c := \frac{57 \cdot f'_{cbeam}{}^{0.5}}{1 \cdot psi^{0.5}} \cdot ksi$$

$$\varepsilon_{bi} := \frac{M_{initial} \cdot Y_b}{I_g \cdot E_c} - \frac{P_e}{A_c \cdot E_c} \cdot \left[1 + \frac{(Y_b - Y_s) \cdot Y_b}{\frac{I_g}{A_c}} \right]$$

$$Controlling\_Factor := if\left[(\varepsilon_{total} < \varepsilon_{fu} + \varepsilon_{bi}), "Concrete\ crushing", "FRP\ rupture" \right]$$

$Controlling\_Factor =$

Note: It is recommended that the design be altered if concrete crushing is the failure mode. Reduce the number of FRP layers or reduce the width of the strips used. If the controlling factor cannot be changed, proceed with Step 6A; if the controlling factor is FRP rupture, proceed with Step 6B.

Step 6A: When failure is governed by concrete crushing, the strain in the concrete at failure will be at its maximum usable strain, ε_{cu}.

$$\varepsilon_c := \varepsilon_{cu}$$

The strain in the FRP may be determined by finding the strain in the concrete substrate at ultimate and subtracting the strain in the concrete substrate at the time of FRP installation.

$$\varepsilon_f := \varepsilon_c \cdot \left(\frac{H + t_s - C}{C} \right) - \varepsilon_{bi}$$

ε_{bi} = Strain in concrete substrate at time of FRP installation.

Because the concrete is at its maximum usable strain level, the rectangular stress block specified in ACI 318 may be used to aproximate the actual non-linear stress distribution in the concrete.
The FRP sheet may be taken as linear-elastic to failure.

$$f_f := E_f \cdot \varepsilon_f$$

The estimated value of C is then checked against the value obtained, c, to satisfy equilibirum of the internal stress resultants.

$$c := \frac{A_{FRP} \cdot f_f + A_{ps} \cdot f_u}{0.85 \cdot f'_c \cdot 0.85 \cdot b} \qquad c = \blacksquare \text{ in} \qquad C = \blacksquare \text{ in}$$

Repeat Step 4 through Step 6 by adjusting C in Step 4 until C=c, then proceed to Step 10.

Step 6B: When the failure mode is controlled by FRP rupture, the calculation procedure used to compute the nominal moment capacity of a section is similar to that used when there is concrete crushing. In this case, the known value of strain in the FRP may be used in conjunction with the estimated neutral axis location to determine the strain level in each of the materials.
Calculate the concrete strain, ε_c, and the strain in the FRP, ε_f.

$$\varepsilon_c := \left(\varepsilon_{fu} + \varepsilon_{bi} \right) \cdot \frac{C}{H + t_s - C}$$

$$\varepsilon_f := \varepsilon_{fu}$$

Therefore the stress in the FRP = f_f.

$$f_f := \begin{cases} f_{fu} & \text{if } \varepsilon_f \cdot E_f > f_{fu} \\ \left(\varepsilon_f \cdot E_f \right) & \text{otherwise} \end{cases} \qquad f_f = \blacksquare \text{ ksi}$$

Step 7: Determine stress block parameters.

Because the concrete does not reach its ultimate compressive strain in Step 6B, the Whitney stress block is not applicable. The stress resultant for concrete should be determined from an appropriate non-linear stress-strain relationship or by a rectangular stress block suitable for the particular level of strain in the concrete. Parameters for the stress block are given below.

$$E_{beam} := \frac{57 \cdot f'_{cbeam}{}^{0.5}}{psi^{0.5}} \cdot ksi \qquad E_{slab} := \frac{57 \cdot f'_c{}^{.5}}{1 \cdot psi^{0.5}} \cdot ksi$$

$$n_{transformed} := \frac{E_{slab}}{E_{beam}}$$

$$\varepsilon_{pc} := \frac{1.71 \cdot f'_c}{E_{slab}} \qquad \varepsilon_n := \frac{\varepsilon_c}{\varepsilon_{pc}}$$

$$\beta_1 := \left[2 - 4 \cdot \frac{\left(\varepsilon_n - \operatorname{atan}\left(\varepsilon_n\right)\right)}{\varepsilon_n \cdot \ln\left(1 + \varepsilon_n{}^2\right)} \right]$$

$$\gamma := \frac{0.90 \cdot \ln\left(1 + \varepsilon_n{}^2\right)}{\beta_1 \cdot \varepsilon_n}$$

Step 8: Determine the strain in the prestressing strands. Total strain in the prestressing strands is due to strains at three load stages. Load stage 1 is the prestress alone, stage 2 is the decompression of the concrete, and stage 3 is the ultimate load. Total strain = $\varepsilon_1 + \varepsilon_2 + \varepsilon_3$

ε_1 = Strain in the tendons due to the initial application of the prestress force and any subsequent losses that occur.

$$\varepsilon_1 := \frac{P_e}{A_{ps} \cdot E_p}$$

ε_2 = Strain in the tendons due to decompression of the concrete at the level of the tendons.

$$\varepsilon_2 := \frac{P_e}{A_c \cdot E_c} \cdot \left[1 + \frac{\left(Y_b - Y_s\right)^2}{\frac{I_g}{A_c}} \right]$$

ε_3 = Strain in the tendons due to ultimate loading.

$$\varepsilon_3 := \begin{cases} \left[\varepsilon_f \cdot \frac{(H + t_s - Y_s - C)}{H + t_s - C}\right] & \text{if } \varepsilon_{total} > \varepsilon_{fu} + \varepsilon_{bi} \quad \text{FRP rupture} \\ \left[\varepsilon_c \cdot \left(\frac{H + t_s - Y_s - C}{C}\right)\right] & \text{otherwise} \quad \text{Concrete crushing} \end{cases}$$

$$\varepsilon_{ps} := \varepsilon_1 + \varepsilon_2 + \varepsilon_3 \qquad \varepsilon_p := \begin{cases} \varepsilon_{ps} & \text{if } \varepsilon_{ps} < 0.03 \\ 0.03 & \text{otherwise} \end{cases}$$

Step 9: Calculate the stress in prestressing strands so that c may be calculated.

$$f_{ps} := \begin{cases} \varepsilon_p \cdot E_p & \text{if } \varepsilon_p \le 0.008 \\ \text{otherwise} & \\ \quad \begin{cases} \left(\left(f_u - \frac{75 \cdot psi}{\varepsilon_p - 0.0065} - 2000 \cdot psi\right)\right) & \text{if } f_u = 270000 \cdot psi \\ \left(\left(f_u - \frac{58 \cdot psi}{\varepsilon_p - 0.006} - 2000 \cdot psi\right)\right) & \text{otherwise} \end{cases} & \end{cases}$$

Force in FRP sheets

$$T_{FRP} := A_{FRP} \cdot f_f$$

Force in strands

$$T_{ps} := A_{ps} \cdot f_{ps}$$

Estimate of neutral axis location

$$c := \frac{T_{ps} + T_{FRP}}{\gamma \cdot f'_c \cdot \beta_1 \cdot b} \qquad c = \blacksquare\,in \qquad C = \blacksquare\,in$$

Re-iterate until c = C by changing C in Step 4. Then proceed to Step 10.

Step 10: Compute the nominal capacity of the beam.

Assuming $\beta_1 * C < t_s$

$\beta_1 \cdot C = \blacksquare$ in $\qquad t_s = \blacksquare$ in

$$M_n := \left[T_{ps} \cdot \left(H + t_s - Y_s - \frac{\beta_1 \cdot C}{2}\right) + T_{FRP} \cdot \left(H + t_s - \frac{\beta_1 \cdot C}{2}\right)\right]$$

$\phi := 0.9$

$\phi \cdot M_n := \blacksquare$

Step 11: Check all allowable stresses that haven't been checked already.

$M_{LL\_I} := \blacksquare \cdot ft \cdot kip$ $M_{DL1} := \blacksquare \cdot ft \cdot kip$ $M_{DL2} := \blacksquare \cdot ft \cdot kip$

M_{LL_I} = live load with impact

M_{DL1} = dead load on the non composite section

M_{DL2} = superimposed dead load on the composite section

$f_{available}$ is the available stress capacity for live load.

$$f_{available} := \frac{P_e}{A_c} + \frac{P_e \cdot (Y_b - Y_s)}{S_{beam}} - \frac{M_{DL1}}{S_{beam}} - \frac{M_{DL2}}{S_{3n}}$$

$$f_{LL\_I} := \frac{M_{LL\_I}}{S_n}$$

Calculate $f_{available}$ -f_{LL_I}. If this stress is negative this is the stress to be carried by the FRP.

$$check_1 := \begin{cases} \text{"stress carried by FRP"} & \text{if } f_{available} - f_{LL\_I} < 0 \\ \text{"stress carried by tendons"} & \text{otherwise} \end{cases}$$

$check_1 = \blacksquare$

$f_{carriedbyFRP} := -(f_{available} - f_{LL\_I})$ $f_{carriedbyFRP} = \blacksquare$ ksi

Allowable stress for FRP

$f_{FRP} := 0.33 \cdot 0.95 \cdot 0.65 \cdot f_f$

$f_{FRP} = \blacksquare$ ksi

f_{FRP} must be higher than the stress to be carried by the FRP .

$$check_2 := \begin{cases} \text{"Good"} & \text{if } f_{FRP} > f_{carriedbyFRP} \\ \text{"No good"} & \text{otherwise} \end{cases}$$

$check_2 = \blacksquare$

Allowable concrete compressive stresses:

$$f_1 := \frac{-P_e}{A_c} + \frac{P_e \cdot (Y_b - Y_s)}{S_{top}} - \frac{M_{DL1}}{S_{top}} - \frac{M_{DL2}}{S_{3n\_top}} - \frac{M_{LL\_I}}{S_{n\_top}} + 0.6 \cdot f'_{cbeam}$$

$$f_2 := \frac{-P_e}{A_c} + \frac{P_e \cdot (Y_b - Y_s)}{S_{top}} - 0.5 \cdot \left(\frac{M_{DL1}}{S_{top}} + \frac{M_{DL2}}{S_{3n\_top}} \right) - \frac{M_{LL\_I}}{S_{n\_top}} + 0.4 \cdot f'_{cbeam}$$

$$f_3 := \frac{-P_e}{A_c} + \frac{P_e \cdot (Y_b - Y_s)}{S_{top}} - \frac{M_{DL1}}{S_{top}} - \frac{M_{DL2}}{S_{3n\_top}} + 0.4 \cdot f'_{cbeam}$$

If f_1, f_2, and f_3 are positive, compression in concrete is O.K.

$$check_3 := \begin{cases} \text{"Good"} & \text{if } f_1 > 0 \\ \text{"Good"} & \text{if } f_2 > 0 \\ \text{"Good"} & \text{if } f_3 > 0 \\ \text{"No good"} & \text{otherwise} \end{cases}$$

$check_3 =$ ▮

$f_1 =$ ▮ ksi $\quad f_2 =$ ▮ ksi $\quad f_3 =$ ▮ ksi

Allowable stress in prestressing steel

$$f_{allowable} := \min(0.74 \cdot f_u, 0.82 \cdot 0.85 \cdot f_u)$$ Stress Relieved Strand

Final stress in strands

$$P_{final} := \frac{\frac{M_{LL\_I}}{S_n} + \frac{M_{DL1}}{S_{beam}} + \frac{M_{DL2}}{S_{3n}} - 6 \cdot f'_{cbeam}{}^{0.5} \cdot psi^{0.5}}{\frac{1}{A_c} + \frac{Y_b - Y_s}{S_{beam}}}$$

$$f_{final} := \frac{P_{final}}{A_{ps}}$$ f_{final} must be less than $f_{allowable}$

$f_{final} =$ ▮ ksi $\quad f_{allowable} =$ ▮ ksi

$$check_4 := \begin{cases} \text{"Good"} & \text{if } f_{final} < f_{allowable} \\ \text{"No good"} & \text{otherwise} \end{cases}$$

$check_4 =$ ▮

Step 12: Determine development length of the FRP according to manufacturer's recommendations

$$l_{df} := \frac{f_{fu} \cdot t_f \cdot n}{3 \cdot f'_{cbeam}{}^{0.5} \cdot psi^{0.5}}$$

$$l_{used} := \left(l_{df} + 1 \cdot in\right)$$

Find location where M = Mcr along the beam

$Length := \blacksquare \cdot ft$ $\qquad$ $M_{cr} := \blacksquare \cdot ft \cdot kip$

$$k := \frac{Mu_{original}}{\left(\frac{Length}{2}\right)^2}$$

$$x := \left(\frac{M_{cr}}{k}\right)^{0.5}$$

x = distance from centerline of beam to location where M = Mcr

Length of FRP required

$$L := 2 \cdot \left(x + l_{used}\right)$$

If more than one ply is used, extend each underlying sheet 6 inches on each end.

CFRP APPLICATION PROCEDURES

The following is a guide designed to aid in the application of CFRP. The pictures shown are from a bridge beam, but similar steps are followed for any other sort of repair/retrofit. Mbrace CFRP materials were used in this repair, thus any differences in manufacturer's materials could warrant adjustments of this procedure. The five aspects of CFRP application include: primer, putty, saturant, carbon fiber sheets/plates, and top coat.

Concrete Repair

Step 1: Repair concrete using mortar and epoxy injections according to current standards available. Forms must be used to maintain the original shape of the beam. Figures C1 and C2 show formwork and a completed patch.

Step 2: Grind off edges to a minimum of 1/2 inch for better bonding action.

Figure C1. Formwork example.

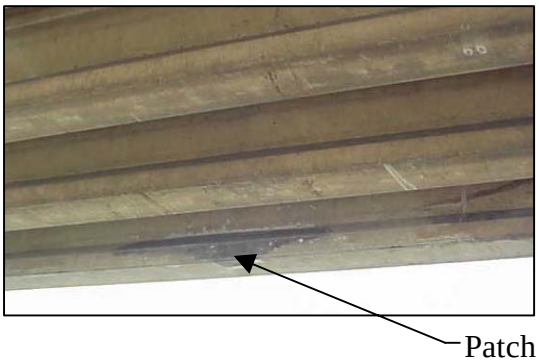

Figure C2. Cured Patch.

CFRP Installation

Application of primer:

Step 1: Clean off surface using high-pressure air or a damp cloth. Remove all dust.

Step 2: Weigh appropriate amounts of primer to be mixed, 3 parts A and 1 part B (may be different for other manufacturers). Measure only what is needed since primer has only a 35-minute pot life and will harden soon after mixing. A complete batch of primer covers 150-200 sq ft/gal. Figure C3 shows the weighing of the components.

Step 3: Mix for 3 minutes using a hammer-drill and mixing bit, shown in Figure C4.

Step 4: Pour primer into a paint tray and roll on with a medium nap roller. This can actually be completed quite quickly as long as the entire surface gets covered well. Figures C5 and C6 show the application of the primer.

Figure C3. Weighing of the primer components.

Figure C4. Mixing of the primer components with mixing drill bit.

Figure C5. Applying primer with nap roller.

Figure C6. Another view of primer application.

Application of putty:

The putty is used to plug bug holes and other small cracks for a better bond.

Step 1: Measure desired amount of both putty components with a scale.

Step 2: Premix white component for 3 minutes. Mix with other component for 3 more minutes, similar to the primer. Figures C7 and C8 show the mixing.

Step 3: Generously smear putty onto wet primer using an ordinary hand trowel. Press into any small holes that may exist. Coverage for the putty on smooth surfaces is 24 sq ft/gal and for rough surfaces about 12 sq ft/gal. Figure C9 and C10 show the putty application.

Figure C7. Putty mixture.

Figure C8. Mixing of the two components.

Figure C9. Applying putty with hand trowel.

Figure C10. View with putty step completed.

Application of Saturant:

The saturant impregnates the dry fibers and holds the CFRP in place while the epoxy cures.

Step 1: Weigh desired amount of saturant components. Pot life for the saturant is 30 minutes and coverage is 110-130 sq ft/gal.

Step 2: Premix the blue component for 3 minutes. Mix another 3 minutes while the colorless component is slowly added as shown in Figure C11.

Step 3: Roll the saturant directly on the wet putty with a clean nap roller. The roller should be soaked with saturant, which allows for easier application. This step should go fairly quickly as long the entire surface gets covered with saturant. Figures C12 and C13 show application of the saturant.

Figure C11. Mixing the blue and color-less component of the saturant layer.

Figure C12. Beginning the application of saturant layer with nap roller.

Figure C13. Applying saturant.

Application of carbon fiber:

Step 1: Determine the size of carbon fiber sheets required and cut to length using a utility knife and a straight edge, shown in Figure C14. Ideal length is between 6 and 10 ft.

Step 2: Roll precut strips for ease in application. A rolled up strip is shown in Figure C16.

Step 3: Begin unrolling longitudinal carbon fiber onto the wet saturant. Press along the length of the material with gloved hands. Use a ribbed roller to remove air pockets and impregnate the fibers with saturant. An installed longitudinal strip is shown in Figure C15.

Step 4: Continue applying all of the longitudinal strips. A 4 in. overlap is recommended when starting the next strip (see Figure C17). A thin strip of saturant should be applied to the last 4 in. of the previous strip so the next one will stick to it.

Step 5: One half hour after the carbon fiber strips have been applied, spread a 2nd layer of saturant over the existing carbon fiber strips.

Step 6: If applicable, apply a 2nd layer of carbon fiber strips in the new layer of saturant. If another layer is not needed, the 2nd layer of saturant should be left to dry.

Step 7: Repeat steps 5 and 6 for the desired number of layers.

Step 8: Apply transverse wrap in similar fashion. No overlap of the transverse FRP is required (see Figures C18 through C20).

Figure C14. Cutting FRP to the predetermined size.

Figure C15. One strip of longitudinal FRP.

Figure C16. Unrolling a strip of FRP.

Figure C17. Four inch overlap splice.

Figure C18. Transverse wrap over the longitudinal FRP.

Figure C19. Transverse wrap (cut to designed length).

Figure C20. Entire beam after the longitudinal and transverse FRP are installed.

Application of topcoat:

The topcoat is similar to a final layer of paint. It is applied mainly for aesthetic purposes so the repair is not noticeable while driving past the structure.

Step 1: Weigh components of topcoat, a 4:1 ratio. Pot life of the topcoat is 3 hours. Coverage is 350 sq ft/gal.

Step 2: Mix using hammer-drill and mixing bit for 5 minutes.

Step 3: Apply over the dried saturant and FRP using rollers and brushes. Figures C21 through C23 show the painting of the topcoat and the complete repaired structure.

Figure C21. The painting of the topcoat.

Figure C22. Using a roller to paint bottom flange.

Figure C23. Final view of completely repaired bridge.

REFERENCES

AASHTO LRFD Bridge Design Specifications, Second Edition, American Association of State Highway and Transportation Officials, Washington, D.C., 1998.

Aboutaha, R., R. Leon, A.H. Zureick, "Rehabilitation of Damaged AASHTO Type II Prestressed Girder Using CFRP," Second Symposium on Practical Solutions For Bridge Strengthening and Rehabilitation, 1997.

Alexander, J. and J.J. Cheng, "Field Application and Studies of Using CFRP Sheets To Strengthen Concrete Bridge Girders," Advanced Composite Materials in Bridges and Structures, 1996.

Al-Sulaimani, G. J., A. Sharif, I.A. Basunbul, M.H. Baluch, and B.N. Ghaleb, "Shear repair for reinforced concrete by fibreglass plate bonding," ACI Structural Journal, V.91, No.3, pp. 458-464, 1994.

American Concrete Institute, "ACI Manual of Concrete Practice, Part 1," ACI 209R-94, American Concrete Institute, Farmington Hills, Michigan, 1994.

Arduini, Marco and Antonio Nanni, "Behavior of Precracked RC Beams Strengthened with Carbon FRP Sheets," Journal of Composites for Construction, May 1997, pp. 63-70.

Arduini, Marco, Angelo Di Tommaso, and Antonio Nanni, "Brittle Failure in FRP Plate and Sheet Bonded Beams," ACI Structural Journal, July-August 1997, pp. 363-370.

Barnes, R.A. and G.C. Mays, "Fatigue Performance of Concrete Beams Strengthened with CFRP," Journal of Composites for Construction, Vol. 3, No. 2, pp. 95-104, May 1999.

Breña, S.F., R.M. Bramblett, S.L. Wood, M.E. Kreger, "Flexural Strengthening of Existing Reinforced Concrete Bridges Using Carbon Fiber Reinforced Polymer Composites," 9th International Conference and Exhibition, Structural Faults and Repairs, London, UK, July 2001.

Capozucco, R., and M. Nilde Cerri, "Static and Dynamic Behaviour of RC Beam Model Strengthened by CFRP Sheets," Construction and Building Materials, 2002, pp. 91-99.

Chaallel, O., M.J. Nollet, and D. Perraton, "Strengthening of Reinforced Concrete Beams with Externally Bonded FRP Plates: Design Guidelines for Shear and Flexure," Canadian Journal of Civil Engineering, Volume 25, 1998, pp. 692-704.

Chaallal, O., M. Shahawy, and M. Hassan, "Performance of Reinforced Concrete T-Girders Strengthened in Shear with Carbon Fiber-Reinforced Polymer Fabric," ACI Structural Journal, May-June 2002, pp. 335-343.

Chajes, M. J., T.F. Januszka, D.R. Mertz, T.A. Thomason, and W.W. Finch, "Shear strengthening of reinforced concrete beams using externally applied composite fabrics," ACI Structural J., V.92, No.3, pp. 295-303, 1995.

Chajes, M.J., T. Thomson, and C. Farschman, "Durability of Concrete Beams Externally, Reinforced with Composite Fabrics," Construction and Building Materials, Volume 9, Number 3, 1995, pp. 141-148.

Drimoussis, Efronisi and J.H. Roger Cheng, "Strengthening of Existing Concrete Bridge Girders For Shear Deficiencies Using Externally Bonded CFRP Sheets," Developments in Short and Medium Span Bridge Engineering, 1994.

Feldman, L.R., J.O. Jirsa, D.W. Fowler, and R.L. Cassasquillo, "Current Practice in the Repair of Prestressed Bridge Girders," Research Report 1370-1, University of Texas at Austin, June 1996.

Green, Mark and Khaled A. Soudki, "FRP Strengthened Concrete Structures in Cold Regions," Recent Advances in Bridge Engineering – Advanced Rehabilitation, Durable Materials, Nondestructive Evaluation and Management, 1997.

Hoa, S.V., M. Xie, X.R. Xiao, "Repair of Steel Reinforced Concrete with Carbon/Epoxy Composites," Advanced Composite Materials in Bridges and Structures, 1996.

Hooks, John and Jim Siebels, et al., "Advanced Composites in Bridges in Europe and Japan," U.S. Department of Transportation, Federal Highway Administration, December 1997.

Hutchinson, R., A. Abdelrahman, and S. Rizkalla, "Shear Strengthening Using CFRP Sheets For a Prestressed Concrete Highway Bridge in Manitoba, Canada," Recent Advances in Bridge Engineering – Advanced Rehabilitation, Durable Materials, Nondestructive Evaluation and Management, 1997.

Kachlakev, D.I., "Horsetaile Creek Bridge-Design Method Calibration and Experimental Results of Structural Strengthening with CFRP and GFRP Laminates," 9th International Conference and Exhibition, Structural Faults and Repairs, London, UK, July 2001.

Keble, D., G. Marshall, N. Thoday, "Strengthening of M60 Barnes Bridge, Manchester with Carbon Fibre Composites," 9th International Conference and Exhibition, Structural Faults and Repairs, London, UK, July 2001.

Klaiber, F.W., T.J. Wipf, F.M. Russo, R.R. Paradis, and R.E. Mateega, "Field/Laboratory Testing of Damaged Prestressed Concrete Girder Bridges," Iowa Department of Transportation, HR-397, December 1999.

Ligday, F.J., S.V. Kumar, and H.V.S. Gangarao, "Creep of Concrete Beams with Externally Bonded Carbon Fiber Tow Sheets," Advanced Composite Material in Bridges and Structures, 1996.

Malek, A.M., H. Saadatmanesh, and M.R. Ehsani, "Shear and Normal Stress Concentrations in RC Beams Strengthened with FRP Plates," Advanced Composite Material in Bridges and Structures, 1996.

Masoud, S., K. Soudki, "Blah Blah" 3rd Structural Specialty Conference of the Canadian Society of Civil Engineers, London, Ontario, June 2000.

Master Builders, Inc., EMACO S88 Cl – Performance Data and Specifications, Cleveland, OH, 1998.

Master Builders, Inc., MBrace Composite Strengthening System – Engineering Design Guidelines, Second Edition, Cleveland, OH, 1998.

Muller, John and Peter Dux, "Fatigue of Prestressed Concrete Beams with Inclined Strands," Journal of Structural Engineering, Volume 120, Number 4, April, 1994, pp. 1122-1139.

Nanni, A., P.C. Huang, J.G. Tumialan, "Strengthening of Impact-Damaged Bridge Girder Using FRP Laminates," 9th International Conference and Exhibition, Structural Faults and Repairs, London, UK, July 2001.

Norris, T., H. Saadatmanesh, and M. R. Ehsani, "Shear and Flexural Strengthening of R/C Beams with Carbon Fiber Sheets," Journal of Structural Engineering, July 1997, pp. 903-911.

Olson, S.A., C.W. French, R.T. Leon, "Reusability and Impact Damage Repair of Twenty-Year-Old AASHTO Type III Girders," University of Minnesota, May 1992.

Overman, T.R., J.E. Breen, and K.H. Frank, "Fatigue Behavior of Pretensioned Concrete Girders," Research Report 300-2F, University of Texas at Austin, November 1984.

Phillips, L., L. Ornberg, G. Kotlers, and D. Bierwagen, "Committee Report on Overheight Collision Damage on Bridges," Iowa Department of Transportation, 1995.

Plevris, Nikolaos and Thanasis Triantafillou, "Time-Dependent Behavior of RC Members Strengthened with FRP Laminates," Journal of Structural Engineering, March 1994, pp. 1016-1042.

Precast/Prestressed Concrete Institute, PCI Design Handbook, 5th Edition, Chicago, IL, 1999.

Quantill, R.J., L.C. Hollaway, and A.M. Thorne, "Predictions of the maximum plate end stresses of FRP strengthened beams: Part II," Magazine of Concrete Research, 1996, pp. 343-351.

Raker, Erik E., "Effective Concrete Repair," M.S. Thesis in preparation, Iowa State University, Ames, IA, 2000.

Rao, Chetana and Gregory Frantz, "Fatigue Tests of 27-Year-Old Prestressed Concrete Bridge Box Beams," PCI Journal, September-October, 1996, pp.74-83.

Roberts, T.M., "Approximate Analysis of Shear and Normal Stress Concentrations in the Adhesive Layer of Plated RC Beams," The Structural Engineer, Volume 67, Number 12/20, June 1989, pp. 229-233.

Saadatmanesh, H. and A.M. Malek, "Design Guidelines for Flexural Strengthening of RC Beams with FRP Plates," Journal of Composites for Construction, November 1998, pp. 158-164.

Sato, Y., T. Maeda, and Y. Asano, "A study on bond mechanism of carbon fibre sheet," Proceedings 3 rd International Symposium on Non-Metallic Reinforcement for Concrete Structures (FRPRCS-3), V.1, Japan Concrete Society, pp. 279-286, 1997.

Sen, Rajan, M. Shahawy, G. Mullins, and J. Spain, "Durability of CFRP/Epoxy/Concrete Bond in Marine Environment," ACI Structural Journal, November-December 1999, pp. 906-914.

Shahawy, M.A. and T. Beitelman, "Structural Repair and Strengthening of Damaged Prestressed Concrete Bridges Utilizing Externally Bonded Carbon Materials," 41st International SAMPE Symposium, 1996.

Shahawy, M. A. and T. Beitelman, "Static and Fatigue Performance of RC Beams Strengthened with CFRP Laminates," Journal of Structural Engineering, June 1999, pp. 613-621.

Shahawy, M.A., T. Beitelman, M. Arockiasamy, and R. Sowrirajan, "Experimental Investigation on Structural Repair and Strengthening of Damaged Prestressed Concrete Slabs Utilizing Externally Bonded Carbon Laminates," Construction and Building Materials, September 1995, pp. 217-224.

Shanafelt, G.O. and W.B. Horn, "Damage Evaluation and Repair Methods for Prestressed Concrete Bridge Members," National Cooperative Highway Research Program Report 226, Washington, D.C., November 1980.

Shanafelt, G.O. and W.B. Horn, "Guidelines For Evaluation and Repair of Prestressed Concrete Bridge Members," National Cooperative Highway Research Program Report 280, Washington, D.C., December 1985.

Sharif, Al-Sulamimani, Basunbul, Baluch, and Ghaleb, "Strengthening of Initially Loaded Reinforced Concrete Beams Using FRP Plates," ACI Structural Journal, Volume 91, Number 2, March-April 1994, pp. 160-168.

Stallings, J.M., J.W. Tedesco, M. El-Mihilmy, M. McCauley, "Field Performance of FRP Bridge Repairs," Journal of Bridge Engineering, May 2000, pp. 107-113.

Standard Prestressed Beam Details, Iowa Department of Transportation, Ames, IA, 1990.

Swamy, R. N., P. Mukhopadhyaya, and C.J. Lynsdale, "Strengthening for shear of RC beams by external plate bonding," The Structural Engineer, V.77, No.12, pp19-30, 1999.

Taljsten, Bjorn and Anders Carolin, "Strengthening of a Concrete Railway Bridge in Lulea with Carbon Fibre Reinforced Polymers – CFRP," Lulea University of Technology, 1998.

Tann, D.B., R. Delpak, E. Andreon, "Design Aspects of Shear Strengthening of RC Beams Using Externally Bonded FRP Sheets," 9th International Conference and Exhibition, Structural Faults and Repairs, London, UK, July 2001.

Triantafillou, T. C., "Shear strengthening of reinforced concrete beams using epoxy-bonded FRP composites," ACI Structural J., V.95, No.2, March-April, pp107-115, 1998.

Touranji, Houssam, and William Gomez, "Durability Characteristics of Concrete Beams Externally Bonded with FRP Composite Sheets," Construction and Building Materials, July 1997, pp. 351-358.

Varastehpour, H. and P. Hamelin, "Experimental Study of RC Beams Strengthened with CFRP Plate," Advanced Composite Materials in Bridges and Structures, 1996.

Watson, R.J., "Extending the Life of Bridges Using Fiber Reinforced Polymers," 9th International Conference and Exhibition, Structural Faults and Repairs, London, UK, July 2001.

Zobel, R.S., J.O. Jirsa, D.W. Fowler, and R.L. Carrasquillo, "Evaluation and Repair of Impact-Damaged Prestressed Concrete Bridge Girders," Texas Department of Transportation, Report Number 1370-3F, May 1996.

ACKNOWLEDGMENTS

The research presented in this report was conducted by the Bridge Engineering Center at Iowa State University and was sponsored by the Highway Division of the Iowa Department of Transportation and the Iowa Highway Research Board and under Research project TR-428.

The authors wish to thank all the Iowa Department of Transportation employees, especially those who helped with the field portion of the study, for their assistance. We would also like to thank Master Builders, Inc. for the generous donation of the CFRP materials used in the laboratory tests. Specially, we would like to thank Steve Tysl and Tony Conn for all of their guidance. A special thanks is also accorded to Brent Phares for his work on the Design/Application guide and Curtis Monk, FHWA Iowa Division Bridge Engineer, for his help in the development of the project.

The experimental portion of this project would not have been possible without the help of Doug Wood, Manager of the Structural Engineering Laboratory. Thanks are also due to the following Civil Engineering undergraduates for all of their assistance in the laboratory: Ben Dreier, Emily Allison, Travis Hosteng, Elizabeth Kash, Ken Hoevelkamp, Katie Bell, and Scott Ingersoll.